Quantifying the Role of Coarse Aggregate Strength on Resistance to Load in HMA

Research Report 0-5268-2

TxDOT Project Number 0-5268

Performed in cooperation with the Texas Department of Transportation & Federal Highway Administration

June 2008

Center for Transportation Infrastructure Systems
The University of Texas at El Paso
El Paso, TX 79968
(915) 747-6925
http://ctis.utep.edu

TECHNICAL REPORT STANDARD TITLE PAGE

1. Report No. FHWA/TX 08/0-5268-2	**2. Government Accession No.**	**3. Recipient's Catalog No.**
4. Title and Subtitle Quantifying the Role of Coarse Aggregate Strength on Resistance to Load in HMA		**5. Report Date** June 2008 **6. Performing Organization Code**
7. Authors J. Reyes, E. Mahmoud, I. Abdallah, E. Masad, S. Nazarian, Richard Langford, and V. Tandon		**8. Performing Organization Report No.** 0-5268-2
9. Performing Organization Name and Address Center for Transportation Infrastructure Systems The University of Texas at El Paso, El Paso, Texas 79968-0516		**10. Work Unit No.** **11. Contract or Grant No.** Project No. 0-5268
12. Sponsoring Agency Name and Address Texas Department of Transportation Research and Technology Implementation Office P.O. Box 5080, Austin, Texas 78763-5080		**13. Type of Report and Period Covered** Technical Report Sept. 1, 2005 –October, 2006 **14. Sponsoring Agency Code**

15. Supplementary Notes
Research Performed in Cooperation with TxDOT and the Federal Highway Administration
Research Study Title: The Role of Coarse Aggregate Point and Mass Strength on Resistance to Load in HMA.

16. Abstract

Several methods are available to determine aggregate characteristics, but their relationship to field performance, aggregate structure in HMA, and traffic loading needs to be further investigated and defined. Current laboratory protocols do not correlate well with aggregate abrasion, toughness, and strength requirements during handling, construction, and service. Specifications should ensure that aggregate particles possess the necessary strengths to avoid degradation during handling, construction, and trafficking.

This report discusses the determination of protocols and recommendations on the characteristics of the aggregates in a multifaceted way, considering the geological, geotechnical and mix design, to ensure accurate, economical, and time efficient testing methods. The use of these parameters in a micro-mechanical model to predict the performance is also discussed.

Correlations and analytical investigations were performed on the results of existing TxDOT tests methods, as well as those not currently specified by TxDOT. The recommended tests were found to be promising with advantageous relationships with existing tests as alternatives. The Schmidt Hammer, Seismic Modulus (V-meter), and Indirect Tensile Strength tests were beneficial to be performed on bulk rock samples and cored rock specimens for the simplicity and time consumption. British Standards tests, i.e. Aggregate Crushing Value (ACV), prove to be very reliable methods in finding aggregate properties; for example, rock strength and modulus. Traditional tests are mentioned in this report as effective tests to characterize aggregate angularity and texture.

The same investigation was done in HMA Performance tests to discover methods that may prove to be useful and accurate. Dynamic Modulus and Flow Time are time consuming. Three other performance methods are tested to consider alternatives. The Indirect Tensile Strength, Seismic Modulus (V-meter), and the Hamburg Wheel Tracking Device tests demonstrate very good results to portray HMA performance and the role of aggregates in the new generation HMA mixes.

17. Key Words Aggregate Interaction, Aggregate Gradation, Hot Mix Asphalt, Micromechanical Models	**18. Distribution Statement** No restrictions. This document is available to the public through the National Technical Information Service, 5285 Port Royal Road, Springfield, Virginia 22161, www.ntis.gov		
19. Security Classified (of this report) Unclassified	**20. Security Classified (of this page)** Unclassified	**21. No. of Pages** 162	**22. Price**

Form DOT F 1700.7 (8-69)

DISCLAIMERS

The contents of this report reflect the view of the authors who are responsible for the facts and the accuracy of the data presented herein. The contents do not necessarily reflect the official views or policies of the Texas Department of Transportation or the Federal Highway Administration. This report does not constitute a standard, a specification or a regulation.

The material contained in this report is experimental in nature and is published for informational purposes only. Any discrepancies with official views or policies of the Texas Department of Transportation or the Federal Highway Administration should be discussed with the appropriate Austin Division prior to implementation of the procedures or results.

NOT INTENDED FOR CONSTRUCTION, BIDDING, OR PERMIT PURPOSES

Jaime Reyes, BSCE
Enad Mahmoud, MSCE
Imad Abdallah, MSCE
Eyad Masad, Ph.D., PE (96368)
Soheil Nazarian, Ph.D., PE (66495)
Richard Langford, Ph.D.
Vivek Tandon, Ph.D., PE (88219)

Quantifying the Role of Coarse Aggregate Strength on Resistance to Load in HMA

By

Jaime Reyes, BSCE
Enad Mahmoud, MSCE
Imad Abdallah, MSCE, EIT
Eyad Masad, Ph.D., PE
Soheil Nazarian, Ph.D., PE
Richard Langford, Ph.D.
Vivek Tandon, Ph.D., PE

Research Project 0-5268

The Role of Coarse Aggregate Point and Mass Strength on Resistance to Load in HMA

Performed in cooperation with the
Texas Department of Transportation and
Federal Highway Administration

Research Report TX 0-5268-2

June 2008

Center for Transportation Infrastructure Systems
The University of Texas at El Paso
El Paso, TX 79968-0516

ACKNOWLEDGEMENTS

The successful progress of this project could not have happened without the help and input of many personnel of TxDOT. The authors acknowledge Mr. Richard Williammee, P.E., the project PD and Mr. Elias Rmeili, P.E., the project PC for facilitating the collaboration and with TxDOT Districts. They have also provided valuable guidance and input.

Special thanks are extended to the PAs, Dr. K.C. Evans, P.G., Dr. Zhiming Si, P.E., Mr. Jim Black, Mr. Joel Carrizales, and Mr. Josiah Yuen whom have been very supportive on this project and were helpful in finalizing the literature review portion of this report.

ABSTRACT

The performance of the new generation of HMA mixtures that rely more on a stone-to-stone contact is greatly influenced by the properties of the aggregate blends such as gradation and strength. As a result, aggregates have a significant and direct effect on the performance of asphalt pavements and it is important to maximize the quality of aggregates to ensure the proper performance of roadways.

The objective of this research is to evaluate the effect of stress concentrations at contact points on coarse aggregates that could cause aggregate fracture. To achieve the objectives, an extensive series of tests from geological evaluation of quarries and rocks retrieved from them, to rock strength tests, to traditional and new aggregate tests, to geotechnical strength tests were carried out on six aggregates to rank them. To establish the performance of mixes, specimens of four different mix types were prepared and subjected to a number of performance-related tests. The laboratory activities were supplemented with micro-mechanical modeling to understand the internal behavior of the mixes. Through correlation and statistical analyses, the redundant aggregate-related and performance-related tests were identified and the optimum test methods were recommended. Based on these activities, several tests for characterizing and ranking aggregates were proposed.

From the tests characterizing the aggregate point and bulk strength results, the Aggregate Crushing Value (ACV) test and its surrogate parameters were found to correlate well with performance.

The compressive strength obtained using the Schmidt hammer seems to be the most appropriate test for estimating the quality of the bulk rock before crushing in the field or lab. The V-meter seems to be an appropriate tool for estimating the modulus as well as the quality of the rock in tension.

From the traditional tests, the Los Angeles Abrasion test, Mg Soundness test, the Micro-Deval test, and AIMS angularity after micro-Deval are appropriate.

An approach for modeling the response of HMA was developed in this study. The aggregate properties (stiffness, compressive strength and tensile strength) were determined by matching the model results to experimental measurements conducted on aggregate samples. The PFC mixes are shown to have more localized high stresses within the aggregates than the Superpave and

CMHB mixes. This finding indicates that aggregates with higher resistance to fracture need to be used in PFC mixes.

A database of the information was assembled and a ranking scheme was implemented that can be readily used to rank the aggregates. Based on the average value of each parameter and the coefficient of variation of the test associated with those parameters, the acceptance limits can be set rationally considering the aggregate sources available to TxDOT. However, more aggregate types are needed to set the limits.

IMPLEMENTATION STATEMENT

In this report a number of recommendations have been made to estimate the strength of the aggregates for different mixes. The recommendations are based on the results from six sites.

At this time, the recommendations should be implemented on a number of aggregates to confirm the recommendations, and to adjust the limits and/or criteria. As part of the implementation, a guide should be developed to disseminate to the TxDOT staff.

TABLE OF CONTENTS

LIST OF FIGURES

LIST OF TABLES

CHAPTER ONE - INTRODUCTION

INTRODUCTION

The ever-increasing traffic volumes, including increased truck traffic and higher tire pressures, are putting greater stresses on the asphalt pavements which manifest in the form of pavement distresses such as rutting and fatigue cracking. To address these issues, improvements in the hot asphalt mix (HMA) blends are being implemented. The new generation of asphalt pavements such as coarse-graded Superpave mixtures, Stone Matrix Asphalt (SMA) and Porous Friction Course (PFC) rely more on stone-on-stone contact for a stronger coarse aggregate skeleton.

The performance of HMA mixtures is greatly influenced by the properties of the aggregate blends such as gradation and strength; therefore they have a significant and direct effect on the performance of asphalt pavements. It is important to maximize the quality of aggregates to ensure a proper performance of roadways.

Several methods are available to determine aggregate characteristics, but their relationship to field performance, aggregate structure in HMA, and traffic loading needs to be further investigated and defined. Current laboratory protocols do not correlate well with aggregate abrasion, toughness, and strength requirements during handling, construction, and service. Specifications should ensure that aggregate particles possess the necessary strengths to avoid degradation during handling, construction, and trafficking.

To address these issues, the characteristics of the aggregates have to be considered in a multifaceted way, considering the geological, geotechnical, mix design and construction. These parameters can be input in a micro-mechanical model to predict the performance. The effects of stress concentration at contact points on coarse aggregates and means of reducing them are also of interest. The geological aspects consist of characterizing the hardness and nature of rock mass. The geotechnical aspects are necessary to optimize the gradation, to consider the shape and size of the aggregates in the mix and to assess the strength of the aggregate mass as a whole. A proper HMA mix is needed to ensure the adequate durability, structural capacity and performance after the gradation is optimized.

ORGANIZATION

The work presented in this report represents an analytical and experimental investigation to evaluate the effect of stress concentration at contact points on coarse aggregates that could cause aggregate fracture. Chapter 2 gives an overview of current and new methods used for measuring the strength, shape and hardness of individual aggregates, and the bulk strength and deformation characteristics of the aggregate skeleton. The focus of Chapter 2 is on the description of the aggregates and mix selection, whereas Appendix A describes the geological aspects of the aggregates.

The next three chapters further detail the development of the methods discussed in Chapter 2. Chapter 3 describes the tests used to identify and evaluate the toughness and abrasion resistance in aggregates as well as those to evaluate the aggregate shape characteristics and those used to evaluate aggregate breakdown. Chapter 3 also presents a series of strength and stiffness tests to characterize the aggregate quality which is needed for the micromechanics modeling. Chapter 4 explains a series of methods related to the evaluation of the effects of different aggregate particle characteristics on aggregate interaction and shear strength. Chapter 5 discusses the tests used in this research to characterize the HMA performance such as the Hamburg Wheel Tracking test, indirect tensile strength test, dynamic modulus test, and flowtime test. Chapter 6 explains the micromechanical modeling to describe the behavior of materials considering their grain-to-grain interaction. In Chapter 7, based on the information gathered in Chapters 3 through 6, statistical and other advanced analyses of the results are presented. Finally, Chapter 8 provides the conclusions and recommendations for future work.

CHAPTER TWO - BACKGROUND

REVIEW OF LITERATURE

An extensive literature review documenting aggregate properties that significantly impact HMA performance was detailed in Research Report 5268-1 by Alvarado et al. (2007). Some of the conventional and recently developed aggregate tests as well as the significance of aggregate stone-on-stone interaction were described in that report. The readers are referred to Alvarado et al. so that they can become familiar with the background of this research. Excerpts from that document are included here.

Gradation is a primary concern in HMA design and thus most agencies specify allowable aggregate gradations. Gradation of a HMA influences almost all important properties including stiffness, stability, durability, permeability, workability, fatigue resistance, frictional resistance and resistance to moisture damage. Inappropriate selections of aggregate gradation, aggregate properties, and binder grade, type and content are major contributors to rutting and cracking of asphalt pavements. Strong opinions exist among industry experts as to which gradation type, ranging from fine to coarse to open-graded or stone matrix asphalt gradations, will provide the best performance (Hand et al., 2002).

Aggregate gradation can be described as dense-graded, gap-graded, uniformly-graded or open-graded. Dense-graded aggregates produce low air void content and maximum weight when compacted. The gap-graded aggregates refer to the gradation that certain intermediate sizes are substantially absent. The strength of gap-graded mixes (e.g., Stone-Matrix Asphalt, SMA) relies heavily on the stone-on-stone aggregate skeleton. It is imperative that the mixture be designed and placed with a strong coarse aggregate skeleton (Brown and Haddock, 1997). Uniformly-graded aggregates refer to a gradation that contains most of the particles in a very narrow size range. Open-Graded Friction Course (OGFC) mix designs are composed of this type of gradation.

Masad et al. (2003) indicate that the particle geometry of an aggregate can be fully expressed in terms of three independent properties which influence the performance of HMA: shape (or form), angularity (roundness), and surface texture.

Aggregates must be tough and abrasion resistant to resist crushing, degradation, and disintegration when stockpiled, placed with a paver, compacted with rollers, and subjected to

traffic loadings (Wu et al., 1998). These properties are especially critical for open- or gap-graded asphalt mixtures where coarse particles are subjected to high contact stresses. Aggregate degradation or breakdown may result in significant loss of pavement life.

Aggregate toughness refers to the property of an aggregate to resist breakdown. Such breakdown can alter the HMA gradation, resulting in a mixture that does not meet the volumetric properties (Prowell et al., 2005). Abrasion refers to the wearing of the aggregates in the pavement structure. Therefore, abrasion resistance is the resistance of an aggregate to wearing. Aggregates lacking adequate toughness and abrasion resistance may cause construction and performance problems. In addition, aggregates must also be resistant to breakdown when subjected to wetting and drying or freezing and thawing.

Another important aggregate property is hardness. Hardness of a rock is the resistance to deformation when it is loaded. Hardness is another major component in aggregates for a proper pavement performance.

One of the major components in aggregate degradation is the breaking up of the aggregates. The permanence of aggregates depends on their ability to retain their shape after being subjected to mechanical loads and applied disruptive forces (Oztas et al., 1999). The more strongly the particles in an aggregate are held together, the greater the work that has to be done to break the bonds. The performance of HMA is considered the combined resistance (shear strength) of the mineral aggregates and bituminous cement. Aggregates must provide support from traffic loads without deforming excessively (Cheung and Dawson, 2002).

The strength of an aggregate may be selected as a key factor in providing a qualitative evaluation of the interior quality of aggregates. The coarse aggregate strength is traditionally estimated indirectly by well known tests such as the Los Angeles abrasion test, the hardness and soundness tests, the aggregate crushing value test, etc. However, the indirect tensile and compressive strengths tests are preferred.

The Discrete Element Method (DEM) can be effectively used to model the interaction among HMA aggregate particles. Cundall and Hart (1992) summarized the advancements in discrete element codes. The DEM has been mainly utilized as a research tool in many studies in the last few years to study the grain-to-grain contact.

In Phase I of this study, the effectiveness of integrating experimental results on quarry rock and aggregates and numerical analysis to realistically predict the performance of mixes was demonstrated for the first time (see Alvarado et al., 2007).

AGGREGATES AND MIX SELECTION

The main object of this study is to evaluate the effect of stress concentration at contact points on coarse aggregates that could cause aggregate to fracture. Six aggregate types (three in Phase I and three in Phase II) were selected from six TxDOT Districts. A total of 21 mixes with three or four mix types were used in this study for the six aggregate sources (see Table 2.1). Most of

Table 2.1 - Selection of Aggregates and Mixtures

Phase I		Phase II	
Aggregate Type	**Mix Type**	**Aggregate Type**	**Mix Type**
Hard Limestone	CMHB-C Superpave-C PFC Type-D*	Sandstone	CMHB-C Superpave-C PFC Type-D
Granite	CMHB-C Superpave-C PFC Type-D*	Gravel	CMHB-C Superpave-C PFC Type-D
Soft Limestone	CMHB-C Superpave-C PFC Type-D*	Lightweight	CMHB-C Superpave-C PFC Type-D

***- Type-D mix for Phase I aggregates was actually added in Phase II of the project.**

these aggregates are commonly used in TxDOT paving and their performance histories are well known. For each of these aggregates, three mix types were chosen in Phase I: Porous Friction Course (PFC), Superpave-C, and Coarse Matrix High Binder (CMHB-C). In Phase II, a traditional Type D mix was also added. The same asphalt binder (PG 76-22) was used for all mixes to minimize the impact of the binder properties on the results.

The average gradation curve for each mix type, as illustrated in Figure 2.1, was selected to be in the middle of the gradation band specified by TxDOT. These gradations differ from one another to provide different grain-to-grain contact. The PFC is a coarse, almost uniform-graded mixture with a high percentage by weight of coarse aggregates. It is composed of 89% aggregates larger than a No. 8 sieve. In contrast, Superpave-C is a fine-graded mixture. It consists of 35% coarse aggregates (retained on the No. 8 sieve, hereinafter) and 65% fine aggregates. The CMHB-C mix is a coarse-graded mixture that is composed of 63% coarse aggregates and 37% fine aggregates. The Type-D mix demonstrates a well-graded gradation with 40% coarse aggregates and 60% fine aggregates. Although the gradation needs to be adjusted depending on mix design, this step was taken to make sure that an average estimate of crushing can be obtained for each mix type.

Since the main focus of this study is to evaluate the effect of stress concentration at contact points on coarse aggregates that could cause aggregate fracture, only coarse aggregates (Retained No. 8) from different sources were used while the fine portion (Passing No. 8) was obtained from one source only.

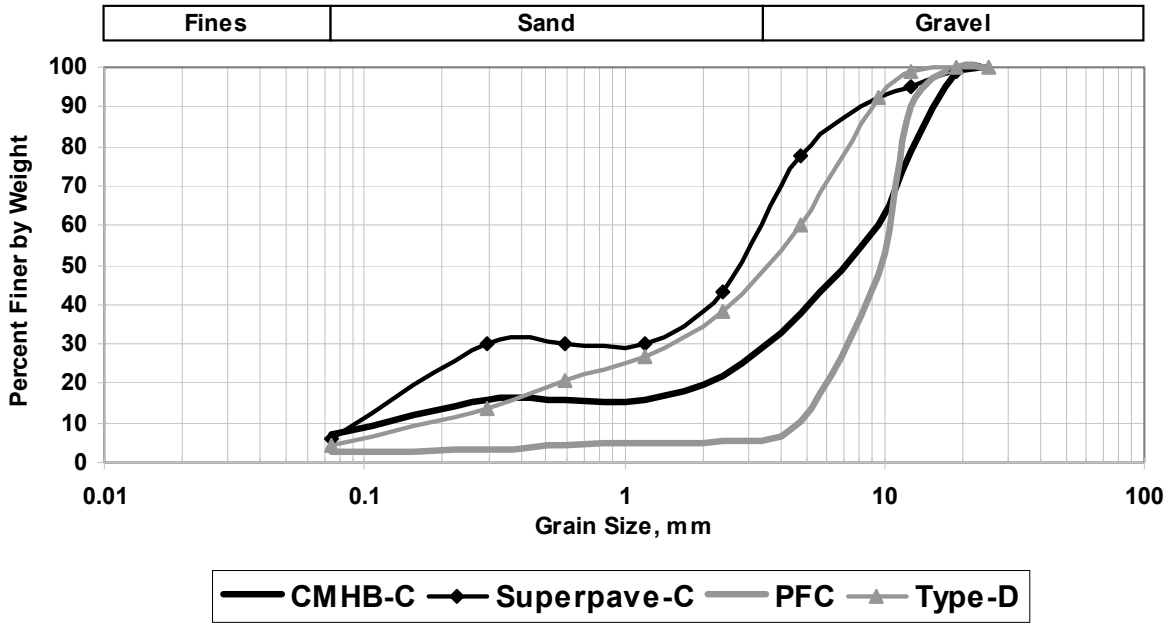

Figure 2.1 – Gradations of Mixes Used in This Study

GEOLOGICAL ASPECTS OF AGGREGATE

The geological description and the petrography analysis of the three Phase I aggregates were described in Research Report 5268-1. Due to the importance of the mineralogical aspects of aggregates, that section is repeated in Appendix A with the information about the three new aggregates added.

TRADITIONAL TESTS TO CHARACTERIZE MIXES AND AGGREGATES

The results of numerous tests, including the Los Angeles abrasion and Micro-Deval tests, currently specified by TxDOT to evaluate the degradation resistance in aggregates are summarized in Table 2.2. The results of the Aggregate IMaging System (AIMS) used to measure the shape characteristics of the aggregates are also provided in Table 2.2.

MIX DESIGN

The mix designs for the four mix types were developed using Tex-241-F and Tex-205-F. All mixes were designed using the Superpave Gyratory Compactor (SGC) regardless of mix types. The mixing, curing and compaction temperatures were selected as per Tex-241-F. The target air void contents for the CMHB-C, Superpave-C and Type D mixes were 4% and for the PFC mixes were 20%. For the PFC mixtures, 1% lime and 0.4% fiber of the total aggregate weight was added, as specified in Tex-241-F. The Job Mix Formula (JMF) for each of the mixes is summarized in Table 2.3 for Phase I mixes and Table 2.4 for the Phase II mixes. Since the lightweight aggregate has a specific gravity less than those of normal weight aggregates, a volumetric approach was considered.

Table 2.2 - Summary Results of Tests to Characterize Aggregates

Source	Test Procedure		Hard Limestone	Granite	Soft Limestone	Sandstone	Gravel	Lightweight Aggregate
TxDOT	Los Angeles Abrasion % Wt. Loss	Tex 410-A	24	38	32	26	19	26
	Mg Soundness Bituminous	Tex 411-A	9	20	29	20	4	7
	Mg Soundness Surface Treatment		8	19	23	19	4	4
	Polish Value	Tex 438-A	20	26	21	35	26	16
	Micro-Deval % Wt. Loss – Bituminous	Tex 461-A	13	13	26	18	4	27
	Coarse Aggregate Acid Insolubility	Tex 612-J	1	91	1	55	81	95
TTI	Micro-Deval %Wt. Loss - Surface Treatment	Tex 461-A	15	9	20	16	2	22
	Texture Before Micro-Deval	AIMS Procedure	193	221	80	265	142	205
	Texture After Micro-Deval		95	187	36	222	108	207
	Angularity Before Micro-Deval		2323	2791	2195	2868	3959	2370
	Angularity After Micro-Deval		1730	2491	1671	1883	2787	1483

*Using HMAC Application Sample Size Fractions

Table 2.3 - Mix Designs Used in Phase I

Property		Hard Limestone				Granite				Soft Limestone			
		CMHB-C	Superpave-C	PFC	Type-D	CMHB-C	Superpave-C	PFC	Type-D	CMHB-C	Superpave-C	PFC	Type-D
Binder Grade		PG 76- 22											
Binder Content,%		4.2	4.0	5.1	5.5	5.3	4.8	6.6	5.1	5.8	5.2	7.1	5.5
Sieve Size, in.	**Sieve No.**	**Percent Passing, %**											
1		100	100	100	100	100	100	100	100	100	100	100	100
0.75	**(3/4)**	99	99	100	100	99	99	100	100	100	100	100	100
0.492	**(1/2)**	78.5	95	90	99	78.5	95	90	99	84	97.5	91	99.5
0.375	**(3/8)**	60	92.5	47.5	92.5	60	92.5	47.5	92.5	69.5	92.5	52.5	95
0.187	**(No. 4)**	37.5	77.5	10.5	60	37.5	77.5	10.5	60	50	76	15.5	70.5
0.0929	**(No. 8)**	22	43	5.5	38	22	43	5.5	38	36	59	10.5	53.5
0.0469	**(No. 16)**	16	30	5	27	16	30	5	27	26	41	9.5	38
0.0234	**(No. 30)**	-	-	4.5	21	-	-	4.5	21	-	-	8.5	29.5
0.0117	**(No. 50)**	-	-	3.5	13.5	-	-	3.5	13.5	-	-	6.5	19
0.0029	**(No. 200)**	7	6	2.5	4.5	7	6	2.5	4.5	11.5	8.5	4.5	6.5
Maximum SG		2.554	2.554	2.572	2.756	2.471	2.520	2.469	2.744	2.450	2.515	2.445	2.738
Aggregate Bulk SG		2.696	2.696	2.715	2.710	2.601	2.655	2.526	2.696	2.587	2.653	2.527	2.638
Binder SG		1.02											
AV at N_{design}=100,%		4.0	4.0	20	4	4.0	4.0	20.0	4	4.0	4.0	20.0	4
VMA at N_{design}=100, %		12.7	12.7	27.2	12.9	13.7	13.2	27	15.5	14.3	13.7	28.0	13.9
VFA at N_{design}=100,%		70.2	68.5	26.4	69.8	69.7	69.9	25.8	74.2	72.5	70.9	28.8	72.2
Effective Asphalt Content, %		3.7	3.6	3.7	3.7	4.1	3.9	3.6	4.0	4.5	4.1	4.2	4.2
Dust Proportion		1.7	1.5	0.5	1.2	1.3	1.3	0.4	1.1	1.2	1.2	0.4	1.5

Table 2.4 – Mix Designs Used in Phase II

Property		Sandstone				Gravel				Lightweight Aggregate			
		CMHB-C	Superpave-C	PFC	Type-D	CMHB-C	Superpave-C	PFC	Type-D	CMHB-C	Superpave-C	PFC	Type-D
Binder Grade		PG 76- 22											
Binder Content,%		5.3	4.4	5.5	5.2	5.7	4.6	6.8	4.9	10.4	9.3	11.0	10.0
Sieve Size, in.	**Sieve No.**	**Percent Passing, %**											
1		100	100	100	100	100	100	100	100	100	100	100	100
0.75	**(3/4)**	99	99	100	100	99	99	100	100	100	100	100	100
0.492	**(1/2)**	78.5	95	90	99	78.5	95	90	99	84	97.5	91	99.5
0.375	**(3/8)**	60	92.5	47.5	92.5	60	92.5	47.5	92.5	69.5	92.5	52.5	95
0.187	**(No. 4)**	37.5	77.5	10.5	60	37.5	77.5	10.5	60	50	76	15.5	70.5
0.0929	**(No. 8)**	22	43	5.5	38	22	43	5.5	38	36	59	10.5	53.5
0.0469	**(No. 16)**	16	30	5	27	16	30	5	27	26	41	9.5	38
0.0234	**(No. 30)**	-	-	4.5	21	-	-	4.5	21	-	-	8.5	29.5
0.0117	**(No. 50)**	-	-	3.5	13.5	-	-	3.5	13.5	-	-	6.5	19
0.0029	**(No. 200)**	7	6	2.5	4.5	7	6	2.5	4.5	11.5	8.5	4.5	6.5
Maximum SG		2.430	2.488	2.374	2.450	2.433	2.502	2.376	2.485	1.625	1.879	1.427	1.823
Aggregate Bulk SG		2.585	2.621	2.555	2.608	2.616	2.655	2.594	2.649	1.605	1.914	1.365	1.850
Binder SG		1.02											
AV at N_{design}=100,%		4	4	20	4	4	4	20	4	4	4	20	4
VMA at N_{design}=100, %		14.3	12.9	27.9	14.0	15.7	13.5	31.7	14.2	12.9	16.8	32.8	14.9
VFA at N_{design}=100,%		69.3	69.7	30.7	74.4	74.7	70.8	36.9	71.9	69.6	71.2	20.4	72.8
Effective Asphalt Content, %		4.8	4.2	5.2	4.3	5.1	4.8	5.7	4.9	5.8	6.0	5.0	6.3
Dust Proportion		1.5	1.4	0.5	1.0	1.4	1.3	0.4	0.9	1.2	1.0	0.5	0.7

As shown in Table 2.4, a higher percentage passing for the lightweight coarse aggregate is calculated to reduce the weights to design the HMA with the distribution of coarse lightweight aggregate to those of fines to be the same as those as the normal weight aggregate mix design.

The asphalt contents for the five normal weight aggregates varied from 4% to 7.1%, and for the lightweight aggregate varied from 9.3% to 11.0% due to the high absorption of the aggregates. For each coarse aggregate type, the Superpave-C mixes had the lowest asphalt content whereas the PFC had the highest. The CMHB-C mix designs do not meet the TxDOT specifications of 15% Voids in Mineral Aggregates (VMA). Similarly, the dust proportion of 0.6 to 1.2 was not met for some of the mixes. The desired VMA or dust proportions could not be achieved because the gradations of the mixes had to be fixed for this study, to ensure that all coarse aggregates are evaluated in the same manner. Changing the gradation would bring in other parameters into the study that would impact the rigorousness of the conclusions drawn.

The mix designs presented herein are primarily for achieving the goals of this project. To actually lay down the proposed mixes, a number of other parameters should be evaluated. This evaluation process was outside the scope of this project.

SPECIMEN PREPARATION

All HMA specimens were prepared using a Pine Instrument Co. Superpave Gyratory Compactor (SGC) with the same compactor parameters; the angle of gyration, vertical pressure, and rotational speed. Two different sets of HMA specimens were prepared for this project at two different compaction efforts. First, the specimens were compacted to achieve a nominal air void content of 7% (20% for PFC), as specified in the TxDOT specifications. This generally occurred between 50 and 75 gyrations. Second, another set of lab specimens was compacted to 250 revolutions. Such variation in the compaction effort or number of gyrations was important to evaluate the potential of crushing in the aggregates. The design of Type-D mixes in TxDOT is usually carried out using a Texas Gyratory Compactor (TGC). For uniformity in compaction effort, these mixes were also designed using an SGC in concurrence with the PMC of the project.

Once compacted, the specimens were tested to characterize the HMA performance utilizing the Hamburg Wheel Tracking Device (HWTD) test, InDirect Tensile test (IDT), dynamic modulus test, and flow time (simple performance) test. After testing, the aggregate breakdown was examined. Specimens compacted to the nominal 7% (or 20% for PFC) air voids and to 250 gyrations were heated and broken down. The asphalt was then burned from the aggregates using an ignition oven according to Tex-236-F, and a sieve analysis was performed on each mix.

CHAPTER THREE - CHARACTERIZATION OF AGGREGATES AND ROCK MASSES

INTRODUCTION

A detailed description of test methods used to characterize the aggregates and rock masses are given in Research Report 5268-1. In this chapter a brief description of each test is given and the results are presented. The tests carried out on the aggregates include the Aggregate Impact Value (AIV) and Aggregate Crushing Value (ACV). Rock masses were subjected to the InDirect Tensile test (IDT), compressive strength test, Schmidt Hammer, Free-Free Resonant Column (FFRC) test, and ultrasonic test (V-meter).

AGGREGATE IMPACT VALUE (AIV)

The Aggregate Impact Value (British Standard 812-Part 112) provides a measure of the resistance of aggregates to impact. A specimen of the material passing the 1/2 in. sieve and retained on the 3/8 in. sieve is compacted into a 4-in. diameter, 2 in. high cylindrical steel cup by 25 strokes of a tamping rod. The sample is subjected to 25 vertical impacts dropped from a height of 15 in. using a 30-lb metal hammer, each being delivered at an interval of not less than 1 second. This action breaks the aggregate to a degree which is dependent on the vertical impact resistance of the material. Following the impacts, the crushed aggregate is then removed from the steel cup and weighed to record its mass. A sieve analysis is performed afterwards and the material passing the No. 8 sieve is weighed and recorded. The aggregate impact value (AIV) is then determined as a percentage using the following equation:

$$AIV = (M2 / M1) \, x \, 100 \tag{3.1}$$

where *M2* is the mass of the crushed material passed on the No. 4 sieve and *M1* is the mass of the total material after crushing. Traditionally, a maximum dry AIV of 30% is specified as the borderline between acceptable and unacceptable aggregates. The AIV tests can also be performed on aggregates soaked for 24 hours before testing.

The AIV values for the test conducted on the six aggregates in the dry and soaked conditions are summarized in Table 3.1. From the dry AIVs, the hard limestone, sandstone and gravel are of

Table 3.1 - Aggregate Impact Values for Aggregates

Aggregate Type	Dry AIV		Soaked AIV	
	Mean, %	COV, %	Mean, %	COV, %
Hard Limestone	13	*5*	31	*1*
Granite	29	*6*	35	*2*
Soft Limestone	28	*7*	34	*2*
Sandstone	21	*1*	21	*3*
Gravel	14	*8*	12	*7*
Lightweight Aggregate	38	*14*	27	*3*

high quality, the lightweight aggregate is unacceptable, and the granite and soft limestone are marginal. In the soaked conditions, the hard limestone is significantly worse than the dry condition, and the granite and soft limestone are equal or marginally worse. The crushing potential of the lightweight aggregate, unlike the others, decreases in soaked conditions. This perhaps occurs because the lightweight aggregate becomes much less brittle and softer after soaking than in the dry state, reducing the crushing of aggregates in compression (i.e., aggregates deform significantly more before breaking in compression or tension).

AGGREGATE CRUSHING VALUE (ACV)

The Aggregate Crushing Value Test (British Standard 812-Part 110) provides a measure of the resistance to crushing under gradually applied compressive loads by a compression testing machine. The material passing the 1/2 in. and retained on the 3/8 in. sieves is used to fill a 6-in. diameter by 4-in. high steel cylinder in three equal layers, each tamped 25 times. The sample is then subjected to a continuous loading up to 90,000 lb applied through a freely moving plunger by a compression testing machine over a period of 10 minutes. The crushed material is sieved and Equation 3.1 is used to calculate the ACV as well. Similar to the AIV tests, a maximum dry ACV of 30% is specified as the borderline between acceptable and unacceptable aggregates

To quantify the behaviors of aggregates under loading, the load and deformation of the specimen can be recorded during loading and plotted as shown in Figure 3.1. Four parameters (Compaction Modulus, Crushing Modulus, Maximum Compacting Stress, and Maximum Compacting Strain) can be estimated from that curve.

The ACV values for the six aggregates are reported in Table 3.2. The gravel and sandstone exhibited the least amount of crushing, and the lightweight aggregate the most. From the compacting moduli, the gravel will be the most resistant to compaction, and the lightweight aggregate, granite and soft limestone the least. From the crushing modulus, the gravel is the most resistant to crushing and the soft limestone the least. Based on the maximum compacting stress, the gravel can handle by far a greater compaction energy compared to the other materials shown, whereas the soft limestone and granite the least. In terms of maximum compacting stress, the lightweight aggregate is performing reasonably well.

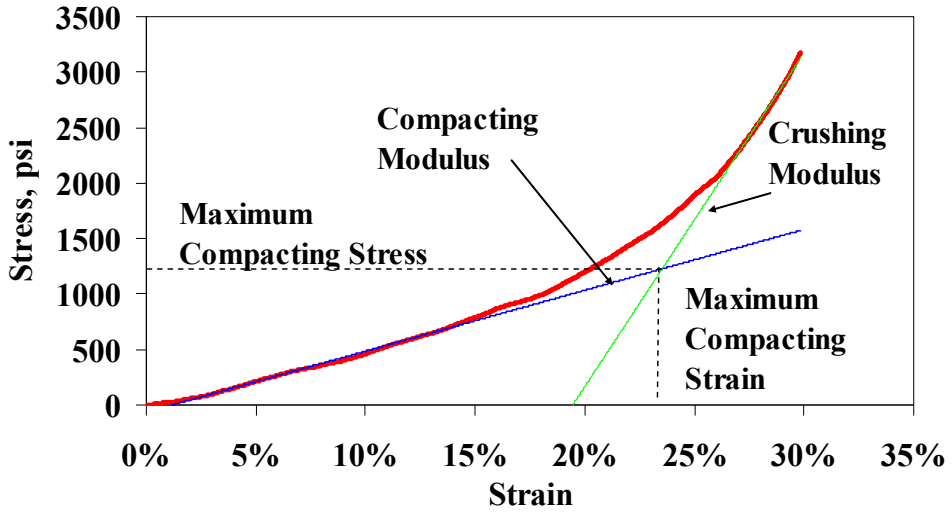

Figure 3.1 - Typical Results for an ACV Test

Table 3.2 - Results from Aggregate Crushing Value Tests on Aggregates

Aggregate Type	ACV	Compacting Modulus	Crushing Modulus	Maximum Compacting Stress
	%	ksi	ksi	psi
Hard Limestone	22 (1%)	6.8 (9%)	26.0 (3%)	1371 (2%)
Granite	27 (13%)	4.9 (7%)	27.2 (6%)	1008 (11%)
Soft Limestone	32 (2%)	4.1 (30%)	31.5 (4%)	988 (25%)
Sandstone	18 (4%)	8.4 (8%)	28.5 (5%)	1575 (4%)
Gravel	16 (1%)	12.8 (7%)	24.0 (6%)	2027 (8%)
Lightweight Aggregate	43 (0%)	4.9 (4%)	26.2 (4%)	1462 (6%)

*** Numbers in the parentheses are the coefficients of variation from triplicate tests.**

TEN PERCENT FINES VALUE (TFV)

The protocol for conducting the TFV tests is identical to the ACV with one exception. The applied load is reduced to the approximate load required to achieve the maximum compacting stress. The force is then released and the crushed material in the cylinder is sieved through the No. 8 sieve. The weight of the fraction passing the sieve is measured. The empirical relationship to obtain the force that yields ten percent fines value (TFV) is:

$$F = 14 \times f / (m + 4) \tag{3.2}$$

where F is the force (in kN) required to produce 10% of fines for each test specimen, f is the maximum force (400 kN or 90,000 lbs) applied to produce the required penetration, and m is the percent weight of material passing the No. 8 sieve from the ACV test.

The TFV values from all aggregates, except for the lightweight aggregate, are close to 10% (between 9 and 12) indicating that Equation 3.2 is reasonable in predicting the 10% crushing threshold. The stresses corresponding to the required forces from Equation 3.2 are also shown in Table 3.3. These stresses are normally greater than the maximum compacting stress except for the lightweight aggregate.

Table 3.3 - Results from Ten Percent Fines Value Tests on Aggregates

Aggregate Type	Max. Compacting Stress from ACV Test, psi	Stress for 10% Fines from TFV Test, psi	TFV	
			Mean, %	COV, %
Hard Limestone	1371	1531	9	*0*
Granite	1008	1362	12	*5*
Soft Limestone	988	1419	10	*6*
Sandstone	1575	1943	11	*7*
Gravel	2027	2054	16	*5*
Lightweight Aggregate	1462	317	17	*11*

SHAPE CHARACTERISTICS USING AIMS

Al-Rousan (2004) gives detailed background information about the AIMS operation and analysis methods. AIMS is a computer automated system that includes a lighting table where aggregates are placed in order to measure their shape, angularity and texture through image processing and analysis techniques. A coarse aggregate sample is placed on specified grid points, while a fine aggregate sample is spread uniformly on the entire tray. Texture is measured by analyzing gray scale images captured at the aggregate surface using the wavelet analysis method (Chandan et al., 2004). AIMS provides three different indices for aggregate shape characterization: texture, angularity, and sphericity.

AIMS was used to characterize the form, texture and angularity of the six aggregates for the three aggregate sizes required for the Micro-Deval tests (see Table 3.4). The results from AIMS are summarized in Table 3.5.

A high texture index means that the aggregate has more texture. The soft limestone is the least textured (the smoothest) and the sandstone has the highest texture. A high angularity index indicates a higher aggregate angularity. The granite has the highest angularity and the soft limestone the lowest. Finally, a high sphericity index indicates a more spherical shape while a low value corresponds to more flat/elongated aggregates. The sphericity indices fall into a narrow range for all aggregates because all the aggregate sources complied with the flat/ elongated fraction required by TxDOT.

The shape characteristics were also measured on the aggregates after the aggregate crushing tests and aggregate impact tests (see Table 3.6). Comparing the angularity values in Table 3.6 with angularity values in Table 3.5, there was no consistent trend in the change in aggregate

Table 3.4 - Aggregate Sizes Used for Characterization in AIMS

Passing	Retained
1/2 in. (12.5 mm)	3/8 in. (9.5 mm)
3/8 in. (9.5 mm)	1/4 in.(6.3 mm)
1/4 in. (6.3 mm)	No. 44. (75 mm)

Table 3.5 – Results from AIMS before Crushing

Aggregate Type	Texture Index			Angularity Index			Sphericity Index		
	3/8 in.	1/4 in.	No. 4	3/8 in.	1/4 in.	No. 4	3/8 in.	1/4 in.	No. 4
Hard Limestone	193	147	128	2557	3020	2753	0.689	0.667	0.678
Granite	180	125	131	3356	3709	3664	0.690	0.665	0.557
Soft Limestone	71	50	51	2294	2458	2576	0.710	0.625	0.663
Sandstone	281	275	241	2807	2912	2885	0.706	0.671	0.631
Gravel	138	136	100	2900	2870	2743	0.699	0.675	0.682
LW Aggregate	226	200	188	2594	2210	2306	0.741	0.741	0.732

Table 3.6 – Results from AIMS after Crushing

a) After Aggregate Crushing Value Tests

Aggregate Type	Texture Index			Angularity Index			Sphericity Index		
	3/8 in.	1/4 in.	No. 4	3/8 in.	1/4 in.	No. 4	3/8 in.	1/4 in.	No. 4
Hard Limestone	195	140	105	2675	2947	2952	0.777	0.746	0.700
Granite	180	149	121	3117	3283	3460	0.769	0.758	0.700
Soft Limestone	66	47	41	2643	2797	2887	0.783	0.702	0.635
Sandstone	295	267	239	2536	2834	2814	0.779	0.718	0.698
Gravel	160	111	110	3232	3181	3302	0.742	0.700	0.645
LW Aggregate	242	215	229	2501	2751	3111	0.794	0.751	0.729

b) After Aggregate Impact Value Tests

Aggregate Type	Texture Index			Angularity Index			Sphericity Index		
	3/8 in.	1/4 in.	No. 4	3/8 in.	1/4 in.	No. 4	3/8 in.	1/4 in.	No. 4
Hard Limestone	219	137	135	2562	2659	2742	0.754	0.791	0.713
Granite	172	127	122	2994	3376	3376	0.757	0.697	0.725
Soft Limestone	59	52	50	2608	2555	2601	0.760	0.725	0.731
Sandstone	342	287	264	2440	2475	3074	0.751	0.708	0.738
Gravel	132	114	88	2806	3021	3072	0.750	0.712	0.699
LW Aggregate	249	225	226	2157	2445	2522	0.797	0.738	0.715

angularity. This could be attributed to the fact that all aggregates were crushed as received in the laboratory prior to the crushing and impact tests.

Texture results were also inconsistent; nevertheless, the changes in texture were minimal, and this is expected as both the impact and crushing tests introduce no polishing to the aggregate surface. The sphericity results show that the sphericity index increased after each of the crushing and impact tests in most of the cases indicating that particles become less flat/elongated and more equi-dimensional, which is desirable for HMA mixes.

ABRASION USING MICRO-DEVAL

The Micro-Deval test was conducted in this study according to Tex-461-A. Sieve analysis is conducted after the Micro-Deval test in order to determine the weight loss in the coarse aggregate sample as the material passing the No. 16 (1.18 mm) sieve. The weight losses for the six aggregates from the standard Micro-Deval tests are shown in Table 3.7.

Table 3.7 - Weight Losses from the Standard Micro-Deval Tests

Aggregate	M-D Wt. Loss,%
Hard Limestone	15.0
Granite	8.8
Soft Limestone	20.4
Sandstone	12.7
Gravel	3.6
Lightweight Aggregate	23.4

The lightweight aggregate had the highest Micro-Deval weight loss while the gravel had the least weight loss. The aggregates were characterized using AIMS after the Micro-Deval tests. Table 3.8 shows comparisons of angularity and texture, respectively. The average indices of the three sizes were used in this comparison. The six aggregates lost some of their shape and texture. All aggregates except the granite and the lightweight aggregate lost a considerable amount of texture (more than 15%) after treatment. All the aggregates lost more than 24% of angularity except the granite (11%).

Table 3.8 – Angularity and Texture Index Change in Micro-Deval

Aggregate	Angularity Index			Texture Index		
	Before MD	After MD	Difference	Before MD	After MD	Difference
Hard Limestone	2323	1730	26%	193	95	51%
Granite	2791	2491	11%	221	187	15%
Soft Limestone	2195	1671	24%	80	36	55%
Gravel	3959	2787	30%	142	108	24%
Sandstone	2868	1883	34%	265	222	16%
Lightweight Aggregate	2370	1483	37%	205	207	-1%

The method developed by Mahmoud (2005) was used to characterize the resistance of the three aggregates to polishing. In this method, the aggregate texture was measured after different polishing times in the Micro-Deval as shown in Figure 3.2. The texture versus polishing time is expressed using the relationship:

$$Texture(t) = a + (b \times e^{-ct}) \tag{3.3}$$

where Texture (t) is the aggregate texture index at time t in minutes. The texture reduces to the parameter (a) as time increases or approaches infinity. Therefore, (a) represented the texture value at terminal time. At time equal zero, the initial texture becomes equal to a+b. For any time greater than zero, the texture drops based on the value of c which is a parameter that quantifies the rate of loss of texture.

Mahmoud (2005) also showed that the texture values measured at three specific time periods of 0, 105, and 180 minutes are sufficient to fit Eq. (3.3) to data and determine the values of the coefficients a, b and c. Parameters a, b and c for Equation 3.3 for the six aggregates are shown in Table 3.9. The hard limestone had an initial texture slightly less than the granite; however, the hard limestone lost more texture compared with the granite. The lightweight aggregate exhibited relatively small changes in texture. It can seen from the results in Table 3.9 and Figure 3.2 that the initial texture alone should not be used to rank aggregates based on texture as aggregates vary in their resistance to loss of texture under abrasion and polishing actions.

Table 3.9 - Equation Parameters for Micro-Deval Tests on Aggregates

Aggregate	A	b	C
Granite	182.44	38.49	0.02081
Hard Limestone	93.60	99.15	0.04087
Soft Limestone	39.13	37.46	0.02505
Sandstone	166.70	99.43	0.00553
Gravel	105.67	36.33	0.02617
Lightweight Aggregate	199.78	5.90	0.00874

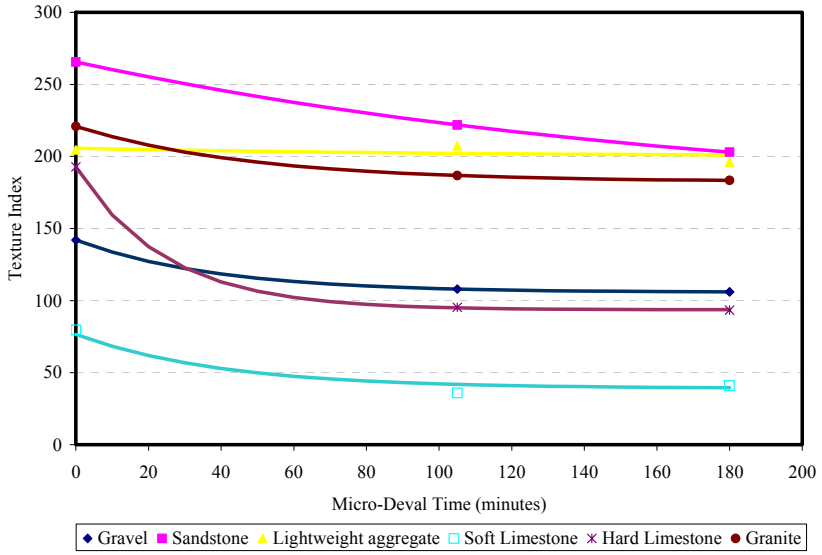

Figure 3.2 - Aggregate Texture as Function of Micro-Deval Time for all Mixes

Figures 3.3 shows the percent change of aggregate passing the 3/8 in. sieve after being compacted to the design air void content for each HMA mix type. The PFC mix showed the most change in gradation, demonstrating that the coarse aggregate is breaking when compacted in coarse gradation mixes. Type-D mixes with the hard limestone, granite and soft limestone was not tested because they were initially not in the scope of this study.

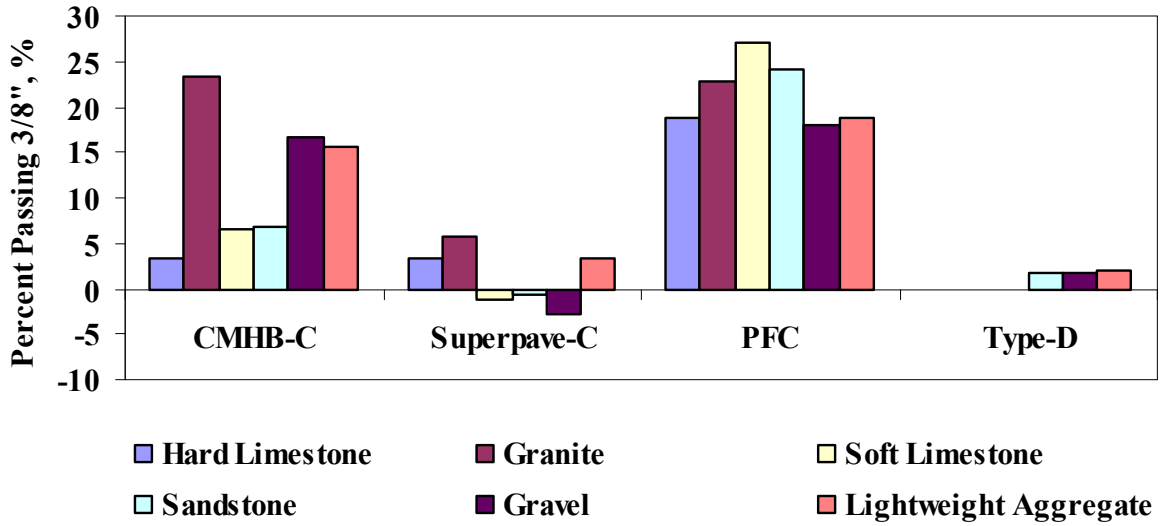

Figure 3.3 - Percentage Change of Aggregate Passing the 3/8 in. Sieve after Compaction

Unlike the PFC and CMHB-C, the finer mixes show little change compared to the coarser mixes. Individually, the granite exhibited more gradation change than the other aggregates for the CMHB-C. Cases with negative or zero change are considered to be a result of the variability in the sieve analysis measurements. The results in Figure 3.3 indicate that some aggregates undergo breakage and crushing during the compaction, which may alter the produced mix design compared with the original laboratory design. This is more severe for the PFC and CMHB-C mixes as compared to the others.

STRENGTH OF INDIVIDUAL AGGREGATE PARTICLES

A single aggregate particle crushing was also performed. Fifty-six particles passing the 1/2 in. sieve and retained on the 3/8 in. sieve from each aggregate source were tested positioned vertically, and another fifty-six particles were tested positioned horizontally as shown in Figure 3.4. The average maximum loads at crushing for each aggregate are shown in Table 3.10. The gravel by far is the strongest aggregate in both directions followed by the sandstone.

The cumulative distributions of the load resistance for the vertical and horizontal tests are shown in Appendix B, and their coefficients of variation (COV's) are summarized in Table 3.10. The strengths exhibit high COV's, indicating that many tests runs should be conducted in order to get a representative distribution of the strength for the aggregates. The distributions were used to introduce variability of the aggregate properties in the micro-mechanical models.

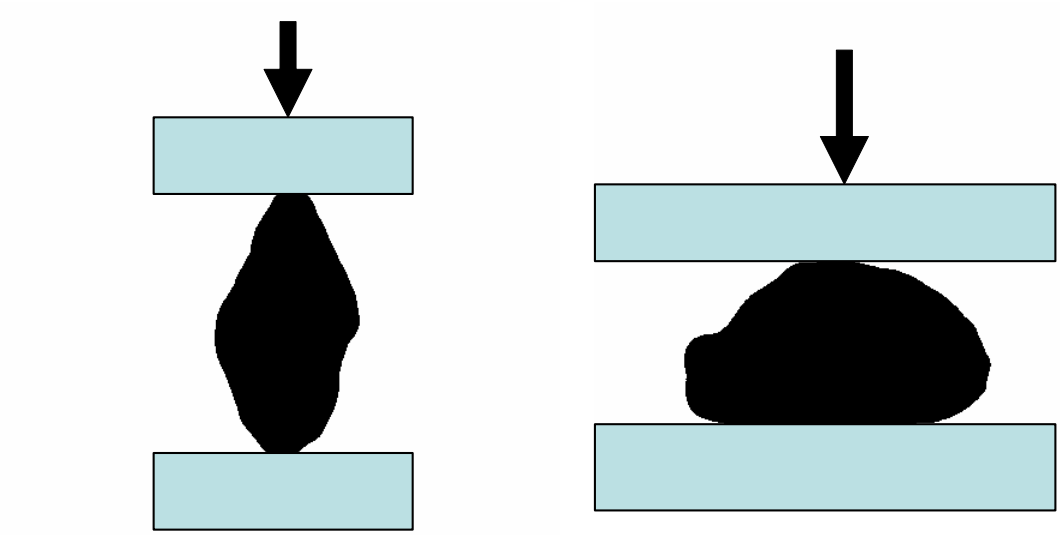

a) Vertically aligned aggregate **b) Horizontally aligned aggregate**

Figure 3.4 - Single Aggregate Crushing Set-up

Table 3.10 – Single Aggregate Crushing Resistance

Aggregate	Load Resistances, lb	
	Vertical	Horizontal
Hard Limestone	173 (*43%*)	171 (*35%*)
Granite	168 (*42%*)	154 (*35%*)
Soft Limestone	153 (*36%*)	130 (*38%*)
Sandstone	235 (*44%*)	268 (*53%*)
Gravel	479 (*54%*)	470 (*58%*)
Lightweight Aggregate	135 (*59%*)	134 (*43%*)

*** - Numbers in the parentheses are the coefficient of variation from triplicate tests.**

PROPERTIES OF ROCK MASSES

A series of strength and stiffness tests were carried out on specimens retrieved from bulk rock samples to characterize the aggregate quality based on the properties of its original rocks. This information was needed for the micro-mechanical models as well. A brief description of each test process is presented in this chapter.

SPLITTING TENSILE TEST

The splitting tensile strength tests (similar to Tex-421-A) on cores from rock masses retrieved from quarries were carried out to determine the potential tensile crushing strength of the aggregates. Rock core samples were first extracted from bulk rocks and cut to 2.3-in. diameter by 2-in. height (standard core barrel size). The samples' dimensions were intentionally kept smaller than standard so that the specimen can be forced to fail in a crushing mode similar to an aggregate. It was impossible to perform this test on the gravel and lightweight aggregate because they are not extractable from rock masses. As shown in Table 3.11, the sandstone exhibited the highest tensile strength and the soft limestone the lowest.

Table 3.11 - Summary Results of IDT and Compressive Strength Tests

Material	Strength, psi		
	IDT	UCS	Schmidt Hammer
Hard Limestone	1412 (20%)	10427 (38%)*	9719
Granite	1062 (23%)	14034 (7%)*	12034
Soft Limestone	682 (-)**	6970 (8%)*	6994
Sandstone	1677 (11%)	13952 (31%)	10868
Gravel	Not feasible		
LW Aggregate			

*** - Numbers in the parentheses are the coefficient of variation from triplicate tests.**
**** - only one specimen was tested for the soft limestone**

COMPRESSIVE STRENGTH TEST

For the purpose of this project, cylindrical rock specimens were tested in a similar manner to Tex-418-A to determine the unconfined compressive crushing strength of the drilled rock cores. Rock cores similar to those for the indirect tensile tests extracted from bulk rocks were used. Table 3.11 also includes the results from the compressive strength tests. The granite and sandstone were the strongest in compression with a strength of about 14,000 psi and the weakest rock was the soft limestone with a strength of about 7,000 psi.

SCHMIDT HAMMER

A Schmidt hammer (Tex-446-A) was also used to estimate the rock compressive strength. The compressive strengths are surprisingly close to those obtained from the compression tests as shown in Table 3.11 except for the sandstone. Since this method can be used both in the laboratory and in the field, and since little sample preparation is required to perform the test, the rebound test performed using the Schmidt hammer may be an excellent test for characterizing the quality of rock masses in compression.

MODULUS OF ROCK

Young's modulus, sometimes referred to as modulus of elasticity, is the measure of a material's resistance to strain and is an extremely important characteristic of a material's stiffness. The Free-Free Resonant Column (FFRC, Tex-149, draft) and Ultrasonic (V-meter) Testing (Tex-254-F, draft) were used to measure the moduli. The moduli, measured using these seismic methods, for the four rocks used in this study are included in Table 3.12. Seismic moduli are typically greater than the regular mechanical elastic moduli because of the differences in the strain levels and strain rates. These tests were performed on 2.3 in. diameter cores from rock masses before they were cut for compressive or tensile strength tests. The hard limestone exhibited the highest modulus of about 10,000 ksi and the soft limestone the lowest with a modulus of about 5,500 ksi. Once again, the granite is less stiff because of the large crystals embedded within the rock.

Table 3.12 - Results of Ultrasonic and FFRC Tests

Material	Modulus, ksi	
	V-Meter	FFRC
Hard Limestone	10328 (13%)*	10299 (6%)*
Granite	6686 (6%)*	7440 (15%)*
Soft Limestone	5473 (11%)*	6309**
Sandstone	8659 (7%)*	8364 (15%)*
Gravel	Not Feasible	
Lightweight Aggregate		

*** - Numbers in the parentheses are the coefficient of variation from triplicate tests.**
**** - FFRC was estimated**

CHAPTER FOUR - CHARACTERIZATION OF AGGREGATE INTERACTION

INTRODUCTION

The coarse aggregate property is traditionally characterized indirectly by widely used tests such as the Los Angeles abrasion test, the hardness and soundness tests, the aggregate crushing value test, etc. Although these indirect test methods provide some information about the aggregate quality, there is still a need to characterize the interaction within the aggregates. The direct shear test and the triaxial compression test methods were utilized to evaluate this interaction.

DIRECT SHEAR TEST

The procedure specified in ASTM D3080 was used to perform the direct shear tests. The sample used for this test was air dried and placed in a direct shear box. A 6-in. diameter direct shear test box was retrofitted into a conventional device for use with larger and coarser aggregate materials used in this project.

This test included drying enough material in the oven at a temperature of 220°F and then letting it cool to room temperature. The coarse portion of the material was then placed in the mold of the direct shear device in three layers, and each layer was rodded 25 times to compaction. Each specimen was subjected to sieve analysis before and after testing to determine the crushing of aggregates due to compaction and shearing. Normal stress was first applied to the sample. Shear stress was gradually increased until the sample failed in shear along a predefined horizontal plane with a horizontal speed of 0.05 in/min.

Triplicate tests were performed on the coarse aggregates at a normal stress of 20 psi. Since the goal was to study the interaction of the aggregates, tests were repeated for the CMHB-C, Superpave-C PFC, and Type-D separately. Figure 4.1 illustrates typical results for this test method. The horizontal stress-horizontal strain curve and the variation in vertical strain with horizontal strain for each specimen were developed. Relevant information, such as the peak strength, horizontal strain at peak strength, the maximum vertical expansion, and the vertical strain at peak strength, was extracted to evaluate the grain-to-grain strength of the mixtures.

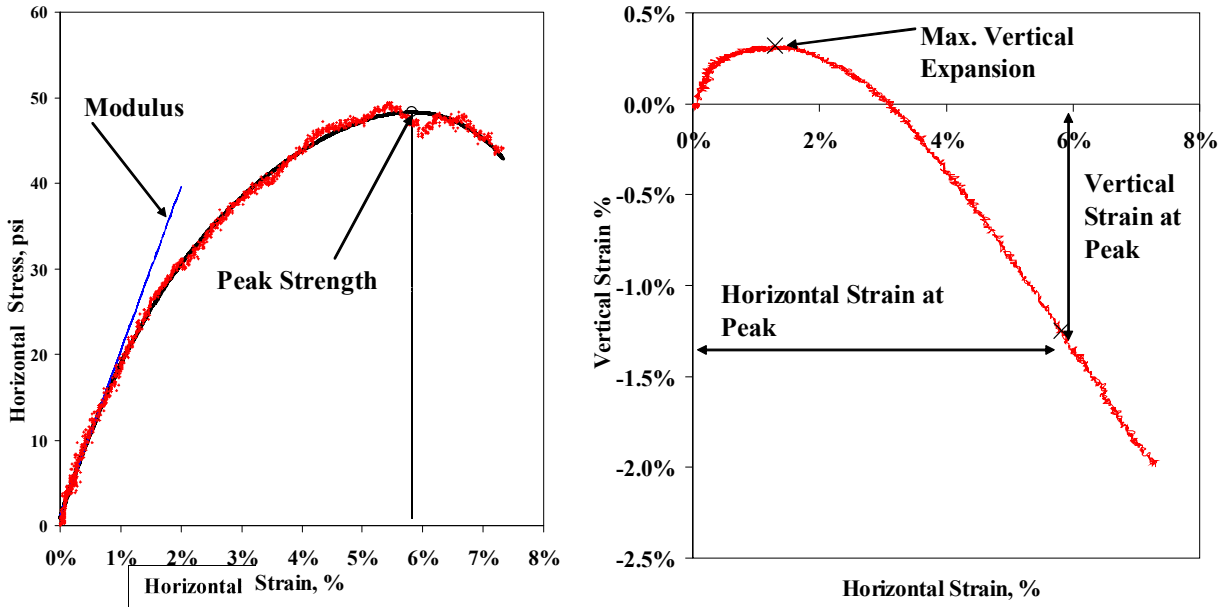

a) Horizontal Stress vs. Horizontal Strain Plot **b) Vertical Strain vs. Horizontal Strain**

Figure 4.1 - Typical Results from Direct Shear Tests

The parameters extracted from the direct shear tests are summarized in Table 4.1. Except for the lightweight aggregates, the mixes yielded dry unit weights ranging from 90 pcf to 97 pcf (see Table 4.1). The PFC mixes from all the aggregate sources yielded unit weights that were 2 to 3 pcf less than the other mixes because of the uniformity in the coarse aggregate gradation. The lightweight aggregates' dry unit weights were between 51 and 53 pcf, simply because the specific gravity of the lightweight aggregates is significantly less than those of the other natural aggregates.

The moduli obtained from the direct shear tests are generally not considered reliable because of the size and rigid boundaries of the shear box and because of high strains applied to the specimen. However, they may provide some relative information with regard to the initial shear resistance to the applied loads. The measured moduli varied from about 1,400 psi to about 2,300 psi (see Table 4.1). The Type-D mix for the lightweight aggregate exhibited the highest modulus and the PFC mix for gravel exhibit the lowest modulus.

The peak strengths for the blends varied from 33 psi to 55 psi (see Table 4.1). The hard limestone generally provided the highest peak strengths. The Superpave-C and Type-D mixes exhibit the lowest peak strength, since these gradations contain smaller particles, causing the least amount of grain-to-grain contact. The CHMB-C and PFC mixes provided the most resistance to shearing due to a good interlocking between the aggregates.

During shearing, a densely-compacted specimen first exhibits a vertical expansion followed by a vertical contraction primarily due to the reorientation and crushing of aggregates, as shown in Figure 4.1b. The initial expansion occurs because of the " reorientation " of the individual particles on top of each other. These values are similar for all the aggregate sources. At this

Table 4.1 - Summary Results from the Direct Shear Tests

Aggregate Source	Mix Type	Dry Unit Weight, pcf*	Modulus, psi	Peak Strength, psi	Strain at Peak Strength, %		Max. Vertical Expansion, %	Φ
					Horizontal	Vertical		
Hard Limestone	CMHB-C	92	2207	55	6.5	-1.6	0.3	70°
		0%	15%	4%	10%	20%	16%	
	Superpave-C	93	1699	45	6.5	-1.3	0.4	67°
		1%	8%	6%	9%	36%	6%	
	PFC	90	1827	50	6.0	-1.0	0.3	68°
		1%	5%	7%	3%	38%	10%	
	Type-D	92	2011	47	8.0	-2	0.2	67
		2	21%	6%	4%	-37%	33%	
Granite	CMHB-C	94	1907	44	6.6	-0.8	0.4	66°
		0%	13%	5%	10%	53%	10%	
	Superpave-C	94	1717	40	6.4	-0.7	0.5	63°
		0%	5%	7%	10%	42%	19%	
	PFC	91	1856	43	6.0	-0.9	0.3	65°
		0%	4%	5%	10%	22%	14%	
	Type D	93	1861	41	7.0	-1.3%	0.2%	64
		4	8%	11%	23%	-79%	47%	
Soft Limestone	CMHB-C	94	1924	46	5.8	-1.6	0.3	67°
		1%	5%	2%	3%	39%	44%	
	Superpave-C	95	2037	45	6.4	-1.7	0.2	66°
		1%	17%	10%	10%	6%	27%	
	PFC	92	1873	48	7.0	-1.0	0.5	67°
		4%	4%	2%	9%	40.0%	27%	
	Type-D	94	2051	45	6.0	-1%	0%	66
		3	6%	3%	20%	-21%	0%	
Sandstone	CMHB-C	95	2078	50	6.6	-1.6	0.7	68°
		0%	3%	2%	8%	9%	11%	
	Superpave-C	94	1798	41	5.0	-1.1	1.6	64°
		1%	6%	2%	16%	26%	8%	
	PFC	92	2027	52	7.6	-2.5	1.6	69°
		1%	1%	5%	1%	11%	7%	
	Type-D	94	1883	43	6.1	-1.5	0.5	65°
		0%	1%	5%	4%	5%	34%	
Gravel	CMHB-C	97	1790	41	4.9	-1.6	0	64°
		0%	16%	6%	12%	23%	0%	
	Superpave-C	97	1624	33	4.4	-0.7	0.8	59°
		0%	3%	4%	3%	54%	18%	
	PFC	95	1415	43	7.1	-2.0	2	65°
		1%	9%	3%	10%	7%	21%	
	Type-D	97	1940	34	6.1	-1.4	1.4	60°
		1%	4%	4%	7%	16%	20%	
LW Aggregate	CMHB-C	53	2038	48	5.2	-1.4	1.6	67°
		1%	4%	6%	5%	5%	5%	
	Superpave-C	53	1998	42	4.6	-0.8	2.0	65°
		1%	2%	4%	3%	18%	24%	
	PFC	51	2137	48	4.6	-1.1	1.8	67°
		2%	1%	2%	3%	0%	11%	
	Type-D	54	2309	43	4.4	-1.0	2.1	65°
		1%	1%	2%	15%	42%	8%	

*** - Numbers with % are the coefficient of variation from triplicate tests.**

point, the maximum expansion strain may not be a parameter that can be used to quantify the interaction of aggregates.

The vertical contraction at higher horizontal strains may be due to the crushing of aggregates or densification due to the reorientation of the aggregates. These values are fairly similar and not very repeatable (see COV values for this parameter in Table 4.1).

The angles of internal friction obtained from the direct shear tests are also included in Table 4.1. The trend is very similar to that from the peak strength for all the aggregate sources. However, it may be easier to use the angle of internal friction than strength in day-to-day operations of TxDOT.

Another matter taken in consideration is to measure how much of the coarse aggregate breaks under a shearing force. Percent aggregates passing the No. 4 sieve after the compaction and shearing are shown in Table 4.2 to see how much aggregate was crushed. The crushing of aggregates is minimal and does not vary significantly within the same aggregate source. Gravel showed the least crushing and the lightweight aggregates the most.

Table 4.2 - Sieve Analysis after Compaction and Shearing

Material	Type	Avg. Percentage Passing No. 4 Sieve, %	COV, %
Hard Limestone	**CMHB-C**	0.6	*4*
	Superpave-C	0.8	*8*
	PFC	0.8	*4*
	Type-D	0.6	*6*
Granite	**CMHB-C**	0.7	*13*
	Superpave-C	0.8	*19*
	PFC	0.7	*9*
	Type-D	0.7	*10*
Soft Limestone	**CMHB-C**	0.9	*5*
	Superpave-C	1.2	*10*
	PFC	1.1	*1*
	Type-D	0.9	*6*
Sandstone	**CMHB-C**	1.1	*1*
	Superpave-C	1.1	*16*
	PFC	0.6	*11*
	Type-D	0.9	*7*
Gravel	**CMHB-C**	0.5	*25*
	Superpave-C	0.6	*38*
	PFC	0.3	*19*
	Type-D	0.8	*13*
Lightweight Aggregate	**CMHB-C**	2.4	*22*
	Superpave-C	2.2	*4*
	PFC	1.7	*13*
	Type-D	2.5	*24*

TRIAXIAL TEST

For a standard triaxial test, in accordance with Tex-143-E, several 6-in. diameter by 8-in. high specimens were prepared at their respective optimum moisture contents. The specimens were encased in rubber membranes, placed between two porous stones, and allowed to mature for at least 24 hours before testing. Each sample was then tested in compression in a triaxial cell at a rate of 1% strain/minute while the stress-strain diagram of material is recorded. The results from different confining pressures can be used to draw the Mohr circles and develop the Mohr-Coulomb failure surfaces.

Typical results for this test are provided in Figure 4.2. Strength parameters, such as the peak strength, residual strength, modulus and strain at peak strength were measured. Triaxial tests could not be carried out on the PFC mixes. Since the PFC blend simply contains almost all coarse aggregates, the specimens were not stable when removed from the mold.

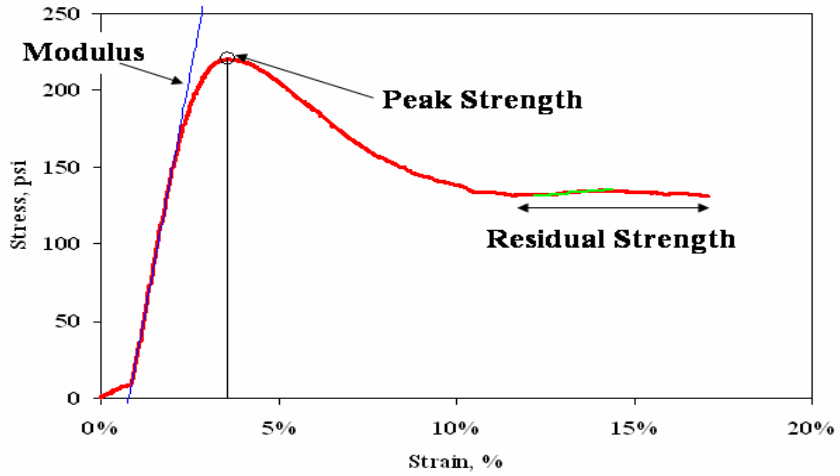

Figure 4.2 - Typical Results from the Triaxial Test

The variations in the dry unit weights for different mixes are included in Table 4.3. These specimens were prepared as per Tex-113-E using a drop hammer. As such, these unit weights are greater than those reported in Table 4.1 for direct shear tests where the specimens were prepared by rodding. The Superpave-C mixes consistently yielded higher dry unit weights as compared to the CMHB-C and Type-D mixes. This occurs because of the more balanced gradation associated with the Superpave-C mixes.

The moduli from these tests, like the direct shear tests, are not considered appropriate. In relative terms, the Superpave-C and Type-D mixes yielded higher moduli as compared to the CMHB-C mixes, indicating that the initial skeletal form of the Superpave-C mixes without binder is more stable.

The peak strengths were higher for the Superpave-C mixes as compared to the CMHB-C and Type-D mixes for all the aggregate sources except for the gravel. For the Superpave-C mixes, the hard limestone exhibited the highest peak strength and the gravel provided the lowest. For the CMHB-C mixes, the soft limestone's peak strength was greater than those of the other five aggregates. For Type-D, the lightweight aggregate yielded the highest peak strength.

Table 4.3 - Summary Results from Triaxial Compression Tests

Material	Type	Dry Unit Weight, pcf	Modulus, psi	Peak Strength, psi	Residual Strength, psi	Strain at Peak Strength, %	Cohesion, psi	Angle of Internal Friction
Hard Limestone	CMHB-C	145	6953	149	130	5.5	23	40°
		*(2%)**		*(13%)**	*(23%)**			
	Superpave-C	152	10945	241	155	4.5	7	59°
		*(2%)**		*(6%)**	*(2%)**			
	Type-D	*133*	7890	*100*	*114.2*	1.2	3	45°
		*(6%)**		*(4%)**	*(4%)**			
Granite	CMHB-C	134	11670	186	159	4.0	11	53°
		*(0%)**		*(5%)**	*(24%)**			
	Superpave-C	146	12286	208	138	3.2	22	49°
		*(3%)**		*(9%)**	*(4%)**			
	Type-D	*144*	10727	*124*	*116.5*	1.5	4	49
		*(5%)**		*(3%)**	*(4%)**			
Soft Limestone	CMHB-C	142	15955	198	178	4.9	12	54°
		*(1%)**		*(3%)**	*(1%)**			
	Superpave-C	150	19344	226	148	4.3	17	53°
		*(1%)**		*(2%)**	*(5%)**			
	Type-D	*145*	13653	*135*	*128.2*	3.2	18	41
		*(7%)**		*(6%)**	*(4%)**			
Sandstone	CMHB-C	134	10975	165	161	3.7	10	45°
		*(1%)**		*(13%)**	*(15%)**			
	Superpave-C	141	17210	203	198	3.2	19	44°
		*(1%)**		*(3%)**	*(2%)**			
	Type-D	132	15157	172	170	2.9	6	49°
		*(2%)**		*(2%)**	*(2%)**			
Gravel	CMHB-C	138	9305	174	171	6.2	10	46°
		*(2%)**		*(4%)**	*(5%)**			
	Superpave-C	141	13886	151	148	3.1	12	41°
		*(1%)**		*(4%)**	*(4%)**			
	Type-D	138	11655	157	154	4.4	8	45°
		*(1%)**		*(2%)**	*(3%)**			
Lightweight Aggregate	CMHB-C	93	13135	171	168	2.5	26	34°
		*(3%)**		*(0%)**	*(2%)**			
	Superpave-C	112	17040	203	201	2.1	15	47°
		*(1%)**		*(2%)**	*(1%)**			
	Type-D	106	10984	201	203	4.0	5	53°
		*(2%)**		*(1%)**	*(2%)**			

**** - Numbers in the parentheses are the coefficient of variation from triplicate tests.***

The cohesions and angles of internal frictions are also reported in Table 4.3 for completeness. The angles of internal friction in this table are different than those in Table 4.1 for direct shear tests simply because the densities were different as discussed above. The trends are hard to interpret because the results from only two confining pressures of 10 psi and 20 psi were available. In the future, more confining pressures should be used.

CHAPTER FIVE - STIFFNESS AND STRENGTH OF MIXES

COMPACTIVE EFFORTS

Two different compacting efforts were used for preparing the lab specimens. A set of specimens was compacted to achieve a nominal in-place air void content of 7% (20% for PFC) while another set was prepared to 250 revolutions to evaluate the potential of crushing in the aggregate due to compaction. Once compacted, the lab specimens were tested to characterize the HMA performance using the Hamburg Wheel Tracking Device, Indirect Tensile test, dynamic modulus test, and flow test.

The numbers of revolutions to achieve the in-place air voids and locking point for all mixes are shown in Table 5.1. For the Superpave-C mixes, about 25 gyrations were needed to achieve 7% air voids for the soft limestone and granite mixes, while about 50 gyrations were needed for the hard limestone mixes, about 73 for sandstone and gravel, and 80 for the lightweight aggregate. About 44 to 79 gyrations were needed to achieve 7% air voids for the CMHB-C mixes. For the PFC mixes (the coarsest mix) between 63 and 94 gyrations were needed to achieve air voids of 20%. Similarly, 62 to 92 gyrations were required for Type D mixes. For the most part, as the mixes got coarser in gradation more effort was needed to achieve the desired air voids (densities). None of the mixes required more gyrations than their corresponding locking points. After 250 gyrations, the air void contents were about 2% to 5% less than the corresponding nominal air void contents of 7% (or 20% for PFC) with a global average reduction in air voids of about 3%.

Measurements were conducted to determine the resistance of aggregates to degradation due to HMA compaction in the Superpave gyratory compactor. Specimens from each mix were placed in an ignition oven to burn off the binder and sieve analysis was performed on the aggregates. Gradations of the compacted specimens to nominal in-place air voids and to 250 gyrations are compared to the original gradations in Table 5.2. The specimens prepared to achieve the nominal in-place air voids exhibit a finer gradation as compared to the original gradation. Further compaction to 250 gyrations caused even more aggregate crushing yielding a finer gradation. The fine contents of the three gradations for each mix are quite similar. Most of the crushing occurs in the gravel-size aggregates (retained on Sieve No. 8). The crushed aggregates are converted to sand or fine size aggregates (passing Sieve No. 8 and retained on Sieve No. 200). The percent reductions in the gravel-size aggregates for different mix types are shown in Figure 5.1 for the nominal in-place air voids. Some variability in the results is attributed to

Table 5.1 – Number of Gyrations for Nominal In-place Air Voids, Locking Point

Material	Mix Type	Number of Gyrations to Nominal in place Air Voids*	Number of Gyrations to Locking Point	Average Air Void Content after 250 Gyrations, %
Hard Limestone	CMHB-C	44	124	5.2
	Superpave-C	50	99	4.0
	PFC	70	130	17.0
	Type D	61	129	5.4
Granite	CMHB-C	49	127	2.8
	Superpave-C	25	94	3.5
	PFC	85	151	17.7
	Type D	64	109	5.7
Soft Limestone	CMHB-C	48	125	2.1
	Superpave-C	24	86	4.6
	PFC	94	163	15.7
	Type D	68	145	6.5
Sandstone	CMHB-C	79	133	4.2
	Superpave-C	72	96	4.9
	PFC	80	141	17.8
	Type-D	82	109	4.0
Gravel	CMHB-C	60	117	3.4
	Superpave-C	74	90	4.2
	PFC	63	173	17.7
	Type-D	92	113	3.8
Lightweight Aggregate	CMHB-C	78	137	4.8
	Superpave-C	81	102	4.1
	PFC	87	178	18.2
	Type-D	78	117	4.7

*** 7% for CMHB-C, Superpave-C, and Type-D and 20% for PFC**

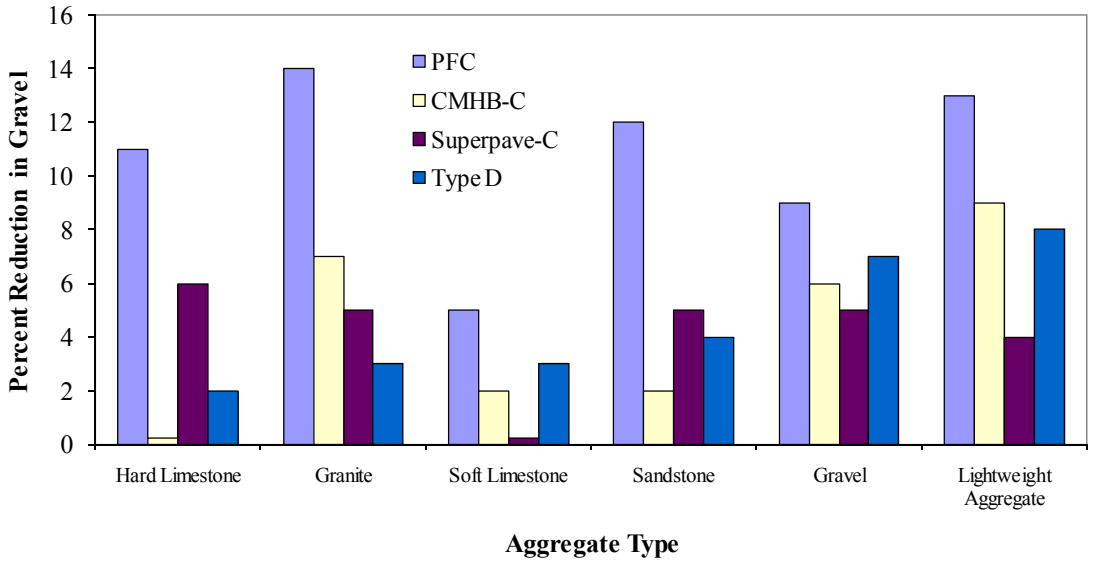

Figure 5.1 – Change in Gravel Contents of Mixes Compacted to Nominal in-place Air Voids

Table 5.2 - Aggregate Crushing Analysis for all Mixes

Sieve No.	Hard Limestone			Granite			Soft Limestone		
	Original Gradation	Nominal in-place Air Voids	250 Gyrations	Original Gradation	Nominal in-place Air Voids	250 Gyrations	Original Gradation	Nominal in-place Air Voids	250 Gyrations
	Percent Passing, %			Percent Passing, %			Percent Passing, %		
CMHB-C									
3/4"	100	100	100	100	100	98	100	100	100
1/2"	79	81	83	79	89	82	79	85	90
3/8"	61	63	61	61	74	66	61	65	66
#4	38	38	39	38	45	47	38	40	40
#8	22	25	25	22	28	30	22	25	25
#16	16	18	17	16	19	20	16	18	16
#30	16	16	15	16	16	18	16	16	14
#50	16	15	15	16	15	16	16	15	13
#200	7	7	6	7	7	7	7	7	5
Superpave-C									
3/4"	100	100	100	100	100	98	100	100	100
1/2"	96	97	96	96	98	97	96	98	96
3/8"	88	91	89	88	93	92	88	87	92
#4	66	72	68	66	71	73	66	65	71
#8	43	52	50	43	48	50	43	45	50
#16	30	37	35	30	33	34	30	30	35
#30	30	35	34	30	31	32	30	28	33
#50	30	33	32	30	30	31	30	27	31
#200	6	10	8	6	10	9	6	8	9
PFC									
3/4"	100	100	100	100	100	100	100	100	100
1/2"	90	91	93	90	89	90	90	92	96
3/8"	48	57	56	48	59	69	48	61	62
#4	11	22	21	11	25	31	11	16	21
#8	6	11	12	6	12	17	6	9	11
#16	5	8	8	5	8	10	5	7	8
#30	4	6	7	4	6	7	4	6	6
#50	3	5	5	3	4	5	3	5	5
#200	3	2	3	3	2	3	3	3	3
Type-D (Test was not performed for Type-D mix at 250 Gyration)									
3/4"	100	100	-	100	100	-	100	100	-
1/2"	99	99	-	99	98	-	99	99	-
3/8"	93	90	-	93	86	-	93	88	-
#4	60	59	-	60	55	-	60	56	-
#8	38	41	-	38	34	-	38	38	-
#16	27	31	-	27	26	-	27	29	-
#30	21	22	-	21	19	-	21	20	-
#50	14	14	-	14	13	-	14	13	-
#200	5	6	-	5	5	-	5	5	-

Table 5.2 cont. - Aggregate Crushing Analysis for all Mixes

Sieve No.	Sandstone			Gravel			Lightweight Aggregates		
	Original Gradation	Nominal in-place Air Voids	250 Gyrations	Original Gradation	Nominal in-place Air Voids	250 Gyrations	Original Gradation	Nominal in-place Air Voids	250 Gyrations
	Percent Passing, %			Percent Passing, %			Percent Passing, %		
CMHB-C									
3/4"	100	100	99	100	100	100	100	100	100
1/2"	79	83	84	79	88	81	84	93	95
3/8"	61	64	63	61	70	64	70	81	84
#4	38	40	42	38	44	45	50	59	66
#8	22	26	27	22	25	28	36	47	50
#16	16	20	18	16	18	20	26	27	28
#30	16	16	16	16	16	18	26	25	27
#50	16	15	15	16	16	17	26	25	25
#200	7	7	7	7	8	8	12	20	18
Superpave-C									
3/4"	100	100	100	100	99	100	100	100	100
1/2"	96	97	98	96	97	96	98	100	97
3/8"	88	92	91	88	90	90	93	96	83
#4	66	71	73	66	70	71	76	80	70
#8	43	50	51	43	47	49	59	64	62
#16	30	36	36	30	33	36	41	60	60
#30	30	32	34	30	33	34	41	59	58
#50	30	32	30	30	30	32	41	52	22
#200	6	9	7	6	7	9	9	20	20
PFC									
3/4"	100	100	100	100	98	100	100	100	100
1/2"	90	92	94	90	92	91	91	96	97
3/8"	48	59	67	48	56	60	53	63	65
#4	11	23	27	11	18	19	16	29	33
#8	6	10	15	6	8	12	11	20	21
#16	5	8	9	5	7	8	10	17	18
#30	4	7	6	4	5	7	9	16	17
#50	3	3	4	3	5	4	7	12	13
#200	3	3	3	3	4	4	5	9	12
Type-D									
3/4"	100	100	100	100	100	100	100	100	100
1/2"	99	100	98	99	100	100	100	100	100
3/8"	93	94	96	92	94	95	95	97	96
#4	60	64	70	60	67	69	71	79	83
#8	38	39	42	38	43	47	54	68	71
#16	27	27	26	27	29	31	38	49	52
#30	21	24	24	21	24	26	30	40	46
#50	14	15	17	13.5	15	14	19	27	31
#200	5	8	6	4.5	6	7	7	12	10

experimental error. The most significant reduction in gravel-size aggregates occurs for the PFC mixes.

HAMBURG WHEEL TRACKING DEVICE TEST

The Hamburg Wheel Tracking Device (Tex-242-F) measures the combined effects of rutting and moisture damage by rolling a steel wheel across the surface of a asphalt concrete test specimen that is immersed in hot water. The measurements are customarily reported as the depth of maximum deformation versus the number of wheel passes. The total number of passes of 20,000 was selected as per Tex-242-F because a PG 76-22 binder was used. The maximum allowable rut depth is 0.5 in.

The results are summarized in Table 5.3. The PFC mixes were not tested because they were not specified in the TxDOT Item 342 specifications, and because our past experience has shown that the specimens fail this test. At the 7% nominal air voids, the mixes with gravel and sandstone deformed the least after 20,000 cycles and the soft limestone and lightweight aggregates the most. The Superpave-C mixes either marginally or significantly faired better than the CMHB-C mixes. Type-D mixes seem to show the most resistance to rutting. The specimens compacted to 250 gyrations rutted more than those prepared at 7% air voids.

Table 5.3 - Summary Results from HWTD Tests

Material	Type	Maximum Rut Depth, in. (Condition)	
		Nominal 7% Air Voids	250 Gyrations
Hard Limestone	CMHB-C	0.49 (marginal)	0.38 (passed)
	Superpave-C	0.40 (passed)	0.73 (failed) @ 14,500 passes
	Type-D	0.35 (passed)	Not tested
Granite	CMHB-C	0.30 (passed)	0.40 (passed)
	Superpave-C	0.22 (passed)	0.63 (failed) @ 19,000 cycles
	Type-D	0.17 (passed)	Not tested
Soft Limestone	CMHB-C	0.53 (marginal)	0.70 (failed) @ 16,000 cycles
	Superpave-C	0.52 (marginal)	0.70 (failed) @ 11,000 cycles
	Type-D	0.44 (marginal)	Not tested
Sandstone	CMHB-C	0.42 (marginal)	0.61 (failed) @ 18,000 cycles
	Superpave-C	0.14 (passed)	0.43 (marginal)
	Type-D	0.14 (passed)	0.20 (passed)
Gravel	CMHB-C	0.16 (passed)	0.29 (passed)
	Superpave-C	0.12 (passed)	0.18 (passed)
	Type-D	0.07 (passed)	0.14 (passed)
Lightweight Aggregate	CMHB-C	0.49 (marginal)	0.62 (failed) @ 18,700 cycles
	Superpave-C	0.47 (marginal)	0.49 (marginal)
	Type-D	0.25 (passed)	0.57 (failed) @ 19,900 cycles

INDIRECT TENSILE TEST

Three replicate specimens of each mix at both compaction levels were tested at a temperature of 77°F as specified by Tex-226-F. The peak strengths and coefficients of variation are summarized in Table 5.4 for all six aggregates. For all aggregates except gravel and Lightweight Aggregate, the Superpave-C and Type-D mixes were the strongest. In all cases, the PFC mixes were the weakest. The gravel and sandstone consistently yield higher strengths than the other aggregates. Comparing the results from the specimens prepared at the nominal air voids and those prepared with 250 gyrations, a clear trend cannot be observed. For the soft limestone, the strengths at 250 gyrations are greater than those prepared at the in-place air void contents. The specimens with the lightweight aggregates provide reasonably high strengths.

Table 5.4 - Summary Results from IDT Tests

Material	Mix Type	Tensile Strength at Failure, psi	
		Nominal in-place Air Voids	250 Gyrations
Hard Limestone	CMHB-C	106 *(1%)*	103 *(1%)*
	Superpave-C	120 *(9%)*	112 *(6%)*
	PFC	39 (11%)	46 (2%)
	Type-D	205 (4%)	-
Granite	CMHB-C	113 *(1%)*	139 *(8%)*
	Superpave-C	116 *(7%)*	132 *(1%)*
	PFC	61 *(0%)*	50 *(1%)*
	Type-D	118 (8%)	-
Soft Limestone	CMHB-C	94 *(5%)*	142 *(2%)*
	Superpave-C	125 *(1%)*	165 *(1%)*
	PFC	50 *(7%)*	68 *(9%)*
	Type-D	148 (4%)	-
Sandstone	CMHB-C	206 *(4%)*	244 *(2%)*
	Superpave-C	226 *(1%)*	112 *(3%)*
	PFC	78 *(9%)*	62 *(3%)*
	Type-D	207 *(1%)*	166 *(6%)*
Gravel	CMHB-C	204 *(7%)*	173 *(9%)*
	Superpave-C	183 *(10%)*	159 *(5%)*
	PFC	58 *(11%)*	26 *(9%)*
	Type-D	203 *(1%)*	90 *(7%)*
Lightweight Aggregate	CMHB-C	175 (1%)	179 *(10%)*
	Superpave-C	211 (0%)	173 *(7%)*
	PFC	67 (1%)	97 *(12%)*
	Type-D	211 (2%)	212 *(3%)*

**** - Numbers in the parentheses are the coefficient of variation from triplicate tests.***

DYNAMIC MODULUS TEST

The dynamic modulus test protocol (as proposed in NCHRP 9-19) is being advocated for characterizing asphalt mixtures. . Briefly described, a sinusoidal axial compressive stress is applied to the specimen at a given temperature and loading frequency. The applied stress and the resulting recoverable axial strain response of the specimen are measured and used to calculate a dynamic modulus and a phase angle. Each specimen is tested at five temperatures: 14, 40, 70, 100 and 130°F. To perform the test at each temperature, the specimen is initially subjected to 200 conditioning cycles at 20 Hz. After the initial conditioning, the specimen is subjected to 50 loading cycles at 10 Hz and 5 Hz. In the end, the specimen is subjected to 7 loading cycles at frequencies of 10, 5, 2 and 1 Hz. The measured moduli are then converted to a variation in modulus with frequency (called a master curve) at a reference temperature of 70^{o}F using the principles of visco-elasticity (see Report 0-5268-1).

The moduli at 10 Hz and a temperature of 70^{o}F, which are representative of those measured with a Falling Weight Deflectometer, are summarized in Table 5.5. For all six aggregate sources, the PFC mixes are the softest simply because of the higher air void contents (about 20%). The Type-D and CMHB-C mixes are in most cases the stiffest mixes. In almost all cases, the specimens prepared at 250 gyrations are stiffer than those prepared at the nominal in-place air voids. This trend is especially pronounced for a number of the PFC mixes because due to higher gyrations, perhaps more intimate grain-to-grain contact is achieved.

SIMPLE PERFORMANCE TEST

The flow time test, which is one of the so-called simple performance tests, is a variation of the static creep test (Tex-231-F) commonly performed by TxDOT to assess the rutting potential of HMAC. In this test, a static load is applied to the specimen, and the resulting strains are recorded as a function of time. The flow time is defined as the time when the minimum rate of change in strain occurs during the creep test. The flow time is determined by differentiating the strain versus time curve.

Three replicate specimens of each mix at the two compaction levels were tested. The results are summarized in Table 5.6. The PFC mixes strained the most. For the other mixes, the amounts of strains are mix-dependent. Comparing the results from the specimens prepared with 250 gyrations and those prepared at the in-place air voids, no apparent trend could be identified.

ULTRASONIC TESTING OF MIXES

The same ultrasonic device (v-meter) used to test the rock masses was also used to measure the seismic moduli of the mixes. The seismic modulus test was performed on the samples prepared for the dynamic modulus tests at room temperature. The test results for the nominal in-place air voids and 250 gyration samples are summarized in Table 5.7. The trends are similar to those reported for the dynamic modulus in Table 5.5. The moduli for the mixes prepared with a compactive effort of 250 gyrations increased by approximately 35% with respect to the samples tested at the nominal in-place air void contents.

Table 5.5 - Summary Results from Dynamic Modulus Tests

Material	Type	Dynamic Modulus at 10 Hz, ksi	
		Nominal in-place Air Voids	250 Gyrations
Hard Limestone	CMHB-C	909	1164
	Superpave-C	827	690
	PFC	239	661
	Type-D	1010	-*
Granite	CMHB-C	847	1041
	Superpave-C	694	665
	PFC	193	319
	Type-D	883	-*
Soft Limestone	CMHB-C	765	1513
	Superpave-C	664	1024
	PFC	198	690
	Type-D	794	-*
Sandstone	CMHB-C	1103	1427
	Superpave-C	937	1012
	PFC	526	518
	Type-D	1056	1373
Gravel	CMHB-C	1180	1460
	Superpave-C	778	1288
	PFC	448	555
	Type-D	926	1394
Lightweight Aggregate	CMHB-C	666	1167
	Superpave-C	618	724
	PFC	291	687
	Type-D	636	828

***Tests were not performed for Type-D mixes at 250 gyrations.**

Table 5.6 - Summary Results from Flow Time Tests

Material	Type	Maximum Strain after 10,000 sec, μ-in./in.	
		Nominal 7% Air Voids	250 Gyrations
Hard Limestone	CMHB-C	3820 *(6%)*	4280 *(16%)*
	Superpave-C	3175 *(0%)*	3980 *(11%)*
	PFC	7860 *(5%)*	7020 *(10%)*
	Type-D	2950 (4%)	-
Granite	CMHB-C	5280 *(3%)*	3380 *(14%)*
	Superpave-C	4860 *(7%)*	5100 *(15%)*
	PFC	7150 *(22%)*	12980 *(24%)*
	Type-D	3683 (9%)	-
Soft Limestone	CMHB-C	6910 *(1%)*	3980 *(11%)*
	Superpave-C	6750 *(7%)*	5790 *(3%)*
	PFC	7320 *(10%)*	7780 *(11%)*
	Type-D	5990 (5%)	-
Sandstone	CMHB-C	4863 *(3%)*	3695 *(2%)*
	Superpave-C	4570 *(4%)*	3235 *(3%)*
	PFC	6826 *(3%)*	6076 *(2%)*
	Type-D	3498 *(6%)*	3434 *(1%)*
Gravel	CMHB-C	3798 *(3%)*	3034 *(3%)*
	Superpave-C	5235 *(6%)*	2442 *(9%)*
	PFC	8881 *(2%)*	7762 *(6%)*
	Type-D	4954 *(1%)*	2848 *(0%)*
Lightweight Aggregate	CMHB-C	5941 *(4%)*	3730 *(0%)*
	Superpave-C	4809 *(3%)*	4878 *(1%)*
	PFC	7850 *(13%)*	8501 *(6%)*
	Type-D	3187 *(6%)*	3109 *(2%)*

*** - Numbers in the parentheses are the coefficient of variation from triplicate tests**
**** Tests were not performed for Type-D mixes at 250 gyrations.**

Table 5.7 - Summary Results from V-Meter Tests

Material	Type	Seismic Modulus, ksi	
		Nominal in-place Air Voids	250 Gyrations
Hard Limestone	CMHB-C	2826 (*2%*)	3803 (*10%*)
	Superpave-C	2800 (*1%*)	3062 (*1%*)
	PFC	1074 (*0%*)	1716 (*14%*)
	Type-D	2820 *(2%)*	-
Granite	CMHB-C	2740 (*6%*)	3385 (*8%*)
	Superpave-C	2276 (*5%*)	3029 (*1%*)
	PFC	856 (*0%*)	1302 (*21%*)
	Type-D	2571 *(5%)*	-
Soft Limestone	CMHB-C	2662 (*1%*)	3445 (*18%*)
	Superpave-C	2101 (*7%*)	3102 (*3%*)
	PFC	922 (*0%*)	1556 (*8%*)
	Type-D	2452 *(3%)*	-
Sandstone	CMHB-C	2930 *(4%)*	2931 (3%)
	Superpave-C	2098 *(3%)*	2562 (7%)
	PFC	1163 *(1%)*	1745 (5%)
	Type-D	2611 *(2%)*	3271 (0%)
Gravel	CMHB-C	3071 *(5%)*	3304 (0%)
	Superpave-C	2103 *(10%)*	3756 (2%)
	PFC	1268 *(2%)*	1869 (8%)
	Type-D	2770 *(7%)*	3065 (6%)
Lightweight Aggregate	CMHB-C	1955 *(2%)*	2820 (2%)
	Superpave-C	1656 *(5%)*	2362 (6%)
	PFC	1390 *(2%)*	1466 (3%)
	Type-D	1798 *(8%)*	2139 (0%)

*** - Numbers in the parentheses are the coefficient of variation from triplicate tests**
**** Tests were not performed for Type-D mixes at 250 gyrations.**

CHAPTER SIX - MICROMECHANICAL MODELING

INTRODUCTION

In this study, a commercially available DEM code called *Particle Flow Code in 2-Dimensions* (PFC2D Version 3.1) was used to model aggregate and asphalt mix properties under different loading conditions. This code includes a user-friendly graphical interface, linear and non-linear contact models, linear and curvilinear boundary conditions, and different types of bond strength.

A detailed description of DEM principles, contact behavior, model geometry, and boundary and loading conditions is given in the Research Report 5268-1. The main reason for using the DEM models is to help us better understand the changes occurring in the interior of the specimens, since all tests described before only provide information about the external changes of the mixes. This chapter includes a summary of the DEM, the calibration results for the aggregate tests, and modeling results of asphalt mixes.

DISCRETE ELEMENT METHOD

DEM is a finite difference scheme used to study the interaction among assemblies of discrete particles. The DEM concept is simple in principle; it is based on successively solving law of motion (Newton's second law) and the force-displacement law for each particle. An explicit time-stepping scheme is employed to integrate Newton's second law for each particle, given a set of contact forces acting on the particle, which results in the updated particles' positions and velocities. Based on the new positions, the relative displacements of each particle are calculated, and used to calculate the contact forces. The DEM is based upon the idea that the time step chosen is sufficiently small so that during a single time step, disturbances cannot propagate from any particle further than its adjacent neighbors. Consequently, forces acting on any particle are determined exclusively by its interaction with particles that it is in contact with.

In PFC2D, particles are circular (balls). They are allowed to overlap at the contact points over a very small area. The amount of overlap is related to the contact force via the force-displacement law. All overlaps are assumed to be small in relation to particle sizes.

Bonds can be added to the contacts between particles to either increase the stiffness of the contact and/or to include a strength parameter above which the bond breaks; PFC2D allows

different types of bonds to be assigned. The contact behavior in PFC2D is described using any of the three models: Contact Stiffness Models, Slip Models, and Bonding Models. These models are activated for all contacts. A contact between two particles exists whenever the distance between the centers of two adjacent particles is equal to or less than the summation of their radii (i.e., the two particles are just touching or overlapping).

DEM OF AGGREGATE TESTS

The PFC2D software was used to model the modulus test, compressive strength test and indirect tensile strength of rock samples representing four aggregates. It was not feasible to conduct these tests on the gravel and the lightweight aggregates that were used in Phase II of this study because these two sources are not available as cores. A comparison between the experimental and modeling results are shown in Figures 6.1 through 6.3, while the model parameters used for each of the aggregates are shown in Table 6.1. The aggregate contact stiffness and strength in the model were determined such that the model results matched the experimental measurements. The parameters determined from this calibration step are then used to represent the aggregates in HMA mix models. The details of the calibration process is given in the Research Report 5268-1, however, the calibration parameters and results are presented herein.

Aggregate samples of a diameter of about 2 in. and a height of about 2 in. were tested under compression and indirect tension loading for four of the aggregates.

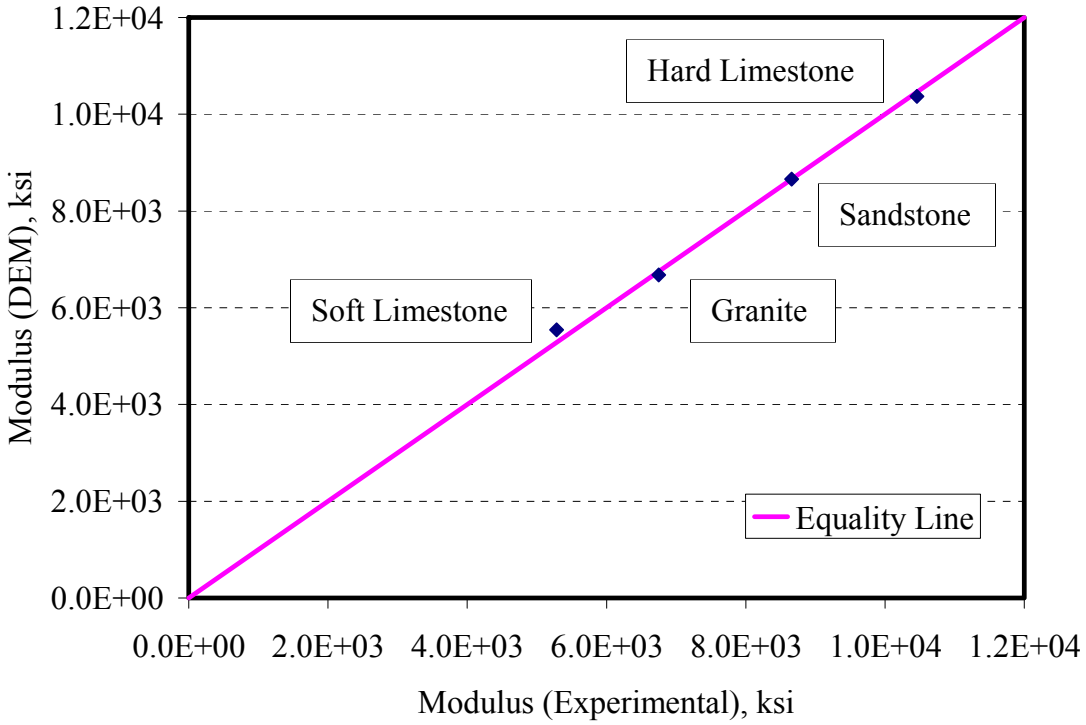

Figure 6.1 - Comparison of Modeling and Experimental Results of Aggregate Modulus

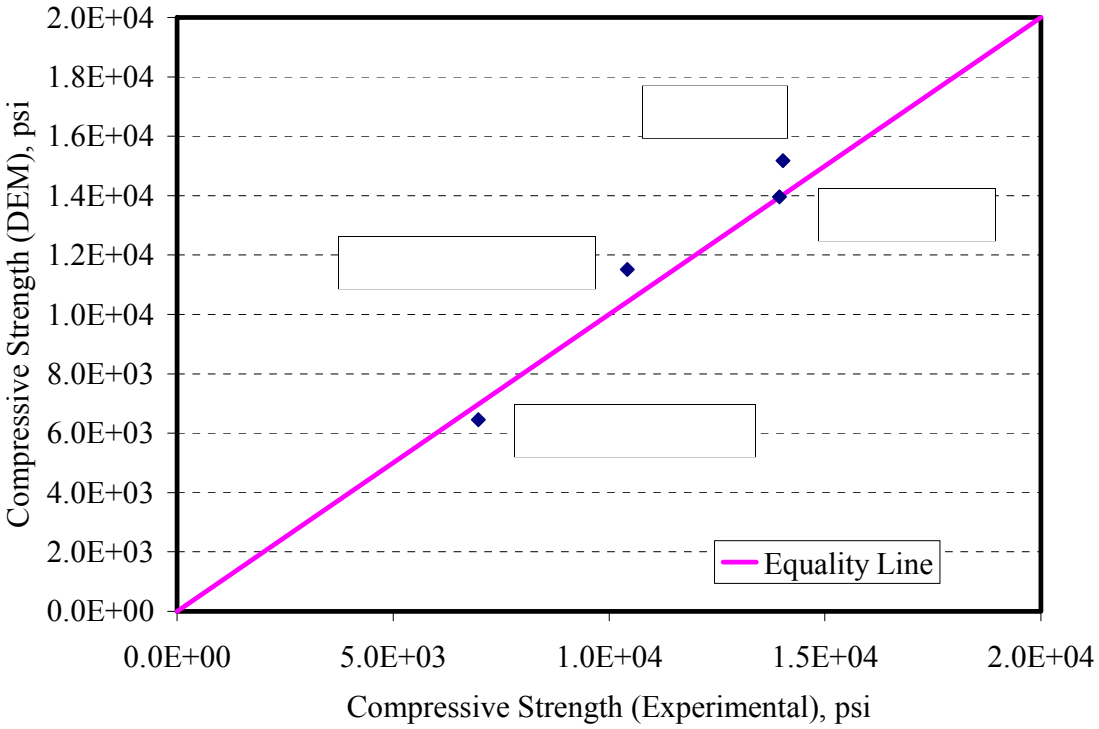

Figure 6.2 - Comparison of Modeling and Experimental Results of Aggregate Compressive Strength

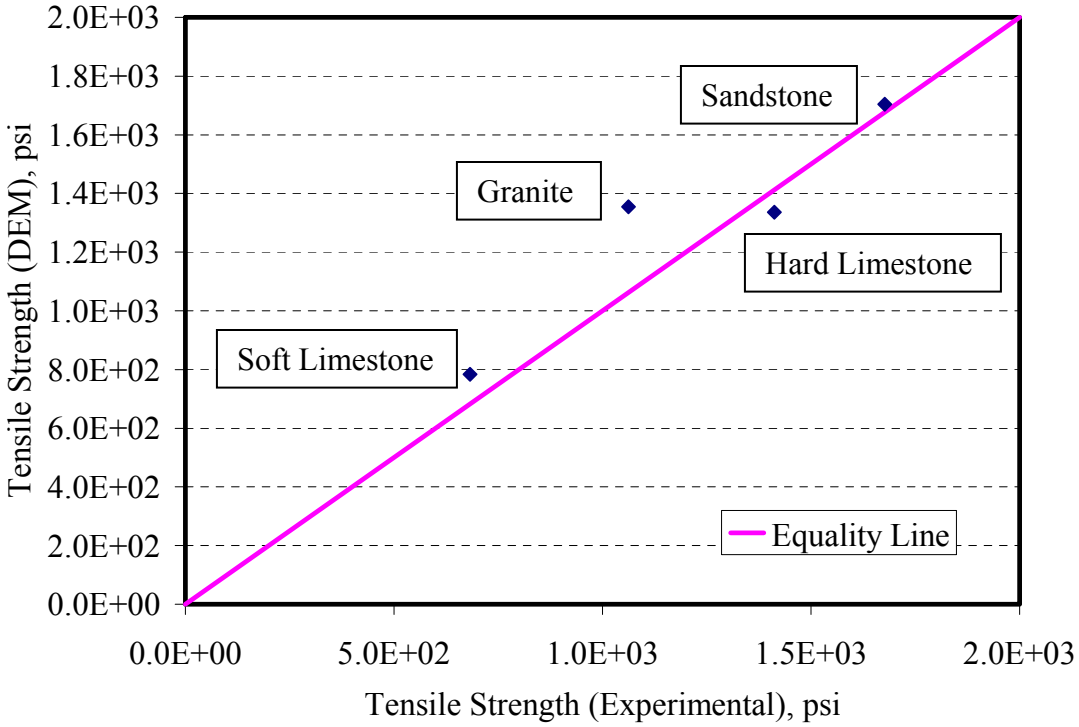

Figure 6.3 - Comparison of Modeling and Experimental Results of Aggregate Tensile Strength

Table 6.1 - Parameters for Bond and Stiffness used to Represent Aggregates Used in DEM

Parameter	Granite	Hard Limestone	Soft Limestone	Sandstone
Bond Strength, lb	45.86	33.72	19.78	42.08
Stiffness, ksi	75.42	145.04	65.27	100.08
Friction Coefficient	0.1	0.1	0.1	0.1

INDIRECT TENSION OF HMA MIXES

Figures 6.4 show the PFC2D model geometries for Superpave-C, CMHB-C, PFC, and Type-D mixtures, respectively. The aggregate stiffness and strength determined in the calibration step were used to represent the properties of the aggregate phase in the HMA mixes. The mastic properties were determined such that the model results match the indirect tensile strengths of the mixes.

The DEM results are compared with the experimental results in Figure 6.5 based on mix type and in Figure 6.6 based on the aggregate type. The mastic properties used in this model are presented in Table 6.2 for the four different mixes. The indirect tensile model for the HMA mixes compared very well with the experimental data.

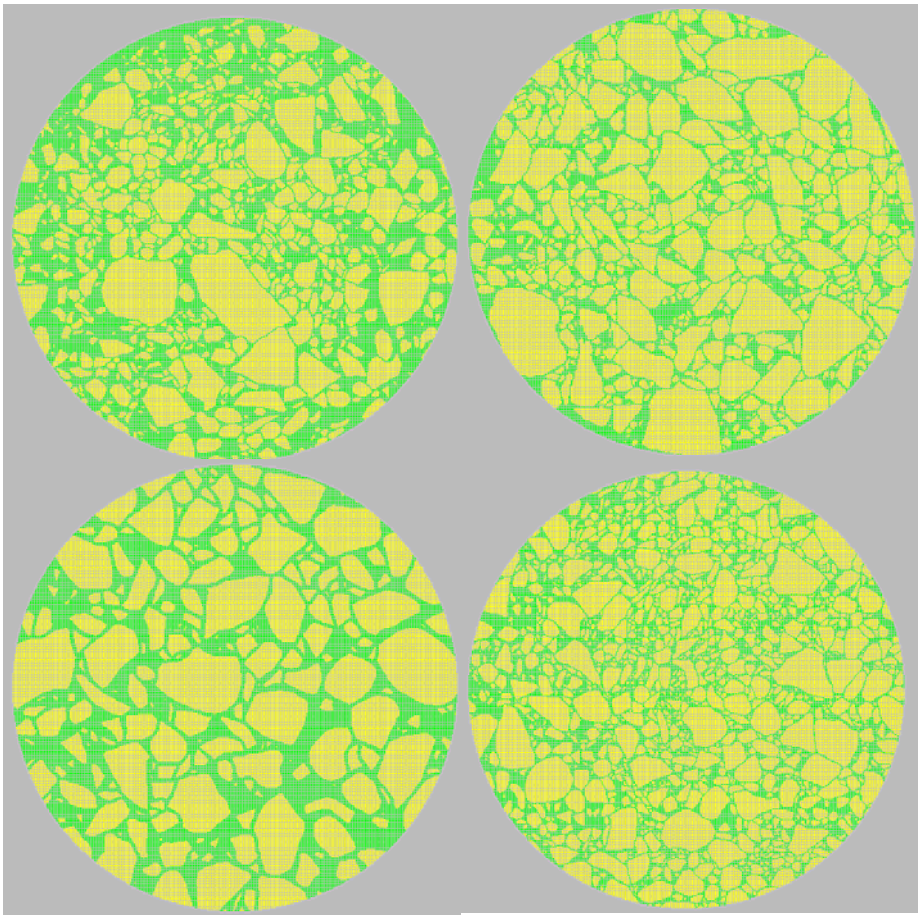

Figure 6.4 - Indirect Tensile Strength Model Superpave-C (Top Left), CMHB-C (Top Right), PFC (Bottom Left), and Type-D (Bottom Right)

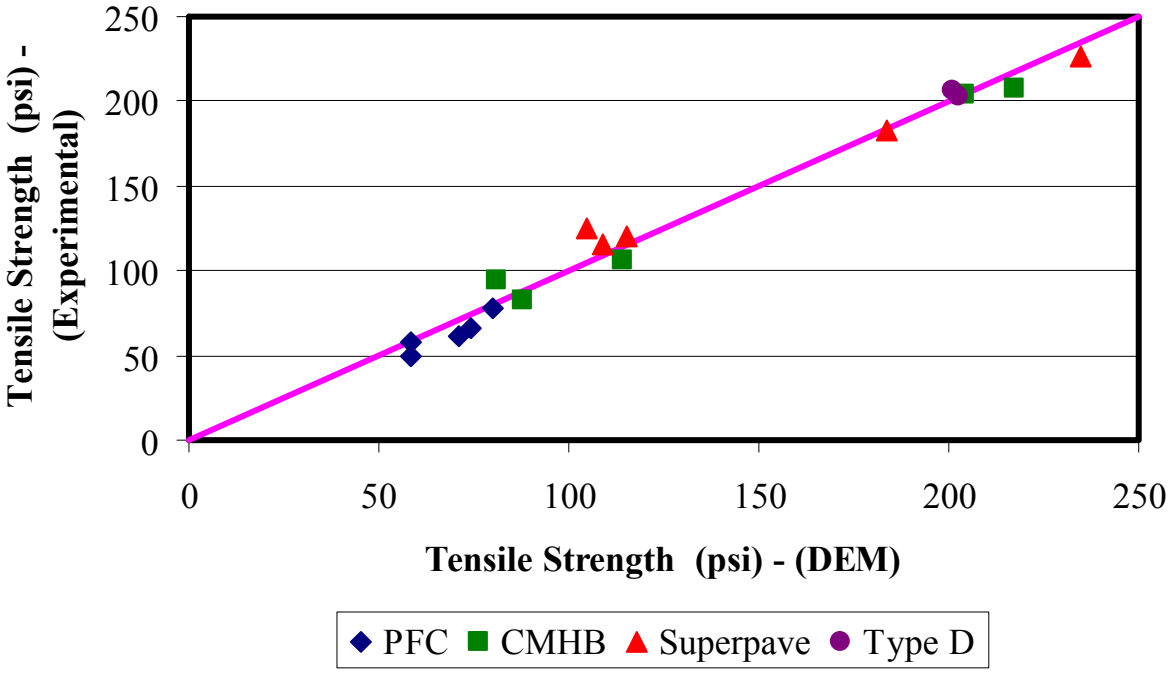

Figure 6.5 - Indirect Tensile Strength Results Grouped According to Mix Type

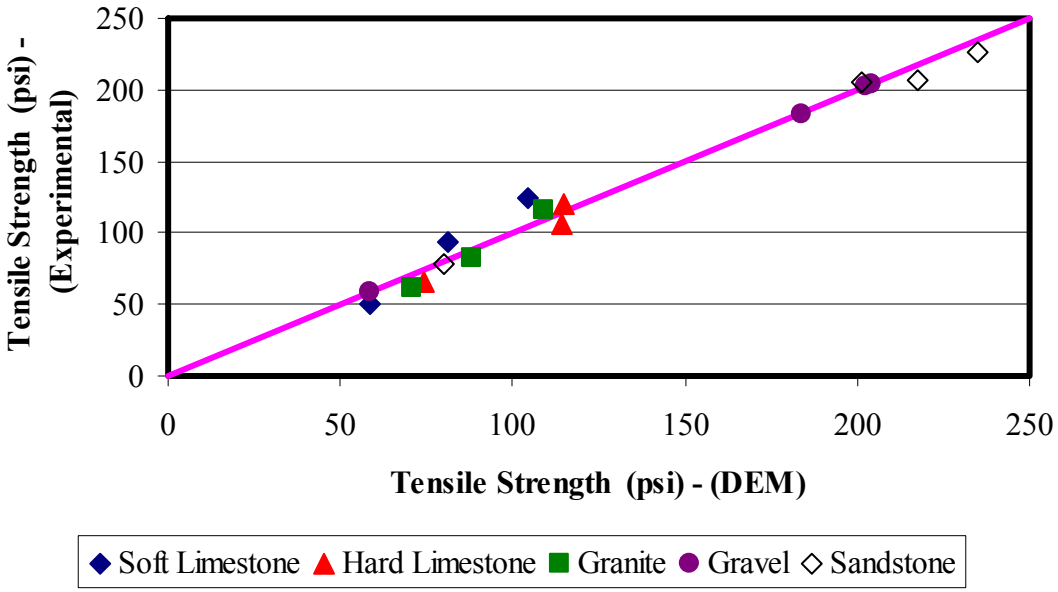

Figure 6.6 - Indirect Tensile Strength Results Grouped According to Aggregate Type

Table 6.2 - Mastic Model Parameters Used in DEM

Parameter	Bond Strength, lb				
	Granite	Hard Limestone	Soft Limestone	Gravel	Sandstone
CMHB-C	7.87	9.22	7.87	14.61	20.23
PFC	2.92	2.92	2.70	2.25	3.82
Superpave-C	8.99	10.57	14.61	20.23	20.23
Type-D	-*	-*	-*	15.74	17.98

** - tests were not performed for Type-D mixes.*

INTERNAL FORCES DISTRIBUTION

The distributions of the internal forces in the mix models were evaluated at an applied force value of 450 lb. As shown in Table 6.3, The PFC mixes had, in general, the highest maximum internal forces among all mixtures. This indicates that aggregates in the PFC mixes experience higher forces than the other mixes. This can be easily seen in Figure 6.7, which compares the maximum internal forces for the different aggregates.

Table 6.3 - Maximum Internal Force at Different Loading Stages (lb)

Aggregate	Mix	Maximum Internal Force
Hard Limestone	CMHB	51.8
	Superpave	67.4
	PFC	113.1
	Type-D	-
Granite	CMHB	45.3
	Superpave	57.5
	PFC	66.8
	Type-D	-
Soft Limestone	CMHB	44.0
	Superpave	58.5
	PFC	64.6
	Type-D	-
Sandstone	CMHB	42.5
	Superpave	54.3
	PFC	59.7
	Type-D	46.4
Gravel	CMHB	41.4
	Superpave	49.3
	PFC	51.3
	Type-D	43.3

Note: the stress distribution in Type-D with fine aggregate would not depend on aggregate type. The stresses are low in Type D so there is no concern of aggregate fracture. This was confirmed by the analysis of aggregate of Phase 2. Also, the test was not conducted for lightweight aggregate.

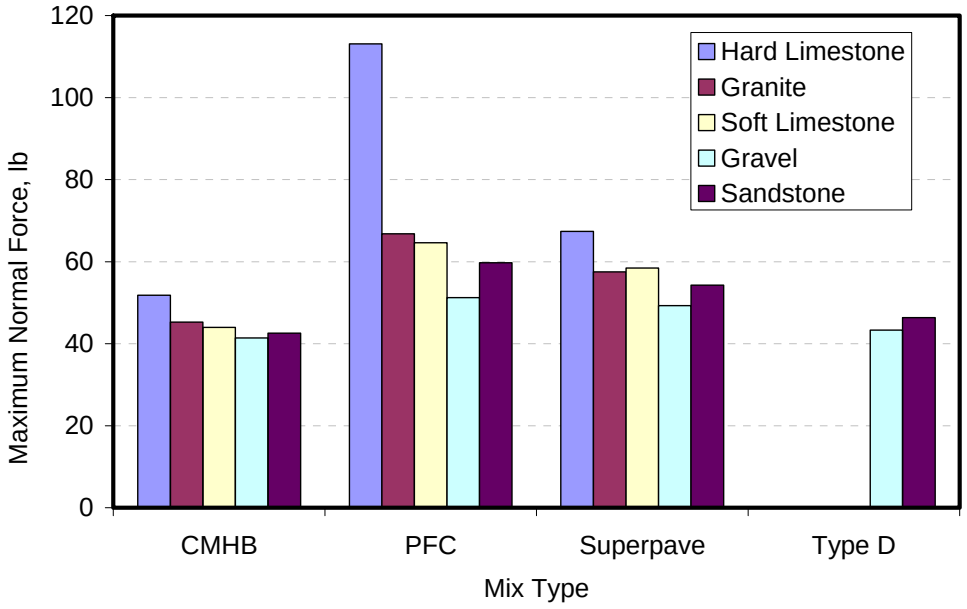

Figure 6.7 – Illustrating Results for the Different Mixes and Aggregates

Figure 6.8 shows examples of the relationships between the maximum internal forces and the three analysis cases representing low, medium and high applied external forces for the soft limestone and gravel mixes. The maximum internal forces increase with an increase in the applied load for different mixes of both aggregates. However, the rate of increase is higher for the gravel mixtures (Figure 6.8b) as compared with the soft limestone mixtures (Figure 6.8a). The rate of increase in the internal forces with an increase in the applied loads is influenced by the aggregate resistance to breakage within the mix. In a controlled displacement test or simulation, breakage of particles reduces the ability of the mixture to sustain applied loads and causes a reduction in the internal forces among aggregate particles. From the aggregate tests and models, the gravel is a much stronger aggregate than the soft limestone, which is reflected in better ability to sustain applied loads and higher rate of increase in build up of internal forces. For the given aggregate types, the PFC mix has the smallest rate of increase in the internal forces among the mixes, which is an indication that the aggregate breakage in the PFC mix is more pronounced than in the other mixes.

In addition to the maximum internal forces, the complete distributions of the internal forces were evaluated. These forces are shown graphically in Figure 6.9 in which the black color represents compression forces, while the red color represents tension forces. Higher forces are represented by thicker lines in these plots. These plots provide a good visual indication of the distribution of internal forces within different mixes. There is less uniform distribution of forces within the PFC mixes as compared to the other mixes for all aggregates. This is evident in the thicker black lines (higher forces).

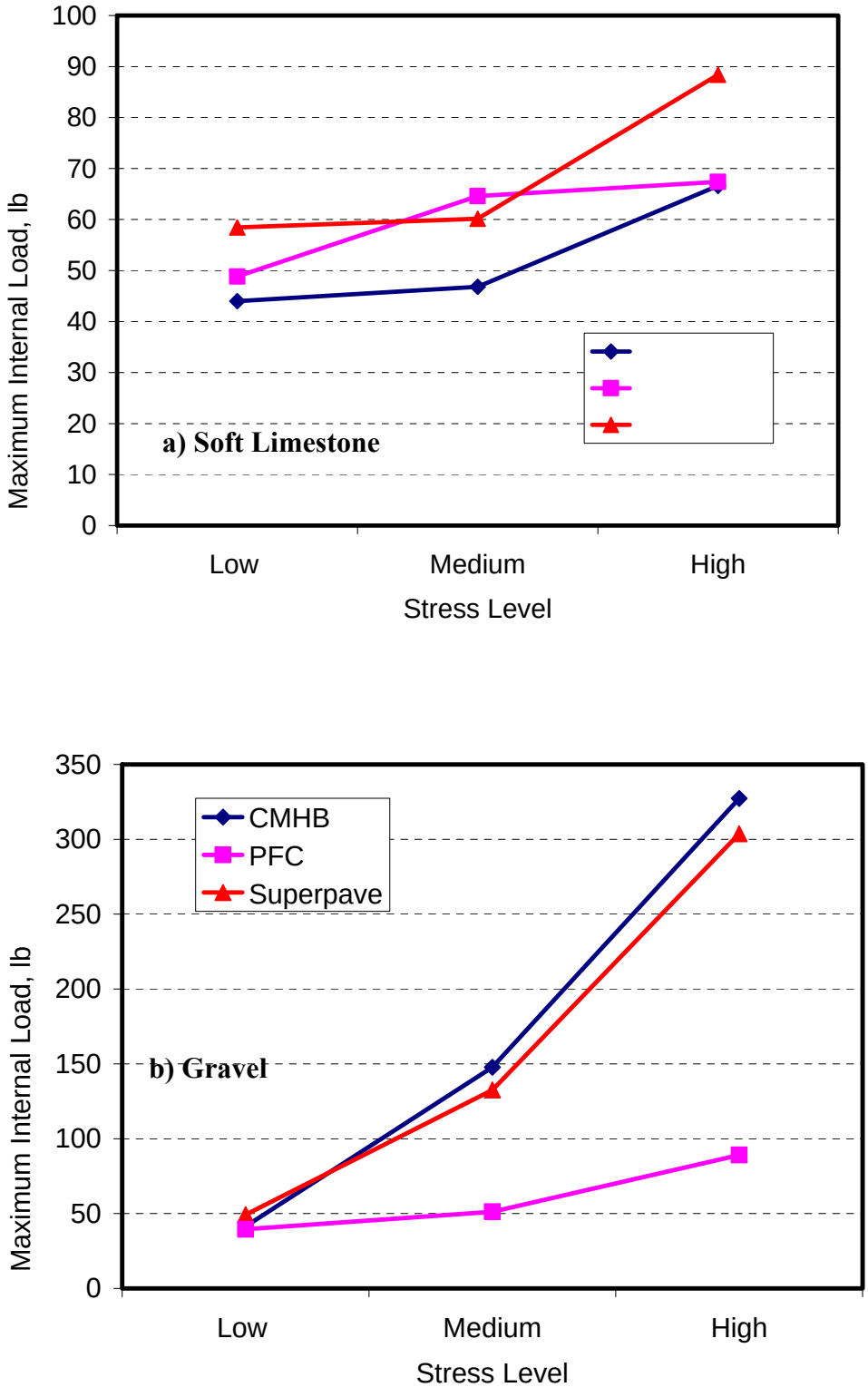

Figure 6.8 – Internal Force Changes with Increasing Applied Load

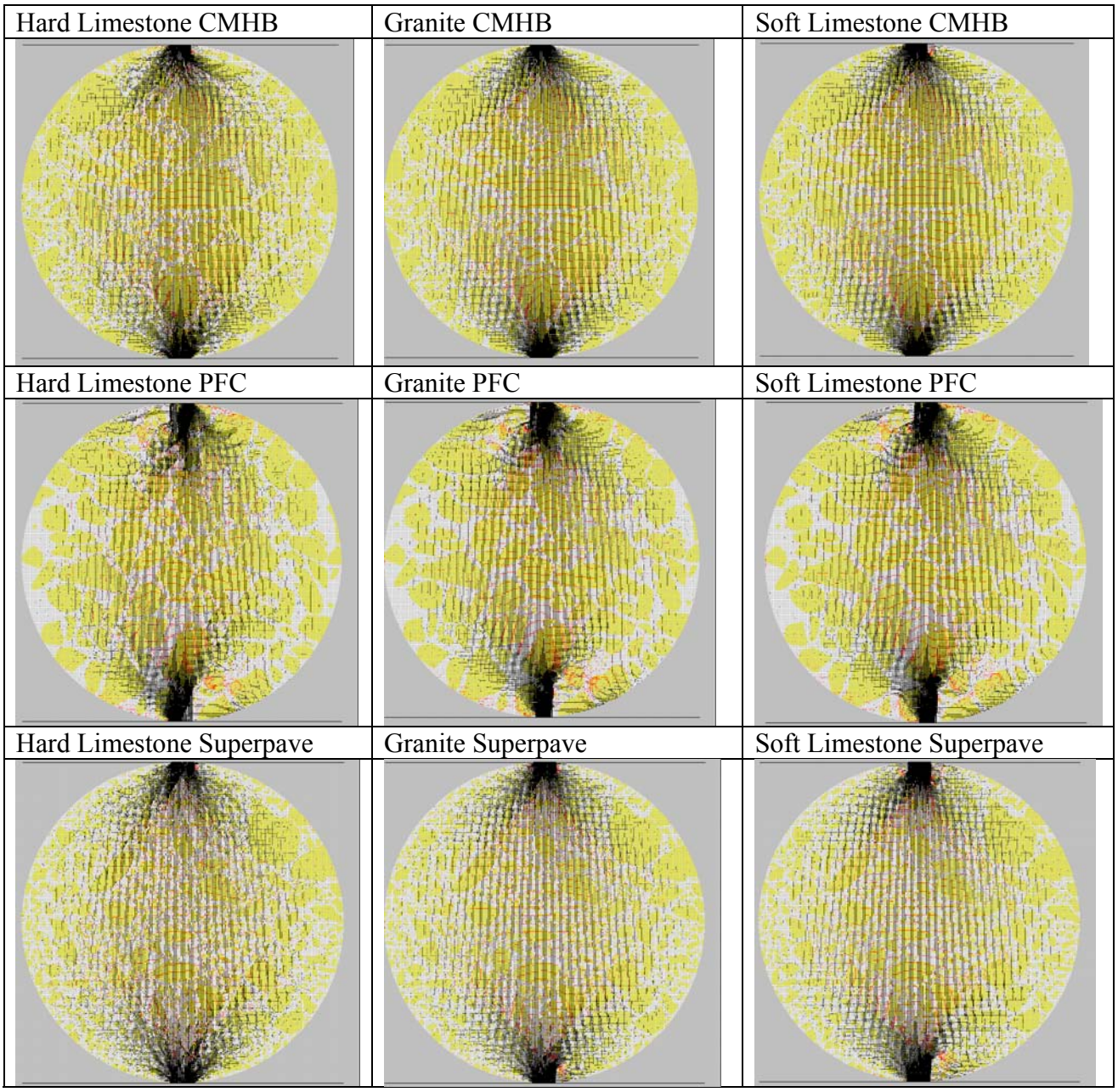

Figure 6.9 - Internal Forces Distribution within Different Mixes at 450 lb Stress State

Gravel Type D	Sandstone Type D
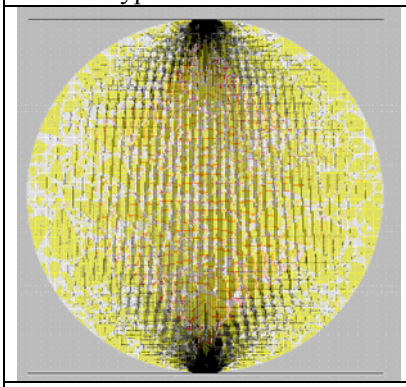	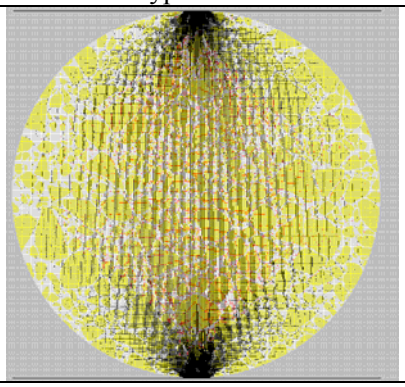
Gravel Type CMHB	Sandstone CMHB
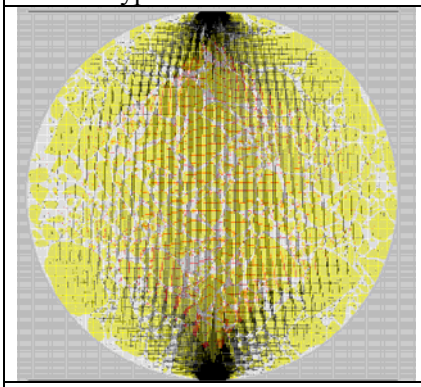	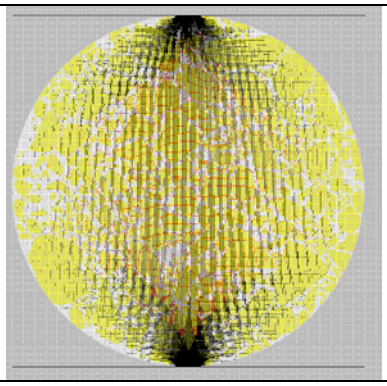
Gravel Type PFC	Sandstone PFC
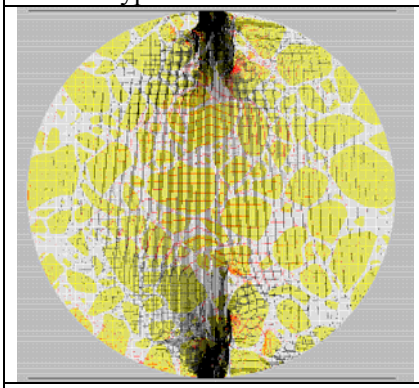	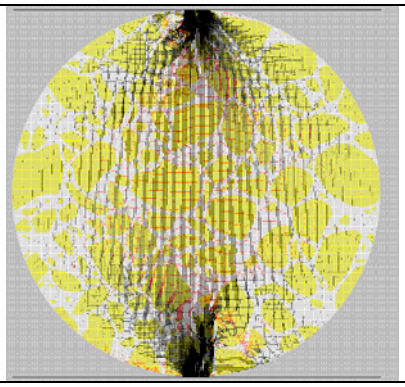
Gravel Superpave	Sandstone Superpave
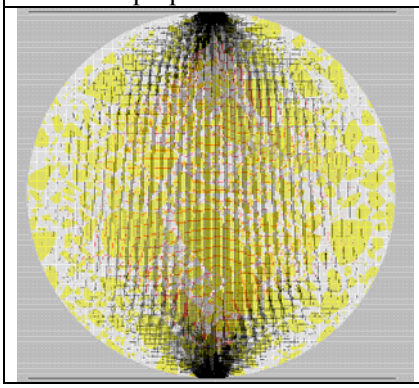	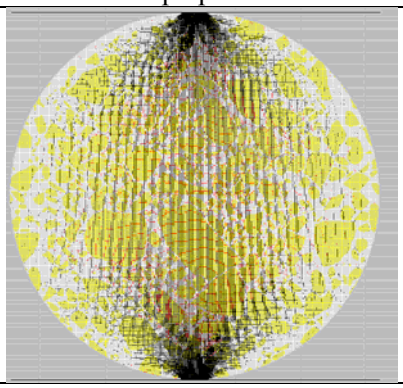

Figure 6.9 cont.- Internal Forces Distribution within Different Mixes at 450 lb Stress State

The cumulative distributions of the compressive forces within different mix types for the hard limestone are shown in Figure 6.10. In generating the figure, forces that were less than 20% of the bond strength were eliminated because they are considered to be too small to affect aggregate breakage. In addition, forces represented in Figure 6.10 are only those within the aggregate phase of the mixture. Forces in the binder or mastic are not included because the focus is on aggregate breakage attributed to forces in these aggregates. Plots similar to Figure 6.10 for other aggregates are given in Appendix C. All plots followed the same trend as in Figure 6.10 with the PFC mix having more forces than the other mixes for all the aggregates. This was also the case for the different types of forces (compression, shear and tension). The average and third quartile of internal forces are summarized in Tables 6.4 and 6.5. The average and third quartile values are higher for the PFC mixes, while there are smaller differences in forces among the remaining mixtures. The ratio of the maximum internal force in the PFC to the maximum internal force in the other mixes ranges from 1.1 to 2.0 with an average of 1.36 (Table 6.4). The average internal forces and the 3rd quartile of the internal forces ratios between PFC and the remaining mixtures is about 1.2 based on the data in Tables 6.4 and 6.5. This comparison would be helpful in specifying minimum requirements for aggregates to be used in PFC mixes.

All the above analysis focused on comparing the different mixes within each aggregate type. The following analysis will evaluate the response of different aggregates within each mix type. Figure 6.11 presents the compressive force distributions within the different aggregate types for the CMHB-C mix. Similar plots are generated for the other mixes in Appendix C. All plots followed the same trend as in Figure 6.11 with the soft limestone experiencing the highest internal forces as compared with the other aggregates. On the other hand, the gravel had the least internal forces for all the different cases. Hard limestone had higher internal forces than the granite and the sandstone, but still below the soft limestone. Finally the sandstone and granite had similar internal forces. Based on these results, aggregates can be ranked for the different mixes as in Table 6.6.

The normalized compression is calculated as the ratio of the contact force to the compressive strength of aggregate. It was decided to use the normalized value instead of absolute value of force in order to account for strength in comparing aggregate performance. For example, an aggregate might experience high contact forces but it has high strength to withstand these forces, consequently, these high contact forces will no be of concern for aggregate fracture. The use of normalized force allows comparing aggregates based on how far they are from reaching their compressive strength and fracture condition.

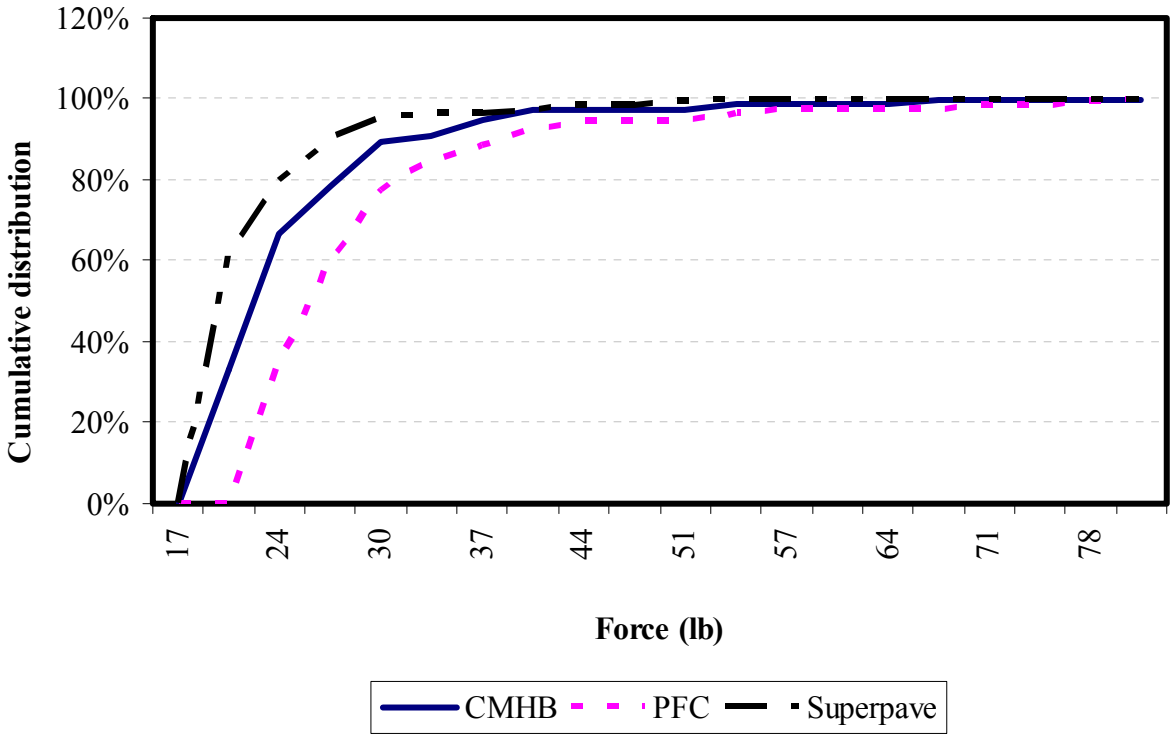

Figure 6.10 - Distribution of Internal Compressive Forces within Different Hard Limestone Mixes

Table 6.4 - Average Values of Internal Forces (lb)

Aggregate	Mix	Compression	Shear	Tension
Hard Limestone	CMHB-C	21.1	6.7	1.3
	Superpave	24.3	6.3	1.9
	PFC	29.0	7.5	3.1
	Type-D	-	-	-
Granite	CMHB	18.6	5.9	0.9
	Superpave	20.6	6.1	2.8
	PFC	25.2	6.7	4.2
	Type-D	-		-
Soft Limestone	CMHB	18.7	6.6	1.5
	Superpave	21.0	6.4	2.9
	PFC	25.1	6.6	4.0
	Type-D	-	-	-
Sandstone	CMHB	18.5	5.8	1.0
	Superpave	20.1	5.8	1.1
	PFC	22.4	6.7	3.4
	Type-D	19.4	6.0	1.0
Gravel	CMHB	18.1	5.8	0.9
	Superpave	18.7	5.4	0.9
	PFC	20.7	6.7	4.3
	Type-D	18.8	5.9	0.9

- : tests were not performed for Type-D mixes.

Table 6.5 - Third Quartile of Internal Forces (lb)

Aggregate	Mix	Compression	Shear	Tension
Hard Limestone	CMHB-C	22.4	7.0	1.3
	Superpave	25.6	6.7	1.4
	PFC	29.6	8.3	3.9
	Type-D	-	-	-
Granite	CMHB	20.7	6.3	0.9
	Superpave	21.9	6.5	2.8
	PFC	26.9	7.4	4.5
	Type-D	-	-	-
Soft Limestone	CMHB	19.6	7.1	1.0
	Superpave	20.1	6.4	2.8
	PFC	26.8	7.5	4.4
	Type-D	-	-	-
Sandstone	CMHB	19.6	6.0	1.1
	Superpave	22.2	5.3	1.1
	PFC	23.8	7.4	3.8
	Type-D	21.2	6.7	1.1
Gravel	CMHB	19.2	5.9	0.9
	Superpave	20.3	5.0	0.9
	PFC	21.9	7.5	4.8
	Type-D	20.3	6.5	0.9

- : tests were not performed for Type-D mixes.

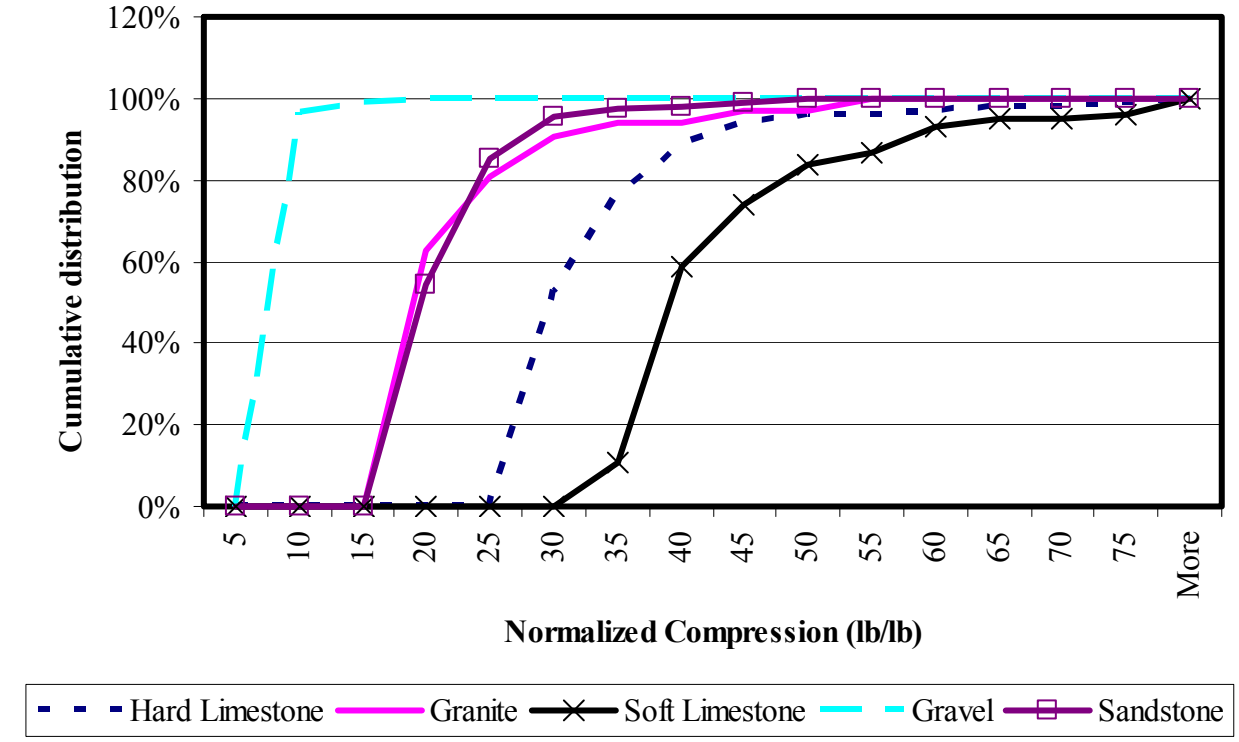

Figure 6.11 - Internal Compression Forces Distribution within Different Aggregates (CMHB-C)

Table 6.6 - Aggregate Ranking for the Different Mixes

Aggregate	Mix Design			
	CMHB-C	Superpave	PFC	Type-D
Hard Limestone	4	4	4	---
Soft Limestone	5	5	5	---
Granite	2	2	2	---
Gravel	1	1	1	1
Sandstone	2	2	2	2

- : tests were not performed for Type-D mixes.

PROBABILISTIC AGGREGATE BOND STRENGTH

All the analysis presented thus far assumed one average value for the bond strength within aggregates. However, aggregate particles from the same source exhibit variability in their properties. In order to account for such variability in the model, the aggregate bond strength is assumed to follow a normal probabilistic distribution. The averages and standard deviations for the distributions were taken to be equal to those obtained from the aggregate experimental measurements.

The probabilistic analysis was repeated seven times (due to time constraints) for each mix and aggregate types. However, the locations or positions for the various bond strength values were determined using a random number generator. In essence, all runs representing the same aggregate type have the same average and standard deviation but the positional distribution of the bonds is different among the different runs. Consequently, this analysis generated distribution of mixture strength.

A comparison of the average and deviation from the average (error bars) between the experimental and model is included in Figure 6.12. The experimental and the numerical values compare reasonably well. The differences in variation between the model and experimental results could be attributed to the use of normal distribution and assuming that the variation in compressive strength tests applies to aggregates within the mix. It is possible that the distribution of strength differs from normal distribution and the variability in aggregates might be not well represented by the compression test. There was no need to do the analysis for the lightweight aggregate, since this was just to demonstrate the procedure of evaluating experimental and model results with consideration to aggregate variability.

SUMMARY OF FINDINGS

- The discrete element model was powerful in modeling the aggregate and mixture tests, as it provided information on the influence of mix design and aggregate properties on resistance to fracture.
- The discrete element model allowed evaluating the internal forces in the HMA mixtures, which cannot be accomplished by the conventional experimental methods.

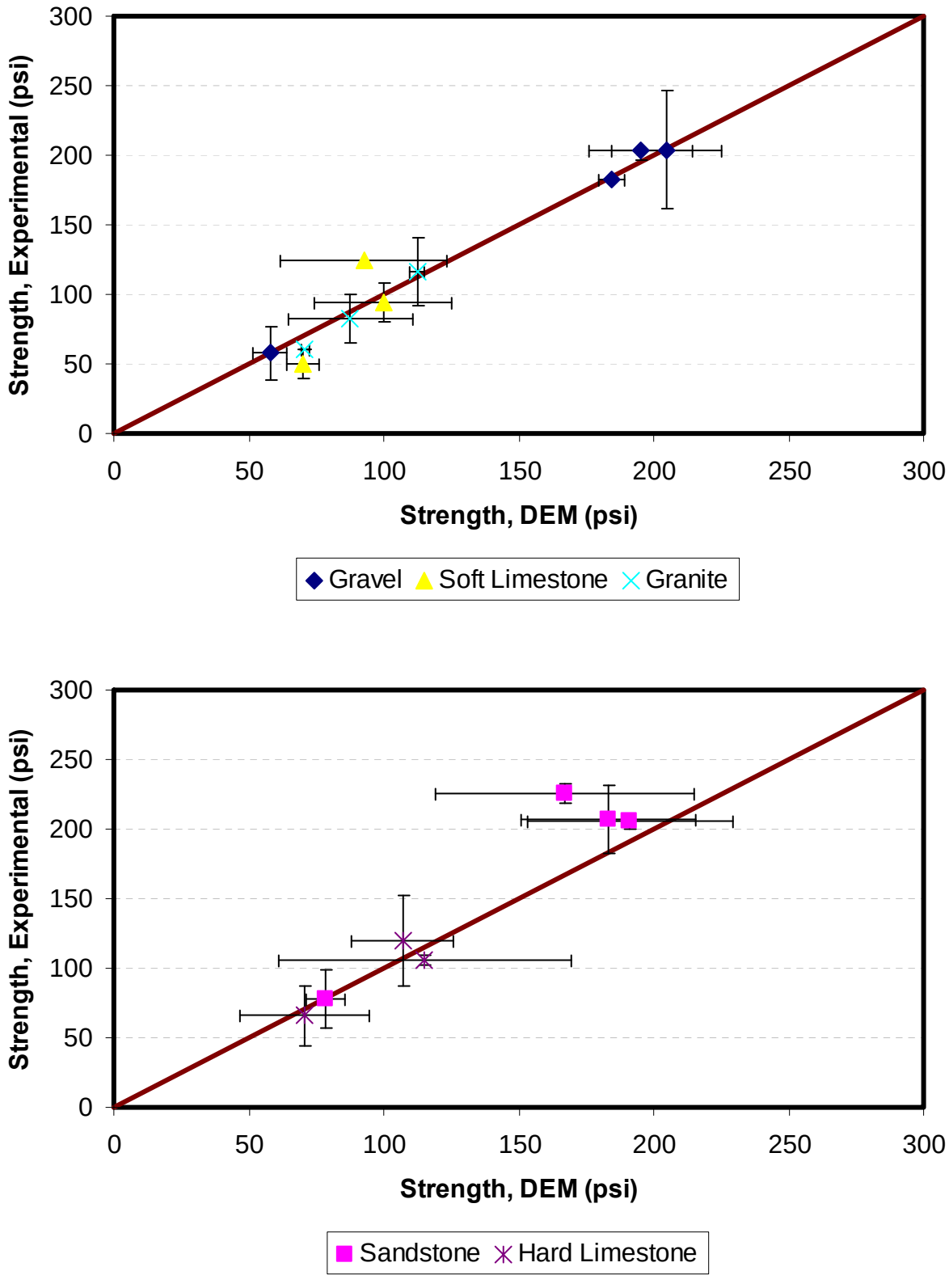

Figure 6.12 - Probabilistic Aggregate Bond Strengths

- The analysis of internal forces revealed that the PFC mixtures experienced higher stresses than all other mixes. Based on the results, it is recommended that aggregate strength in PFC should be about 25% more than the aggregate strength used in the other mixtures.
- With the exception of the PFC, internal forces were comparable for all other mixtures for a given aggregate type.
- The soft limestone experienced the highest internal forces as compared to the other aggregates. Aggregates were ranked based on the internal force values. This ranking can be used to select the appropriate aggregate type given a mixture design.
- The rate of increase in the internal force with an increase in applied loads is an indication of aggregate resistance to breakage. A high increase rate indicates less breakage. PFC mixes experienced the least rate of increase indicating more aggregate breakage when compared with the other mixes.
- The model was successful to a large extent in representing the variability in aggregate properties and the influence of this variability on mixture response.

CHAPTER SEVEN - ANALYSIS OF RESULTS

INTRODUCTION

The experimental and modeling results were presented in the previous chapters for the aggregates and mixes. Chapters 3 and 4 included the test procedures and results of laboratory tests regarding the aggregates and rock properties. Chapters 5 covered the performance of the mixes estimated from a number of laboratory tests. In Chapter 6, the results from micro-mechanical models were presented. In this chapter, the results from these tests are analyzed to draw a number of preliminary conclusions with regard to the applicability of the tests used in this study to estimate the impact of point and mass strength on the performance of the mixes.

The first section of this chapter includes a study on the ranking of the aggregates from a number of diverse points of view. Correlation analysis among all of the aggregate tests is then carried out to identify the redundant, complementary and inconclusive aggregate tests.

The second part of this chapter focuses on the material characterization tests for the mixes. A correlation analysis among the test methods for the characterization of mixes is carried out to once again identify the redundant, complementary and inconclusive mix tests. Finally, a process for developing relationships between individual aggregate tests and tests related to HMA performance is discussed.

After reviewing the analyses, correlations and considerations of expert opinions, a second study in the ranking of the aggregates was done on selected and recommended tests.

AGGREGATE RANKING

The results are categorized in the following three groups:

1. Aggregate properties from tests that may contribute to the identification of point and mass strength,
2. Rock properties of the bulk specimens used to identify the strength and stiffness of rocks before crushing, and
3. Shape and texture properties from the traditional tests commonly carried out by TxDOT for defining the quality of aggregates.

The most ideal way of ranking the aggregates based on the variety of tests carried out, is to know the passing and failing limits for each test. Since there are no defined limits for these tests, especially for the new tests proposed, another approach needs to be taken. A more objective way for ranking the aggregates is based on a scoring system. To implement the process, the normalized score of the aggregate is calculated by using the mean values of each test results. The following equation is used to find the normalized score:

$$r_{ij} = k\frac{x_{ij} - average\{x_j\}}{\max\{x_j\} - \min\{x_j\}} \tag{7.1}$$

where r_{ij} is the normalized value from test *j* for aggregate *i*, x_{ij} is the result from test *j* for aggregate *i*, $average\{x_j\}$ is the average value calculated from test method *j* for the six aggregates; $\max\{x_j\}$ is the maximum value measured from test method *j* for the six aggregates; and $\min\{x_j\}$ is the minimum value measured from test method *j* for the six aggregates. Parameter k is equal to +1 if a higher value from a given test represents a higher quality aggregate, and -1 if a lower value represents a higher quality aggregate.

The value of r_{ij} can vary between -1 for an extremely low quality aggregate to +1 for an extremely high quality aggregate. The final step is to rank the aggregates in each test in a scale of 1 to 5, where 3 being average, 1 being significantly above average and a 5 being significantly below average. To rank the aggregates with similar scores, the same ranges shown in Table 7.1 were used.

Table 7.1 – Definition of Ranking Values

Definition	Significantly Below Average	Below Average	Average	Above Average	Significantly Above Average
Numerical Ranking	5	4	3	2	1
Criteria	$-1<r_{ij}\leq-0.6$	$-0.6<r_{ij}\leq-0.2$	$-0.2<r_{ij}\leq+0.2$	$+0.2<r_{ij}\leq+0.6$	$+0.6<r_{ij}\leq+1$

As an example, consider the ACV of the rocks as shown in Table 7.2. Based on the established criteria of 30, the soft limestone and lightweight aggregates are substandard, while sandstone and gravel of high quality. The numerical ranking captures this established classification quite well.

Table 7.2 – Example of Ranking Process

Aggregate	Hard Limestone	Granite	Soft Limestone	Sandstone	Gravel	Lightweight Aggregate	Average
ACV (%)	22	27	32	18	16	43	26
Normalized Score (r_{ij})	0.16	-0.02	-0.21	0.31	0.38	-0.62	N/A
Numerical Ranking	3	3	4	2	2	5	
Descriptive Ranking	Average	Average	Below Average	Above Average	Above Average	Significantly Below Average	

Of course this ranking is based on only six aggregates. One of the benefits of this method is that as the number of aggregates tested increases, the ranking can be modified based on the properties of aggregates that are available in Texas. For example, consider the case when the lightweight aggregate is eliminated from the database because it is essentially a manufactured aggregate (not a traditional quarried aggregate). As shown in Table 7.3, the average ACV for the data available becomes 23 indicating that on the average the quality of the materials in the database is better than before. Since the maximum ACV is now 32 (as opposed to 43, this indicates that the results fall into a smaller range. Following, the algorithm discussed above, the ranking of the aggregates will change. In this case, the granite will rank as below average, while the other four aggregates rank as in Table 7.2. This example reveals that even though the process is logical, more aggregates should be tested so that the limits for specifications can be refined.

Table 7.3 – Example of Ranking Process Ignoring Lightweight Aggregate

Aggregate	Hard Limestone	Granite	Soft Limestone	Sandstone	Gravel	Average
ACV (%)	22	27	32	18	16	23
Normalized Score (r_{ij})	0.06	-0.25	-0.56	0.31	0.44	N/A
Numerical Ranking	3	4	4	2	2	
Descriptive Ranking	Average	Below Average	Below Average	Above Average	Above Average	

Based on the values reported for each test in the previous chapters, the normalized scores for the aggregates are calculated based on Equation 7.1 and are shown in Table 7.4. The normalized scores are categorized into three areas: a) rock properties, b) aggregate properties, and c) traditional properties. These categorized are followed for the remainder of the chapter.

Table 7.5 shows the ranking score of the normalized values for each of the tests based upon Table 7.1. At a glance, the sandstone and gravel are typically ranked as high-quality (rankings of 2 and 3), and the soft limestone as lower quality (rankings of 4 and 5). For the other three aggregates, the ranking varies depending on the test.

One possible way of globally ranking the aggregates based on all tests is to sum the rankings from all individual tests as done in Table 7.6. The aggregate with the lowest sum of rankings is then considered the best. The qualitative or descriptive rankings are shown for the rock tests, aggregate tests and traditional tests as well as the global rankings and are reported in Table 7.6. Even though these rankings fit the perceptions of the aggregate qualities from previous experience, there are several shortcomings with the ranking process. First, all tests are considered equally important and are weighed the same. Some of the tests may not correlate with performance at all either statistically or heuristically (e.g. coarse aggregate acid insolubility). There are also a number of redundant tests (e.g. modulus of rock from V-meter and FFRC) that are highly correlated since they measure the same parameter. This would essentially give an unfair advantage in ranking to parameters that are measured several ways. These shortcomings are addressed later in this chapter.

Table 7.4 - Normalized Scores for Aggregate Characterization Tests

	Test Parameter	Hard Limestone	Granite	Soft Limestone	Sandstone	Gravel	Lightweight Aggregate
Rock	Compressive Strength	-0.13	0.38	-0.62	0.37	Not Available	
	Indirect Tensile Strength	0.20	-0.15	-0.53	0.47		
	Schmidt Hammer Strength Test	-0.05	0.44	-0.56	0.17		
	V-Meter Modulus	0.52	-0.23	-0.48	0.18		
	FFRC Modulus	0.55	-0.17	-0.45	0.07		
Aggregate	ACV Compacting Modulus	-0.02	-0.24	-0.33	0.16	0.67	-0.24
	ACV Maximum Compacting Stress	-0.03	-0.38	-0.40	0.16	0.60	0.05
	ACV Crushing Modulus	0.16	0.00	-0.57	-0.17	0.43	0.14
	ACV	0.16	-0.02	-0.21	0.31	0.38	-0.62
	ACV #40 Passing	0.20	0.14	-0.33	0.24	0.38	-0.62
	ACV #200 Passing	0.20	0.02	-0.16	0.21	0.36	-0.64
	AIV – Dry	0.43	-0.21	-0.17	0.11	0.39	-0.57
	AIV - Soaked	-0.19	-0.36	-0.32	0.25	0.64	-0.01
	AIV #40 Passing	0.30	-0.01	0.07	0.12	0.23	-0.70
	AIV #200 Passing	0.18	0.06	-0.05	0.17	0.32	-0.68
	Sieve Analysis after Direct Shear	0.23	0.18	0.07	-0.04	0.28	-0.72
Traditional	Los Angeles % Wt. Loss - Bituminous	0.18	-0.55	-0.24	0.08	0.45	0.08
	Mg Soundness Bituminous	0.23	-0.21	-0.57	-0.21	0.43	0.31
	Mg Soundness Surface Treatment	0.25	-0.32	-0.54	-0.32	0.46	0.46
	Micro-Deval %Wt. Loss - Bituminous	0.17	0.17	-0.40	-0.05	0.56	-0.44
	Micro-Deval %Wt. Loss - Surface Treatment	-0.04	0.26	-0.30	-0.10	0.60	-0.40
	Polish Value	-0.21	0.11	-0.16	0.58	0.11	-0.42
	Coarse Aggregate Acid Insolubility	-0.56	0.39	-0.56	0.01	0.29	0.44
	Texture Before Micro-Deval	0.05	0.20	-0.56	0.44	-0.23	0.11
	Texture After Micro-Deval	-0.26	0.24	-0.57	0.43	-0.19	0.35
	Angularity Before Micro-Deval	-0.24	0.02	-0.32	0.07	0.68	-0.22
	Angularity After Micro-Deval	-0.21	0.37	-0.26	-0.10	0.60	-0.40

Table 7.5 - Ranking Score of Aggregates

	Test Parameter	Hard Limestone	Granite	Soft Limestone	Sandstone	Gravel	Lightweight Aggregate
Rock	Compressive Strength	3	2	5	2	Not Available	
	Indirect Tensile Strength	2	3	4	2		
	Schmidt Hammer Strength Test	3	2	4	3		
	V-Meter Modulus	2	4	4	3		
	FFRC Modulus	2	3	4	3		
Aggregate	ACV Compacting Modulus	3	4	4	3	1	4
	ACV Maximum Compacting Stress	3	4	4	3	2	3
	ACV Crushing Modulus	3	3	4	3	2	3
	ACV	3	3	4	2	2	5
	ACV #40 Passing	3	3	4	2	2	5
	ACV #200 Passing	2	3	3	2	2	5
	AIV – Dry	2	4	3	3	2	4
	AIV - Soaked	3	4	4	2	1	3
	AIV #40 Passing	2	3	3	3	2	5
	AIV #200 Passing	3	3	3	3	2	5
	Sieve Analysis after Direct Shear	2	3	3	3	2	5
Traditional	Los Angeles % Wt. Loss - Bituminous	3	4	4	2	2	3
	Mg Soundness Bituminous	2	3	5	3	2	2
	Mg Soundness Surface Treatment	2	3	5	3	2	2
	Micro-Deval %Wt. Loss - Bituminous	3	4	4	3	2	3
	Micro-Deval %Wt. Loss - Surface Treatment	2	4	4	4	2	2
	Polish Value	2	4	4	4	2	2
	Coarse Aggregate Acid Insolubility	3	3	4	3	2	4
	Texture Before Micro-Deval	3	2	4	3	2	4
	Texture After Micro-Deval	4	3	3	2	3	4
	Angularity Before Micro-Deval	4	2	4	3	2	2
	Angularity After Micro-Deval	3	3	4	2	4	3

Table 7.6 – Ranking of Aggregates

a) Rock Tests Only

Aggregate	Summation of Ranks	Qualitative Ranking
Hard Limestone	12	Above Average
Granite	14	Above Average
Soft Limestone	21	Below Average
Sandstone	13	Above Average

b) Aggregate Tests Only

Aggregate	Summation of Ranks	Qualitative Ranking
Hard Limestone	29	Average
Granite	37	Average
Soft Limestone	39	Below Average
Sandstone	29	Average
Gravel	20	Above Average
LW Aggregate	47	Below Average

c) Traditional Tests Only

Aggregate	Summation of Ranks	Qualitative Ranking
Hard Limestone	36	Average
Granite	32	Average
Soft Limestone	43	Significantly Below Avg.
Sandstone	32	Average
Gravel	25	Above Average
LW Aggregate	34	Average

d) All Tests

Aggregate	Summation of Ranks	Qualitative Ranking
Hard Limestone	77	Average
Granite	81	Average
Soft Limestone	106	Below Average
Sandstone	71	Above Average
Gravel	55	Above Average
LW Aggregate	96	Below Average

HMA PERFORMANCE RANKING

The performance of the mixes was also ranked following the process described above. The normalized scores using Equation 7.1 are shown for the mixes compacted to the design air voids in Table 7.7, and the ranking using Table 7.1 by mix type in Table 7.8. For all mixes, the soft limestone was below average, and sandstone at least above average. The ranking for the hard limestone and granite was average for the CMHB-C and Superpave-C, but below average for the PFC. On the contrary, the lightweight aggregate did not rank high for the CMHB-C and Superpave-C, but ranked above average for the PFC. This contradiction can be perhaps due to the fact that the performance tests selected to evaluate mixes may not be appropriate.

Table 7.7 – Normalized Scores for HMA Performance at Design Air Voids

Parameter		Hard Limestone	Granite	Soft Limestone	Sandstone	Gravel	Lightweight Aggregate
CMHB-C	Indirect Tensile Strength	-0.39	-0.33	-0.50	0.50	0.49	0.23
	Dynamic Modulus	-0.01	-0.13	-0.29	0.37	0.52	-0.48
	Seismic Modulus (V-Meter)	0.12	0.04	-0.03	0.21	0.33	-0.67
	Flowtime Maximum Strain	0.41	-0.06	-0.58	0.08	0.42	-0.27
	HWTD Rut Depth	-0.25	0.29	-0.37	-0.05	0.63	-0.25
Superpave-C	Indirect Tensile Strength	-0.40	-0.43	-0.35	0.57	0.18	0.43
	Dynamic Modulus	0.23	-0.18	-0.28	0.58	0.08	-0.42
	Seismic Modulus (V-Meter)	0.55	0.09	-0.06	-0.06	-0.06	-0.45
	Flowtime Maximum Strain	0.48	0.01	-0.52	0.09	-0.09	0.03
	HWTD Rut Depth	-0.22	0.23	-0.52	0.43	0.48	-0.40
PFC	Indirect Tensile Strength	-0.51	0.06	-0.23	0.49	-0.02	0.21
	Dynamic Modulus	-0.23	-0.37	-0.35	0.63	0.40	-0.07
	Seismic Modulus (V-Meter)	-0.07	-0.48	-0.36	0.10	0.29	0.52
	Flowtime Maximum Strain	-0.10	0.24	0.16	0.40	-0.60	-0.10
	HWTD Rut Depth	N/A	N/A	N/A	N/A	N/A	N/A
Type-D	Indirect Tensile Strength	0.25	-0.69	-0.37	0.27	0.23	0.31
	Dynamic Modulus	0.30	0.00	-0.21	0.41	0.10	-0.59
	Seismic Modulus (V-Meter)	0.31	0.07	-0.05	0.11	0.26	-0.69
	Flowtime Maximum Strain	0.36	0.12	-0.64	0.18	-0.30	0.28
	HWTD Rut Depth	-0.31	0.18	-0.55	0.26	0.45	-0.04

Table 7.8 - Ranking of HMA Based on Performance Tests on Specimens Prepared to In Place Air Voids

a) CMHB-C

Aggregate	Summation of Ranks	Qualitative Ranking
Hard Limestone	16	Average
Granite	15	Average
Soft Limestone	19	Below Average
Sandstone	12	Above Average
Gravel	9	Above Average
Lightweight Aggregate	19	Below Average

b) Superpave-C

Aggregate	Summation of Ranks	Qualitative Ranking
Hard Limestone	14	Average
Granite	15	Average
Soft Limestone	19	Below Average
Sandstone	12	Above Average
Gravel	14	Average
Lightweight Aggregate	17	Below Average

c) PFC

Aggregate	Summation of Ranks	Qualitative Ranking
Hard Limestone	14	Below Average
Granite	13	Below Average
Soft Limestone	15	Below Average
Sandstone	8	Significantly Below Avg.
Gravel	12	Average
Lightweight Aggregate	10	Above Average

d) Type-D

Aggregate	Summation of Ranks	Qualitative Ranking
Hard Limestone	12	Above Average
Granite	17	Average
Soft Limestone	20	Below Average
Sandstone	12	Above Average
Gravel	13	Above Average
Lightweight Aggregate	16	Below Average

As specimens were also prepared and tested with 250 gyrations, they were also ranked. Based on field observations by a number of agencies, the HMA mats become compacted during trafficking, and as such their air voids decrease. That is the premise for performing mix design at 4% but placing and testing them at 7% air voids. As reflected in Table 5.1, the air voids of the specimens prepared with 250 gyrations were significantly lower than the in-place air voids used. Preliminarily, it can be assumed that the rankings from the specimens prepared at 250 gyrations may relate to their performance after several years. The normalized scores using Equation 7.1 and the rankings using Table 7.1 of performance based on these specimens are included in Table 7.9 and 7.10, respectively. In this case, the performance of the mixes becomes more similar primarily because of excessive rutting at lower air voids (a well documented phenomenon).

CORRELATION OF TEST METHODS

One of the objectives of this study was to determine which tests are most representative of the aggregate point and bulk strength, shape and texture, and performance of the HMA mixtures. Since some tests may provide redundant information, a correlation analysis among the tests was performed to eliminate the redundant tests and to select complimentary tests. Based on the correlation analysis, tests that provide similar results or are highly correlated can be isolated so that one of them can be selected. Consideration was given to the selection process in terms of cost, test time, and impact on the TxDOT operation.

The correlations between the three categories of tests (aggregate properties, rock properties and traditional properties) are included in Table 7.11 through Table 7.13. Two parameters are considered correlated when the absolute value of their correlation coefficient (CC) is greater than 0.6. As a reminder, a CC of 1 corresponds to a perfect correlation and a CC of zero to no correlation. A negative sign for CC indicated that when one parameter is increasing, the other one is decreasing.

As shown in Table 7.11, the ACV test results and its surrogate parameters (compacting and crushing modulus and maximum compacting stress) correlate well with one another and with the dry AIV test results. The TFV seems to correlate reasonably well with maximum compacting stress, as expected. As such, the ACV test would be an appropriate test to use for characterizing the aggregates, especially since several parameters can be readily determined from the same test. Furthermore, the cost of implementing these tests in the Districts that own a concrete compressive test machine is rather small.

Table 7.12 illustrates the correlation analysis for the tests carried out on rock specimens retrieved from quarries. Three parameters (compressive strength, tensile strength and the modulus) are necessary for micro-mechanical modeling. Since the compressive strength test results and those from the Schmidt hammer are well-correlated, the Schmidt hammer can be used for assessing the compressive strength of the rock. This eliminates the need for coring the rock, and requires minimal training.

Table 7.9 - Normalized Scores for HMA Performance from 250-Gyrations Specimens

Parameter		Hard Limestone	Granite	Soft Limestone	Sandstone	Gravel	Lightweight Aggregate
CMHB-C	Indirect Tensile Strength	-0.43	-0.17	0.57	-0.15	0.07	0.11
	Dynamic Modulus	-0.28	-0.54	0.46	0.28	0.35	-0.27
	Seismic Modulus (V-Meter)	0.53	0.11	0.17	-0.36	0.02	-0.47
	Flowtime Maximum Strain	0.07	0.23	0.12	0.18	-0.77	0.17
	HWTD Rut Depth	0.29	0.24	-0.49	-0.27	0.51	-0.29
Superpave-C	Indirect Tensile Strength	-0.49	-0.17	0.37	-0.49	0.28	0.51
	Dynamic Modulus	-0.34	-0.38	0.20	0.18	0.62	-0.28
	Seismic Modulus (V-Meter)	0.06	0.04	0.09	-0.30	0.56	-0.44
	Flowtime Maximum Strain	0.08	-0.26	-0.46	0.30	0.54	-0.19
	HWTD Rut Depth	-0.37	-0.19	-0.32	0.18	0.63	0.07
PFC	Indirect Tensile Strength	-0.17	-0.12	0.14	0.05	-0.45	0.55
	Dynamic Modulus	0.24	-0.68	0.32	-0.14	-0.04	0.31
	Seismic Modulus (V-Meter)	0.19	-0.54	-0.09	0.24	0.46	-0.25
	Flowtime Maximum Strain	0.29	-0.71	0.16	0.06	0.16	0.04
	HWTD Rut Depth	N/A	N/A	N/A	N/A	N/A	N/A
Type-D	Indirect Tensile Strength	N/A	N/A	N/A	0.08	-0.54	0.46
	Dynamic Modulus	N/A	N/A	N/A	0.31	0.35	-0.65
	Seismic Modulus (V-Meter)	N/A	N/A	N/A	0.39	0.21	-0.61
	Flowtime Maximum Strain	N/A	N/A	N/A	-0.52	0.48	0.04
	HWTD Rut Depth	N/A	N/A	N/A	0.24	0.38	-0.62

Table 7.10 - Ranking of HMA Based on Performance Tests on Specimens Prepared at 250 Gyrations

a) CMHB-C

Aggregate	Summation of Ranks	Qualitative Ranking
Hard Limestone	15	Average
Granite	14	Average
Soft Limestone	14	Average
Sandstone	16	Average
Gravel	15	Average
LW Aggregate	18	Below Average

b) Superpave-C

Aggregate	Summation of Ranks	Qualitative Ranking
Hard Limestone	18	Average
Granite	17	Average
Soft Limestone	16	Average
Sandstone	16	Average
Gravel	8	Above Average
LW Aggregate	16	Average

c) PFC

Aggregate	Summation of Ranks	Qualitative Ranking
Hard Limestone	10	Average
Granite	17	Below Average
Soft Limestone	11	Average
Sandstone	11	Average
Gravel	12	Average
LW Aggregate	11	Average

d) Type-D

Aggregate	Summation of Ranks	Qualitative Ranking
Hard Limestone	--	Not ranked since only three aggregates are available
Granite	--	
Soft Limestone	--	
Sandstone	13	
Gravel	12	
LW Aggregate	20	

Table 7.11 - Correlation Analysis among Different Aggregate Tests

Test	ACV Compacting Modulus	ACV Maximum Compacting Stress	ACV Crushing Modulus	ACV	ACV #40 Passing	ACV #200 Passing	AIV - Dry	AIV - Soaked	AIV #40 Passing	AIV #200 Passing	TFV	Direct Shear Sieve Analysis
ACV Compacting Modulus	1.0											
ACV Maximum Compacting Stress	0.9	1.0										
ACV Crushing Modulus	-0.6	-0.7	1.0									
ACV	-0.8	-0.5	0.3	1.0								
ACV #40 Passing	-0.8	-0.8	0.9	0.9	1.0							
ACV #200 Passing	-0.9	-0.9	0.9	1.0	0.9	1.0						
AIV - Dry	-0.7	-0.5	0.4	0.9	0.7	0.8	1.0					
AIV - Soaked	-0.9	-1.0	0.6	0.5	0.7	0.8	0.4	1.0				
AIV #40 Passing	-0.6	-0.6	0.6	0.6	0.5	0.7	1.0	0.5	1.0			
AIV #200 Passing	-0.9	-0.9	0.9	1.0	0.9	1.0	0.8	0.9	0.7	1.0		
TFV	0.7	0.5	-0.4	-0.4	-0.3	-0.4	-0.3	-0.6	0.0	-0.5	1.0	
Direct Shear Sieve Analysis	-0.4	-0.1	0.1	0.8	0.4	0.4	0.8	0.1	0.5	0.5	-0.4	1.0

Table 7.12 - Correlation Analysis among Different Rock Tests

Test	Compressive Rock Strength	Indirect Tensile Rock Strength	Schmidt Hammer Compressive Strength	V-Meter Rock Modulus	FFRC Rock Modulus
Compressive Rock Strength	1.0				
Indirect Tensile Rock Strength	0.7	1.0			
Schmidt Hammer Strength Test	1.0	0.5	1.0		
V-Meter Rock Modulus	0.3	0.8	0.3	1.0	
FFRC Rock Modulus	0.3	0.7	0.3	1.0	1.0

The tensile strength seems to be well-correlated to the moduli from either FFRC or V-meter tests. This trend makes sense since both the modulus and the tensile strength are to a great extent controlled by the size of the grains composing the rock. If micro-mechanical modeling is not required, it seems that the V-meter will be a good tool for estimating the quality of the aggregates in tension. The V-meter is recommended over the FFRC since the V-meter test can be carried out on the rock samples that are faced without coring. This test also provided the third important property of the aggregates, i.e. modulus.

A strong relationship between the compressive strength and modulus has been reported for many geo-materials and concrete. However, in Table 7.12, these two parameters show very weak correlations. The size of the grains within the rock mass may not impact the compressive strength, but it greatly impacts the modulus.

The third set of correlation analyses performed was for the traditional tests, as shown in Table 7.13. The test results for the aggregate abrasion and soundness resistance, polishing, and physical characteristics such as shape, angularity and texture are included in this table. The test method

Table 7.13 - Correlation Analysis among Different Traditional Tests

Test	Los Angeles % Wt. Loss - Bituminous	Mg Soundness Bituminous	Mg Soundness Surf. Treatment	Micro-Deval %Wt. Loss - Bituminous	Micro-Deval %Wt. Loss - Surf. Treat.	Polish Value	Coarse Aggregate Acid Insolubility	Texture Before Micro-Deval	Texture After Micro-Deval	Angularity Before Micro-Deval	Angularity After Micro-Deval
Los Angeles % Wt. Loss - Bituminous	1.0										
Mg Soundness Bituminous	0.7	1.0									
Mg Soundness Surface Treatment	0.7	1.0	1.0								
Micro-Deval %Wt. Loss - Bituminous	0.6	0.8	0.9	1.0							
Micro-Deval %Wt. Loss - Surf. Treatment	0.4	0.7	0.8	0.9	1.0						
Polish Value	-0.3	0.0	0.1	-0.1	-0.1	1.0					
Coarse Aggregate Acid Insolubility	-0.2	-0.5	-0.4	-0.7	-0.8	0.5	1.0				
Texture Before Micro-Deval	-0.2	-0.4	-0.3	-0.3	-0.1	0.6	0.4	1.0			
Texture After Micro-Deval	-0.1	-0.3	-0.2	-0.3	-0.2	0.8	0.6	0.9	1.0		
Angularity Before Micro-Deval	-0.6	-0.6	-0.6	-0.8	-0.9	0.4	0.8	0.1	0.3	1.0	
Angularity After Micro-Deval	-0.2	-0.6	-0.6	-0.8	-1.0	0.2	0.9	0.1	0.3	0.9	1.0

conducted with AIMS for the characterization of the angularity of the aggregate revealed a fair correlation with most of the tests except for the Polish Value and texture characterization tests. On the other hand, the LA abrasion resistance test showed a poor relationship with almost all the other tests while the Micro-Deval tests exhibited better correlations.

CORRELATION OF PERFORMANCE TESTS

Table 7.14 shows the results of the correlation analysis carried out to identify the relationship between performance tests on HMA specimens and geotechnical tests carried out on specimens prepared with aggregates alone. The direct shear strength on aggregates only correlates with the HWTD rut depth. This correlation is counterintuitive since one expects that with the increase in shear strength of the aggregate skeleton, the rutting potential should decrease (not increase as reflected in Table 7.14). The triaxial strength of aggregates correlates with the dynamic modulus indicating that the aggregate skeleton impacts the stiffness of the mixes. Based on these correlations, it seems that the strength tests on aggregates may not be a good indicator of the performance of the mixes.

The IDT strength of the HMA seems to correlate well with the seismic and dynamic moduli, and to some extent to the flow time and the HWTD rut depth. The seismic and dynamic moduli are well correlated.

Table 7.14 - Correlation Results for Mixture Characterization Tests

	Test	Aggregate		HMA				
		Direct Shear Test - Strength	Triaxial Strength	Indirect Tensile Strength	Dynamic Modulus	Seismic Modulus (V-Meter)	Flow Time Maximum Strain	HWTD Rut Depth
Aggregate	**Direct Shear Test - Strength**	1.0						
	Triaxial Strength	0.2	1.0					
HMA	**Indirect Tensile Strength**	-0.4	-0.4	1.0				
	Dynamic Modulus	-0.2	-0.5	0.9	1.0			
	Seismic Modulus (V-Meter)	-0.1	-0.2	0.7	0.9	1.0		
	Flow Time Maximum Strain	0.1	0.2	-0.7	-0.8	-0.8	1.0	
	HWTD Rut Depth	**0.8**	0.4	-0.7	-0.3	0.2	0.4	1.0

Note: values that are bold and underlined demonstrate high correlations that seem counterintuitive

From Table 7.14, the indirect tensile strength, dynamic modulus, seismic modulus (V-Meter), and flow time correlated well with each other globally. In light of this analysis, the indirect tensile tests and the seismic modulus with the V-meter can be the two candidates to provide information about the strength and stiffness of the HMA. The HWTD is in current TxDOT specifications and can be used if available.

CORRELATION OF PERFORMANCE TESTS TO AGGREGATE-RELATED TESTS

Table 7.15 contains the correlation coefficients among the performance tests and the aggregate-related tests when all mixes are combined. None of the performance tests correlate with the aggregate-related tests, except for the HWTD results. This trend was anticipated because the differences in the proportionality of the coarse aggregates among mixes were impacting the results of the performance tests. For the HWTD tests, the compressive strength of the rock, ACV and its surrogate parameters, as well as Micro-Deval and AIMS angularity are correlated to rutting potential. To establish more rigorous correlations, each mix type was examined individually.

Table 7.16 shows that dynamic modulus, seismic modulus, flow time, and HWDT test for CMHB-C mixes correlate with aggregate properties. These tests show good to reasonable correlations with the rock properties, ACV tests results with nearly all its parameters, and Micro-Deval test results. The IDT is less strongly correlated to the rock and aggregate tests. The binder quality is normally one of the controlling parameters in the IDT strength, which was maintained as a constant in this study.

For the Superpave-C mixes (Table 7.17), the dynamic and seismic moduli, and the flow time value are strongly correlated to the modulus of rock, while the tensile strength of the rock is correlated with all performance tests except seismic modulus. The ACV test results are also correlated to all performance tests except flow time and IDT results. Most of the traditional tests do not correlate with the performance tests.

As shown in Table 7.18, the performance tests on the PFC mixes are occasionally correlated to the aggregate tests. This is unexpected since the PFC is perceived to rely the most on the rock to rock contacts. This lack of correlation can be attributed to perhaps the inappropriateness of the performance test selected for the PFC mixes. To test this hypothesis, the performance tests from the specimens prepared by 250 gyrations were compared to the aggregate tests in Figure 7.19. The indirect tensile and the seismic modulus are impacted by the ACV. This indicates that the performance tests on the PFC mix should be revised in the future, and that the rock-to-rock contact is significant but not at 20% air voids.

Table 7.20 shows that the dynamic modulus, seismic modulus and HWDT tests for Type-D mixes correlate with aggregate properties. All tests show good to reasonable correlations with the rock properties. Most of the traditional tests do not seem to correlate well with the performance tests.

Table 7.15 – Global Correlation Analysis between HMA Performance Tests and Aggregate Properties

Aggregate Test \ Performance Test		HMA				
		Indirect Tensile Strength	Dynamic Modulus	Seismic Modulus (V-Meter)	Flowtime Maximum Strain	HWTD Rut Depth
Rock	Compressive Strength	0.4	0.3	0.1	-0.4	-0.8
	Indirect Tensile Strength	0.5	0.4	0.2	-0.4	-0.5
	Schmidt Hammer Strength Test	0.2	0.2	0.1	-0.4	-0.8
	V-Meter Modulus	0.2	0.2	0.2	-0.4	-0.1
	FFRC Modulus	0.1	0.1	0.2	-0.4	0.0
Aggregate	ACV Compacting Modulus	0.5	0.3	0.2	-0.1	-0.6
	ACV Maximum Compacting Stress	0.5	0.3	0.2	-0.1	-0.6
	ACV Crushing Modulus	-0.2	-0.2	-0.2	0.2	0.6
	ACV	-0.5	-0.4	-0.2	0.3	0.6
	ACV #40 Passing	-0.4	-0.3	-0.2	0.3	0.7
	ACV #200 Passing	-0.4	-0.3	-0.2	0.3	0.6
	AIV – Dry	-0.2	-0.2	-0.2	0.2	0.2
	AIV – Soaked	-0.6	-0.4	-0.1	0.1	0.6
	AIV #40 Passing	-0.1	-0.1	-0.1	0.1	0.0
	AIV #200 Passing	-0.4	-0.3	-0.2	0.2	0.6
	Sieve Analysis after Direct Shear	0.2	0.1	0.1	-0.2	0.2
Traditional Tests	Los Angeles % Wt. Loss - Bituminous	-0.3	-0.2	-0.1	0.1	0.4
	Mg Soundness Bituminous	-0.1	-0.1	-0.2	0.2	0.6
	Mg Soundness Surf. Treat.	-0.1	-0.1	-0.1	0.2	0.6
	Micro-Deval %Wt. Loss - Bituminous	-0.1	0.0	0.0	0.1	0.7
	Micro-Deval %Wt. Loss - Surf. Treat.	-0.2	-0.1	-0.1	0.1	0.7
	Polish Value	0.2	0.1	-0.1	0.0	-0.4
	Coarse Aggregate Acid Insolubility	0.2	0.1	0.0	0.0	-0.8
	Texture Before Micro-Deval	0.0	0.0	0.0	-0.2	-0.2
	Texture After Micro-Deval	0.1	0.1	0.0	-0.2	-0.4
	Angularity Before Micro-Deval	0.3	0.2	0.1	0.0	-0.7
	Angularity After Micro-Deval	0.2	0.1	0.1	0.0	-0.7

Table 7.16 – Correlation Analysis between CMHB-C Performance Tests at Design Air Voids and Aggregate Properties

Aggregate Test \ Performance Test		Indirect Tensile Strength	Dynamic Modulus	Seismic Modulus (V-Meter)	Flow Time Maximum Strain	HWTD Rut Depth
Rock	Compressive Strength	0.6	0.7	0.7	-0.5	-0.9
	Indirect Tensile Strength	0.8	0.9	1.0	-0.8	-0.2
	Schmidt Hammer Strength Test	0.4	0.5	0.5	-0.6	-0.9
	V-Meter Modulus	0.3	0.6	0.8	-1.0	0.1
	FFRC Modulus	0.2	0.5	0.6	-1.0	0.1
Aggregate	ACV Compacting Modulus	0.7	0.9	0.6	-0.8	-0.7
	ACV Maximum Compacting Stress	0.8	0.7	0.3	-0.7	-0.6
	ACV Crushing Modulus	-0.5	-0.4	-0.1	0.8	0.6
	ACV	-0.3	-0.9	-1.0	0.7	0.6
	ACV #40 Passing	-0.2	-0.9	-0.9	0.8	0.7
	ACV #200 Passing	-0.2	-0.9	-1.0	0.7	0.6
	AIV - Dry	-0.1	-0.8	-0.9	0.8	0.4
	AIV - Soaked	-0.9	-0.8	-0.4	0.6	0.6
	AIV #40 Passing	0.2	-0.7	-0.9	0.5	0.3
	AIV #200 Passing	0.0	-0.8	-1.0	0.6	0.5
	Sieve Analysis after Direct Shear	0.3	-0.6	-0.9	0.5	0.5
Traditional	Los Angeles % Wt. Loss - Bituminous	-0.2	-0.2	-0.1	0.3	0.1
	Mg Soundness - Bituminous	-0.1	0.1	0.2	0.4	0.2
	Mg Soundness - Surf. Treat.	-0.2	0.1	0.3	0.4	0.2
	Micro-Deval %Wt. Loss - Bituminous	0.1	-0.5	-0.6	0.6	0.7
	Micro-Deval %Wt. Loss - Surf. Treat.	0.0	-0.5	-0.6	0.5	0.9
	Polish Value	-0.5	0.0	0.4	0.4	-0.1
	Coarse Aggregate Acid Insolubility	0.0	-0.4	-0.4	0.3	-0.4
	Texture Before Micro-Deval	-0.8	-0.8	-0.4	0.6	0.4
	Texture After Micro-Deval	-0.5	-0.8	-0.6	0.8	0.3
	Angularity Before Micro-Deval	0.2	0.5	0.4	-0.3	-0.8
	Angularity After Micro-Deval	0.1	0.5	0.6	-0.4	-0.9

Table 7.17 – Correlation Analysis between Superpave-C Performance Tests at Design Air Voids and Aggregate Properties

	Aggregate Test \ Performance Test	Indirect Tensile Strength	Dynamic Modulus	Seismic Modulus (V-Meter)	Flow Time Maximum Strain	HWTD Rut Depth
Rock	Compressive Strength	0.5	0.5	-0.1	-0.5	-1.0
	Indirect Tensile Strength	0.7	1.0	0.3	-0.8	-0.7
	Schmidt Hammer Strength Test	0.2	0.3	0.1	-0.6	-0.9
	V-Meter Modulus	0.3	0.8	0.7	-0.9	-0.3
	FFRC Modulus	0.1	0.6	0.8	-1.0	-0.2
Aggregate	ACV Compacting Modulus	0.4	0.5	0.1	-0.2	-0.7
	ACV Maximum Compacting Stress	0.6	0.4	-0.2	-0.2	-0.6
	ACV Crushing Modulus	-0.2	-0.1	-0.1	0.6	0.5
	ACV	0.0	-0.8	-0.6	0.3	0.8
	ACV #40 Passing	0.1	-0.8	-0.6	0.4	0.8
	ACV #200 Passing	0.2	-0.8	-0.6	0.3	0.7
	AIV - Dry	0.2	-0.7	-0.7	0.4	0.5
	AIV - Soaked	-0.7	-0.4	0.3	0.1	0.7
	AIV #40 Passing	0.4	-0.7	-0.8	0.1	0.4
	AIV #200 Passing	0.3	-0.7	-0.7	0.1	0.6
	Sieve Analysis after Direct Shear	0.5	-0.5	-0.7	0.1	0.6
Traditional	Los Angeles % Wt. Loss - Bituminous	-0.1	0.0	0.0	0.0	-0.2
	Mg Soundness - Bituminous	0.0	0.4	0.0	0.2	-0.2
	Mg Soundness - Surf. Treat.	-0.1	0.3	0.1	0.3	-0.2
	Micro-Deval %Wt. Loss - Bituminous	0.5	0.0	-0.5	0.0	0.4
	Micro-Deval %Wt. Loss - Surf. Treat.	0.4	0.0	-0.3	-0.1	0.5
	Polish Value	-0.5	-0.2	0.1	0.8	0.1
	Coarse Aggregate Acid Insolubility	0.0	-0.8	-0.6	0.5	0.1
	Texture Before Micro-Deval	-0.7	-0.8	0.0	0.4	0.8
	Texture After Micro-Deval	-0.4	-1.0	-0.4	0.6	0.7
	Angularity Before Micro-Deval	-0.1	-0.2	-0.1	0.4	-0.4
	Angularity After Micro-Deval	-0.3	0.0	0.1	0.2	-0.6

Table 7.18 – Correlation Analysis between PFC Performance Tests at Design Air Voids and Aggregate Properties

Aggregate Test \ Performance Test		Indirect Tensile Strength	Dynamic Modulus	Seismic Modulus (V-Meter)	Flow Time Maximum Strain
Rock	Compressive Strength	0.7	0.5	0.2	-0.5
	Indirect Tensile Strength	0.4	0.8	0.8	-0.2
	Schmidt Hammer Strength Test	0.5	0.3	0.0	-0.3
	V-Meter Modulus	-0.1	0.4	0.7	0.4
	FFRC Modulus	-0.3	0.2	0.6	0.5
Aggregate	ACV Compacting Modulus	0.1	0.8	0.4	0.6
	ACV Maximum Compacting Stress	0.3	0.8	0.8	0.7
	ACV Crushing Modulus	0.0	-0.3	-0.6	-0.7
	ACV	0.0	-0.6	0.1	-0.2
	ACV #40 Passing	0.1	-0.5	0.2	-0.2
	ACV #200 Passing	0.2	-0.4	0.3	-0.2
	AIV - Dry	0.4	-0.4	0.1	-0.4
	AIV - Soaked	-0.4	-0.9	-0.7	-0.6
	AIV #40 Passing	0.4	-0.2	0.5	-0.1
	AIV #200 Passing	0.2	-0.3	0.4	-0.1
	Sieve Analysis after Direct Shear	0.1	-0.3	0.4	-0.1
Traditional	Los Angeles % Wt. Loss - Bituminous	0.4	-0.2	-0.6	-0.8
	Mg Soundness - Bituminous	0.5	0.1	-0.5	-0.9
	Mg Soundness - Surf. Treat.	0.3	0.0	-0.7	-0.9
	Micro-Deval %Wt. Loss - Bituminous	0.6	0.1	0.2	-0.6
	Micro-Deval %Wt. Loss - Surf. Treat.	0.3	0.0	0.2	-0.6
	Polish Value	-0.3	-0.3	-0.7	-0.1
	Coarse Aggregate Acid Insolubility	0.1	-0.3	0.1	0.4
	Texture Before Micro-Deval	-0.6	-0.9	-0.5	0.0
	Texture After Micro-Deval	-0.2	-0.8	-0.2	0.0
	Angularity Before Micro-Deval	-0.2	0.1	0.1	0.7
	Angularity After Micro-Deval	-0.1	0.1	-0.3	0.5

Table 7.19 – Correlation Analysis between PFC Performance Tests at 250 gyrations and Aggregate Properties

Aggregate Test \ Performance Test		Indirect Tensile Strength	Dynamic Modulus	Seismic Modulus (V-Meter)	Flow Time Maximum Strain
Rock	Compressive Strength	-0.4	-0.8	-0.2	0.6
	Indirect Tensile Strength	-0.4	-0.1	0.6	-0.2
	Schmidt Hammer Strength Test	-0.6	-0.9	-0.3	0.7
	V-Meter Modulus	-0.6	0.2	0.7	-0.4
	FFRC Modulus	-0.7	0.2	0.6	-0.4
Aggregate	ACV Compacting Modulus	-0.7	-0.1	0.8	-0.3
	ACV Maximum Compacting Stress	-0.4	0.1	0.8	-0.5
	ACV Crushing Modulus	0.4	0.1	-0.3	0.0
	ACV	0.9	0.4	-0.7	0.1
	ACV #40 Passing	0.9	0.5	-0.5	-0.1
	ACV #200 Passing	0.9	0.4	-0.6	0.1
	AIV - Dry	0.9	0.0	-0.8	0.4
	AIV - Soaked	0.4	0.0	-0.8	0.4
	AIV #40 Passing	0.9	0.2	-0.6	0.2
	AIV #200 Passing	0.9	0.4	-0.6	0.1
	Sieve Analysis after Direct Shear	0.9	0.5	-0.5	-0.1
Traditional	Los Angeles % Wt. Loss - Bituminous	0.2	-0.3	-0.8	0.6
	Mg Soundness - Bituminous	0.2	0.2	-0.2	0.0
	Mg Soundness - Surf. Treat.	0.2	0.1	-0.2	0.0
	Micro-Deval %Wt. Loss - Bituminous	1.0	0.6	-0.5	-0.1
	Micro-Deval %Wt. Loss - Surf. Treat.	0.9	0.6	-0.3	-0.3
	Polish Value	0.7	0.1	-0.2	0.1
	Coarse Aggregate Acid Insolubility	0.1	-0.5	-0.2	0.5
	Texture Before Micro-Deval	0.1	-0.5	-0.1	0.4
	Texture After Micro-Deval	0.3	-0.5	-0.3	0.5
	Angularity Before Micro-Deval	-0.7	-0.4	0.5	0.0
	Angularity After Micro-Deval	-0.8	-0.7	0.2	0.4

Table 7.20 – Correlation Analysis between Type-D Performance Tests at Design Air Voids and Aggregate Properties

Aggregate Test \ Performance Test		Indirect Tensile Strength	Dynamic Modulus	Seismic Modulus (V-Meter)	Flow Time Maximum Strain	HWTD Rut Depth
Rock	Compressive Strength	0.0	0.6	0.7	-0.1	-1.0
	Indirect Tensile Strength	0.8	1.0	0.8	-0.8	-0.6
	Schmidt Hammer Strength Test	-0.1	0.5	0.7	0.0	-0.9
	V-Meter Modulus	0.8	0.9	0.9	-0.9	-0.2
	FFRC Modulus	0.7	0.8	0.9	-0.8	-0.1
Aggregate	ACV Compacting Modulus	0.5	0.5	0.7	-0.2	-0.7
	ACV Maximum Compacting Stress	0.8	0.3	0.4	-0.5	-0.7
	ACV Crushing Modulus	-0.5	-0.1	-0.5	0.3	0.6
	ACV	-0.1	-0.9	-0.9	0.0	0.5
	ACV #40 Passing	0.0	-0.9	-1.0	-0.1	0.5
	ACV #200 Passing	0.0	-0.9	-0.9	-0.1	0.4
	AIV - Dry	-0.3	-0.8	-0.9	0.2	0.2
	AIV - Soaked	-0.6	-0.3	-0.4	0.3	0.7
	AIV #40 Passing	0.1	-0.9	-0.8	-0.2	0.0
	AIV #200 Passing	0.1	-0.9	-0.9	-0.2	0.3
	Sieve Analysis after Direct Shear	0.2	-0.9	-1.0	-0.5	0.9
Traditional	Los Angeles % Wt. Loss - Bituminous	-0.6	0.1	0.0	0.4	-0.1
	Mg Soundness - Bituminous	-0.4	0.4	0.0	0.3	0.1
	Mg Soundness - Surf. Treat.	-0.5	0.4	0.0	0.4	0.1
	Micro-Deval %Wt. Loss - Bituminous	0.2	-0.3	-0.6	-0.4	0.2
	Micro-Deval %Wt. Loss - Surf. Treat.	0.3	-0.3	-0.6	-0.5	0.5
	Polish Value	-0.7	0.0	-0.1	0.8	0.3
	Coarse Aggregate Acid Insolubility	-0.4	-0.8	-0.5	0.5	-0.2
	Texture Before Micro-Deval	-0.6	-0.6	-0.6	0.5	0.7
	Texture After Micro-Deval	-0.6	-0.9	-0.8	0.5	0.5
	Angularity Before Micro-Deval	-0.1	0.0	0.2	0.5	-0.4
	Angularity After Micro-Deval	-0.4	0.2	0.5	0.7	-0.5

ANALYSIS BASED ON SELECT TESTS

After reviewing and analyzing the different tests and on the HMA mixes and aggregates, certain tests are proposed in order to test the quality of the rock and aggregates as well as the performance of HMA mixes. The tests recommended for rock properties are the Schmidt Hammer test, the V-meter seismic modulus test, and the Indirect Tensile test. For the aggregate tests, the ACV tests are recommended. The four traditional tests recommended are the Los

Angeles Abrasion test, Mg Soundness test, and the Micro-Deval test, and AIMS angularity after Micro-Deval. Lastly, the proposed performance tests are the indirect tensile test, V-meter seismic modulus test, and the Hamburg Wheel Tracking Device test. A second series of analysis was carried out with only those tests recommended to demonstrate how well they represent the ranking of the aggregates.

Table 7.21 shows the new ranking of the aggregates by their rock and aggregate properties. Comparing with Table 7.6, only three changes in the ranking of the aggregates occurred. In both ranking schemes these three cases were at the borderlines of the two categories. In general, the sandstone and gravel are the best and the soft limestone and lightweight aggregates the worst.

The selected performance tests on specimens prepared to in-place air voids are ranked in Table 7.22. The ranking for the CMHB-C mixes are similar to those of all tests shown in Table 7.7 except that hard limestone changed from Average (marginally) to below average (marginally). The gravel ranked first followed by the sandstone. For the Superpave-C mix, two changes in the rankings were observed relative to the original ranking. Again, the sandstone and gravel were ranked the highest. For the PFC mixes, the sandstone, gravel and lightweight aggregates ranked similarly and above average. Once again, two of the rankings changed by one level.

To evaluate the results of the aggregate-related tests to performance tests, the rankings from the two tests are compared in Figure 7.1. For a desirable outcome, the results should be concentrated in the lower left and upper right quadrants. A point in the upper left quadrant is considered a false negative condition (considering the aggregate as above average, when the performance is below average). Similarly a point in the lower right quadrant is considered a false positive (considering the aggregate as below average, when the performance is above average). Both of these two conditions are undesirable. Based on the rock tests alone, there are two false negatives. CHMB-C and PFC performed poorly with hard limestone. The aggregate tests do not contain any false negatives. However, it contains one false positive. The PFC shows good performance for light weight aggregate. The traditional tests provide two false negative results. Again, the CHMB-C and PFC mixes performed poorly with the hard limestone aggregate. Based on the three comparisons, the most robust tests are the aggregate tests.

The next issues are the sensitivity of the tests considered and the sensitivity of the performance tests to the change in the properties of aggregates. To evaluate these two issues, the normalized summation of scores in Tables 7.21 and 7.22 were first normalized and then plotted against one another in Figure 7.2. The normalization of the scores was carried out by dividing each score by the average of the scores measured for that case. Since the trends are around the line of equality, it can be concluded that the aggregate-related tests are a reasonable predictor of the performance tests. The more spread the normalized scores for the aggregate-related tests are, the more sensitive to ranking of the aggregates they will be. The spread can be visually assessed from the figure. To quantify further, the coefficient of variation (COV) of the scores for each test method

Table 7.21 – New Ranking of Aggregates from Selected Tests

a) Rock Tests Only

Aggregate	Summation of Ranks	Qualitative Ranking
Hard Limestone	7	Above Average
Granite	9	Average
Soft Limestone	12	Significantly Below Avg. (Below Avg.)*
Sandstone	8	Above Average

b) Aggregate Tests Only

Aggregate	Summation of Ranks	Qualitative Ranking
Hard Limestone	17	Average
Granite	20	Average
Soft Limestone	23	Below Average
Sandstone	15	Average
Gravel	11	Above Average
LW Aggregate	25	Below Average

c) Traditional Tests Only

Aggregate	Summation of Ranks	Qualitative Ranking
Hard Limestone	8	Average
Granite	11	Average
Soft Limestone	12	Below Average (Significantly Below Avg.)
Sandstone	10	Average
Gravel	6	Above Average
LW Aggregate	9	Average

d) All Selected Tests

Aggregate	Summation of Ranks	Qualitative Ranking
Hard Limestone	32	Above Average (Average)
Granite	39	Average
Soft Limestone	48	Below Average
Sandstone	31	Above Average
Gravel	26	Above Average
LW Aggregate	51	Below Average

*** Ranking in the parenthesis are those from Table 7.6.**

Table 7.22 – New Ranking of HMA Based on Selected Performance Tests on Specimens Prepared to In Place Air Voids

a) CMHB-C

Aggregate	Summation of Ranks	Qualitative Ranking
Hard Limestone	11	Below Average (Average)
Granite	9	Average
Soft Limestone	11	Below Average
Sandstone	7	Above Average
Gravel	5	Above Average
LW Aggregate	11	Below Average

b) Superpave-C

Aggregate	Summation of Ranks	Qualitative Ranking
Hard Limestone	10	Average
Granite	9	Average
Soft Limestone	11	Below Average
Sandstone	7	Above Average
Gravel	8	Above Average (Average)
LW Aggregate	10	Average (Below Average)

c) PFC

Aggregate	Summation of Ranks	Qualitative Ranking
Hard Limestone	7	Below Average
Granite	7	Below Average
Soft Limestone	8	Below Average
Sandstone	5	Above Average (Sig. Above Avg.)
Gravel	5	Above Average (Average)
LW Aggregate	4	Above Average

d)Type-D

Aggregate	Summation of Ranks	Qualitative Ranking
Hard Limestone	8	Above Average
Granite	11	Average
Soft Limestone	12	Average (Below Average)
Sandstone	7	Above Average
Gravel	6	Above Average
LW Aggregate	10	Below Average (Average)

*** Ranking in the parenthesis are those from Table 7.8.**

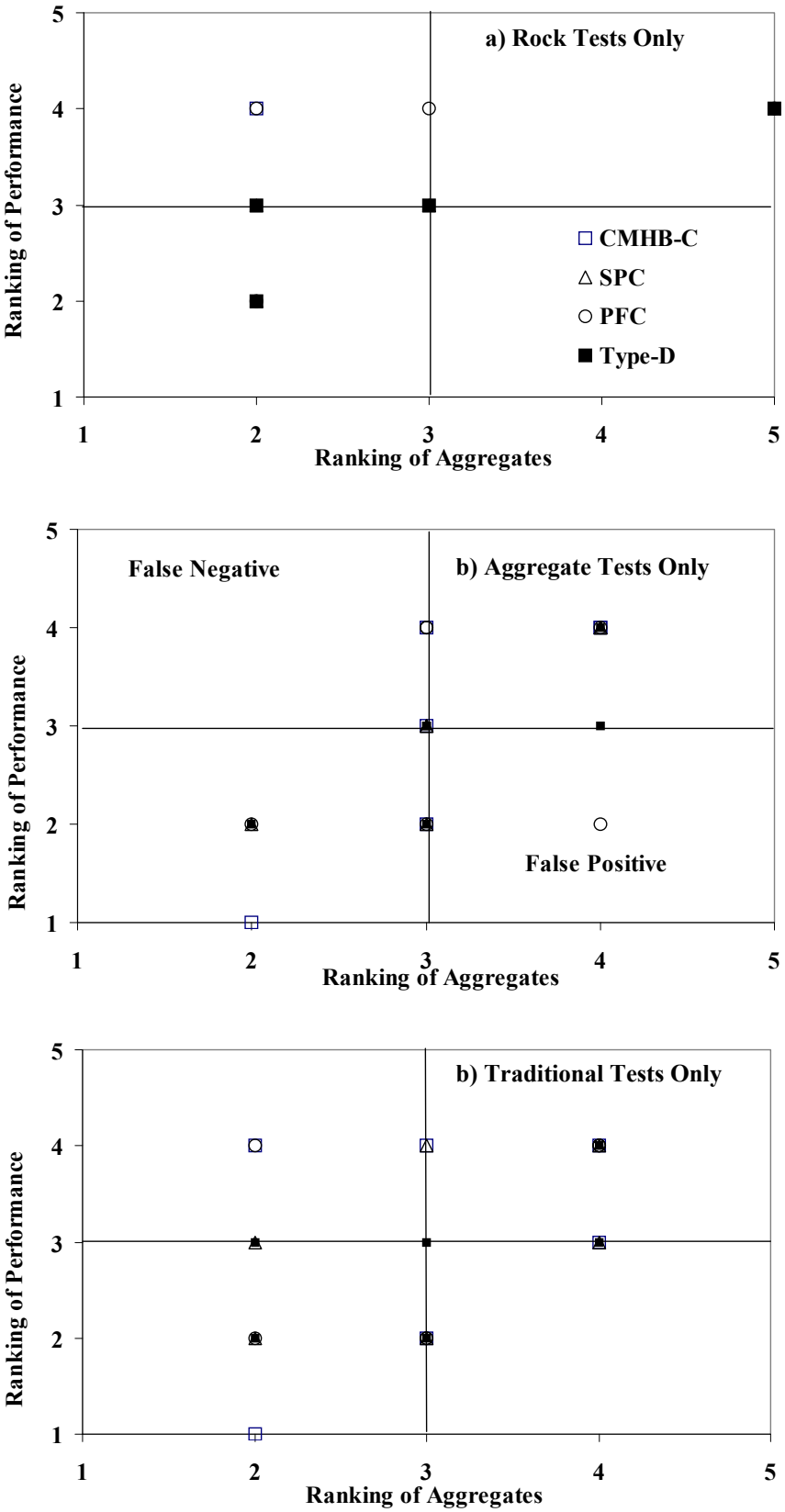

Figure 7.1 – Comparison of Ranking of Aggregate-Related Tests with Ranking of Performance Tests

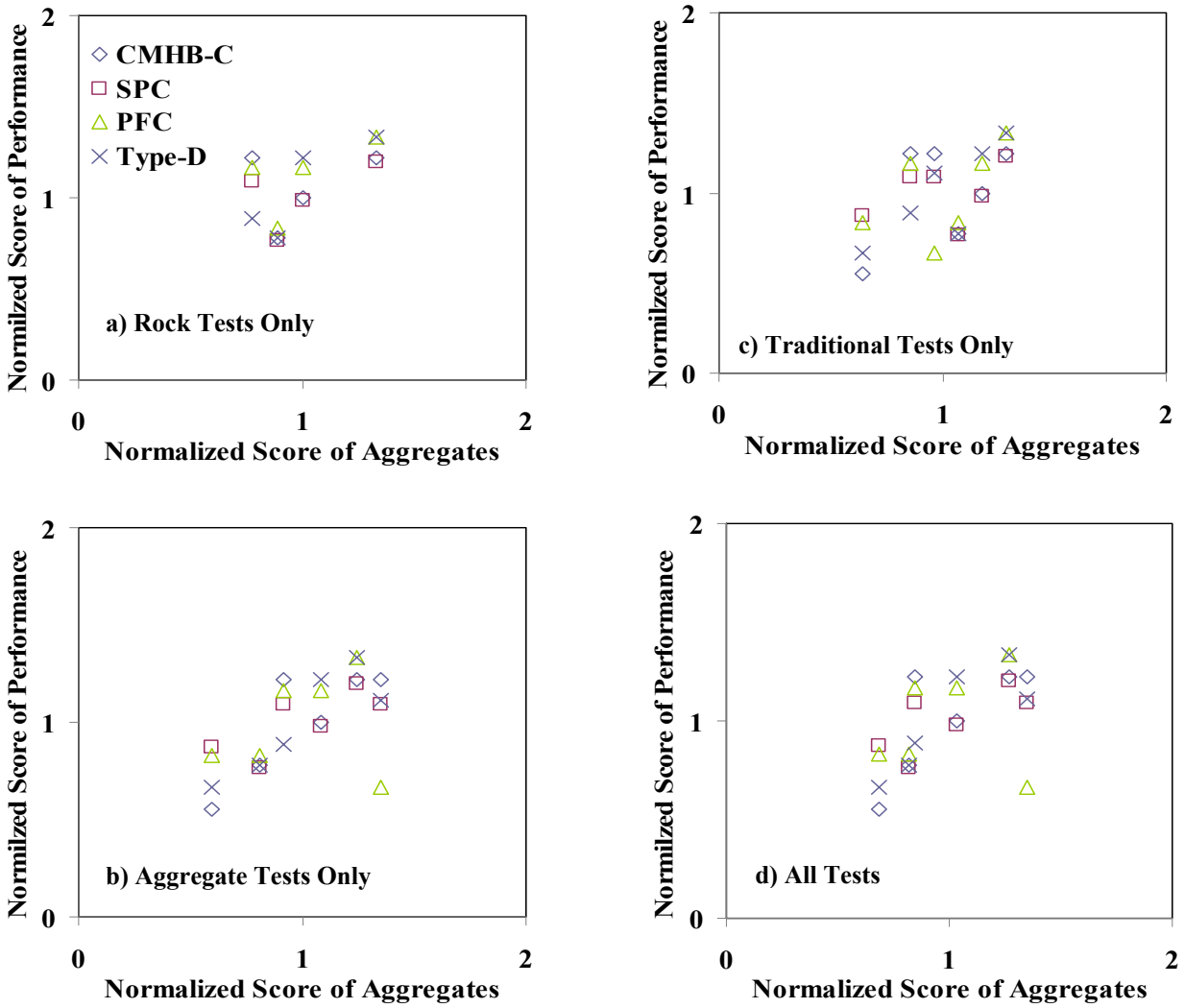

Figure 7.2 – Comparison of Scores of Aggregate-Related Tests with Scores from Performance Tests

is shown in Figure 7.3. For the data set available, the COV's of the aggregate-related tests are between 24% and 28%, indicating that the test methods are almost equally sensitive. The COV of the rock test are lower than others because it does not contain the properties of the lightweight aggregates (the weakest) and gravel (one of the strongest). We feel that if the database is expanded, the rock properties will be more sensitive than the others.

The COV's of the performance tests are also shown in Figure 7.3. The smaller the COV for the performance tests, the least sensitive the performance is to the aggregate quality. Based on Figure 7.3, the Superpave-C mixes are less sensitive to the quality of the rock. The CMHB-C, Type D and PFC are almost equally sensitive to the properties of the rock. The COV of the PFC mixes are counterintuitively lower than the CMHB-C. This occurs because the performance tests selected for the PFC as per the state-of-practice may not be as appropriate for the PFCs with air void contents of 20% as they are for more densely compacted CMHB-C mixes.

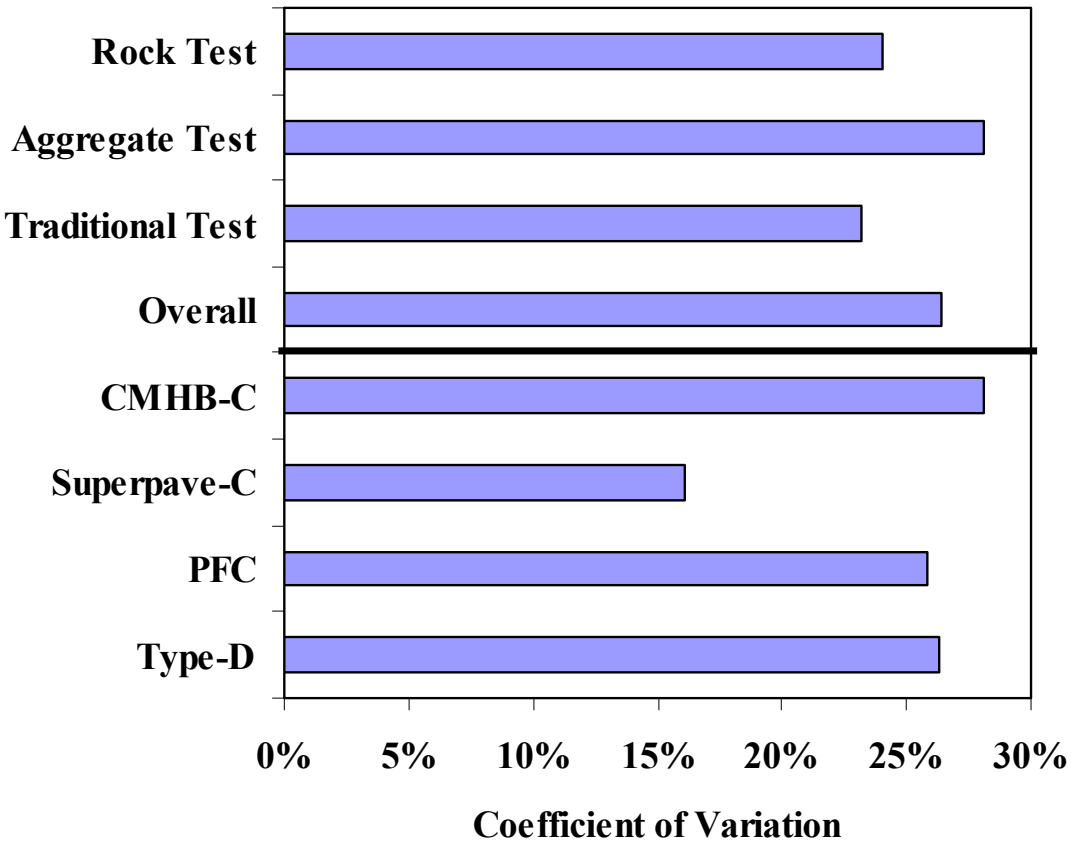

Figure 7.3 – Coefficients of Variations of Different Test Categories

CHAPTER EIGHT - CLOSURE AND RECOMMENDATIONS

SUMMARY

The performance of the new generation of HMA mixtures relying more on a stone-on-stone contact is greatly influenced by the properties of the aggregate blends such as gradation and strength. As a result, aggregates have a significant and direct effect on the performance of asphalt pavements and it is important to maximize the quality of aggregates to ensure the proper performance of roadways.

The objective of this research is to evaluate the effect of stress concentrations at contact points on coarse aggregates that could cause aggregate fracture. To achieve the objectives, an extensive series of tests from geological evaluation of quarries and rocks retrieved from them, to rock strength tests, to traditional and new aggregate tests, to geotechnical strength tests were carried out on six aggregates to rank them. To establish the performance of mixes, specimens of four different mix types were prepared and subjected to a number of performance-related tests. The laboratory activities were supplemented with micro-mechanical modeling to understand the internal behavior of the mixes. Through correlation and statistical analyses, the redundant aggregate-related and performance-related tests were identified and the optimum test methods were recommended. Based on these activities, several tests for characterizing and ranking aggregates and mixes were proposed.

CONCLUSIONS

Aggregates were first ranked according to their performance when subjected to 27 characterization parameters. The ranking was based on three categories of tests (aggregate properties, rock properties, and shape and texture properties) in order to further understand the impact of each method. From such ranking, the following conclusions were drawn:

- From the aggregate properties, gravel ranked above average, hard limestone, granite and sandstone ranked average, and soft limestone and the lightweight aggregate ranked below average.
- From the rock properties, the hard limestone and sandstone ranked above average and granite ranked average. Soft limestone ranked below average. The gravel and

lightweight aggregates could not be subjected to rock tests because they are not originated from rock masses.
- As per the traditional shape and texture tests, the gravel ranked above average, the hard limestone, granite, sandstone and lightweight aggregate ranked as average, with once again the soft limestone being the worst, ranking below average.
- In general, the sandstone and gravel were the best, the hard limestone and granite ranked average, and the soft limestone and lightweight aggregate ranked the worst.

In order to determine which of the tests are the most representative for the characterization of the aggregates, correlation analysis amongst the tests was performed. From this analysis, the following observations are provided:

- From the tests characterizing the aggregate point and bulk strength results, the ACV test and its surrogate parameters were found to correlate well with most of the tests. As a result, the ACV test seems to be the most appropriate test for characterizing the aggregates, especially since several parameters can be readily determined from the same test and the cost of implementing this test in Districts owning a concrete compressive test machine would be insignificant.
- The compressive strength obtained using the Schmidt hammer seems to be the most appropriate test for characterizing this parameter. This test is not only easier and faster than the compressive strength test, but also eliminates the need for coring the rock and requires minimal training.
- The V-meter seems to be an appropriate tool for estimating the modulus as well as the quality of the aggregates in tension. No coring of rock is necessary to perform this test on the rock samples.
- From the traditional tests, the Los Angeles Abrasion test, Mg Soundness test, the Micro-Deval test, and AIMS angularity after Micro-Deval are appropriate.
- The same exercise was carried out on the performance tests. For the purpose of this study, the indirect tensile test and the modulus with the V-meter, and Hamburg Wheel Tracking Device seem to be optimal for characterizing the performance of the HMA.

An approach for modeling the response of HMA mixes was developed in this study. The aggregate properties (stiffness, compressive strength and tensile strength) were determined by matching the model results to experimental measurements conducted on aggregate samples. The model was used to predict the mix response under different loading conditions. The results show that the failure in the soft limestone mixes occurs primarily within the aggregate phase, while the failure in the other mixes occur in the mastic phase. The model was used to investigate the stress or load distributions within the different mixes. The PFC mixes are shown to have more localized high stresses within the aggregates than the Superpave and CMHB mixes. This finding indicates that aggregates with higher resistance to fracture need to be used in PFC mixes.

A database of the information was obtained and a ranking scheme was implemented that can be readily used to rank the aggregates. Based on the average value of each parameter and the coefficient of variation of the test associated with that, parameters for the acceptance limits can be set rationally considering the aggregate sources available to TxDOT. However, more aggregate types are needed to set the limits.

RECOMMENDATIONS

It should be emphasized that these observations are preliminary since the database is rather small. As a result, it is proposed to expand the database with more aggregate sources.

The new tests, such as the ACV, should be implemented by the TxDOT Construction Division and select Districts to ensure their usefulness for TxDOT.

REFERENCE

1. Al-Rousan, T. M. (2004), "Characterization of aggregate shape properties using a computer automated system," PhD Dissertation, Texas A&M University, College Station, Tex.
2. Alvarado, C. (2007), "Feasibility of Quantifying the Role of Coarse Aggregate Strength on Resistance to Load in HMA," Master of Science Thesis, University of Texas at El Paso.
3. Brown, E.R, and J.E. Haddock (1997), "A Method to Ensure Stone-on-Stone Contact in Stone Matrix Asphalt Paving Mixtures," National Center for Asphalt Technology, Auburn University. NCAT Report No. 97-2.
4. Chandan, C., Sivakumar, K., Masad, E., and Fletcher, T. (2004), "Application of imaging techniques to geometry analysis of aggregate particles," Journal of computing in civil engineering, 75-82.
5. Cheung, L.W, and A.R. Dawson (2002), "Effects of Particle and Mix Characteristics on Performance of Some Granular Materials," Transportation Research Record 1787, Transportation Research Board, National Research Council, Washington, DC; pp. 90-98.
6. Cundall, P. A., and R. Hart (1992), "Numerical Modeling of Discontinua," J. Engr. Comp., 9, 101-113.
7. Hand, A.J., J.L. Stiady, T.D. White, A.S. Noureldin, and K. Galal (2002),"Gradation Effects on Hot-Mix Asphalt Performance," Association of Asphalt Paving Technologists, Vol. 70, pp. 132-175.
8. Mahmoud, E. M. (2005), "Development of Experimental Methods for The Evaluation of Aggregate Resistance to Polishing, Abrasion, and Breakage," Master of Science Thesis, Texas A&M University, College Station, Tex.
9. Masad, E., D. N. Little, L. Tashman, S. Saadeh, T. Al-Rousan, and R. Sukhwani (2003), "Evaluation of Aggregate Characteristics Affecting HMA Concrete Performance," Research Report ICAR 203-1, The Aggregate Foundation of Technology, Research, and Education, Arlington, VA.
10. Öztas, T., K. Sönmez, and M.Y. Canbolat (1999), "Strength of Individual Soil Aggregates Against Crushing Forces. I. Influence of Aggregate Characteristics," Journal of Agriculture and Forestry, Vol. 23; pp. 567-57.
11. Prowell, B.D., J. Zhang., and E.R. Brown (2005), "Aggregate Properties and the Performance of Superpave Designed Hot Mix Asphalt," NCHRP Report 539, Transportation Research Board, National Research Council, Washington, DC.

12. Wu, Y., F. Parker, and P.S. Kandhal (1998), “Aggregate Toughness/Abrasion Resistance and Durability/Soundness Tests Related to Asphalt Concrete Performance in Pavements,” Transportation Research Record 1638, Transportation Research Board, National Research Council, Washington, DC. pp. 85–93.

APPENDIX A - GEOLOGICAL ASPECTS OF AGGREGATES

The geological aspects of the three Phase I aggregate sources were described in Research Report 5268-1. Due to the importance of the mineralogical aspects of aggregates, that section is repeated here verbatim. Information about the three new aggregates is also added.

DESCRIPTION OF MATERIAL SOURCES

Hard Limestone Quarry

The hard limestone Quarry is operated by Vulcan Materials Inc and located in Brownwood, Texas where the Pennsylvanian Cisco Formation is mined. The quarry has a large surface area, but only a 25-40 ft thick layer of acceptable limestone. The quarry floor is a thick shale that underlies the limestone and the top is soil that forms the surficial outcrop of the limestone. The Limestone is generally pale gray. Soil processes have tinged the upper 1-3 ft of limestone a tan or orange color. The entire unit thins and pinches out through stratigraphic thinning within half a mile in the northeastern part of the quarry, being replaced by the overlying dark gray shale bed within the same formation, which is not mined.

The entire limestone unit is quarried. Within this, four slightly different layers were noted and specimens were collected from each. Figure A.1 illustrates the layers sampled. The top of the outcrop is approximately 25 ft above the quarry floor. The lowest layer (unit 1) is a dark gray lime mudstone. This is pure limestone, but composed of microscopic (Microcrystalline) crystals that allow the rock to break with smooth curving fractures. The basal layer is approximately 1 ft thick, but above this, thin shale (clay) partings separate the lime mud into layers 3-6 in thick. The layers gradually thicken and become lighter upward until they transition into unit 2.

Unit 2 is a lighter gray lime mud, thicker bedded and more widespread than unit 1. Most of the unit is composed of a 3 ft thick bed of the mud. The entire unit thins and disappears to the northeast, although it continues farther than unit 1. Unit 3 is a grainstone; a limestone composed of large crystals that essentially acted as sand grains when the limestone was deposited. Fossils are common in this unit, the most common being crinoid stems. This unit is darker grey than the underlying lime mud and is continuous throughout the quarry. It forms the base of the quarried interval in the northeastern part of the quarry. The layers in the unit are 0.5 ft to 1 ft thick and pinch and swell in the quarry wall. Unit 4 is a sandy limestone with sparse quartz sand grains disseminated though the bed.

Figure A.1 – Hard Limestone Quarry

interspersed with the limestone grains. The unit is generally tan in color from overlying soil. It is resistant to erosion and the bed holds up the hill in which the quarry is developed. Layers are 0.5 to 2 ft thick. Beds of concentrated fossils are evident in the middle of the layer. Crinoid stems are the most common.

Granite Quarry

The granite quarry is located in El Paso, TX at the McKelligon Canyon plant operated by CEMEX. It exposes a fractured and faulted edge of granite mass. The granite is essentially uniform and, except for alteration along fractures, is granite with ¼ to ½ inch crystals of potassium feldspar, plagioclase feldspar, quartz and amphibole minerals. There is greenish and yellowish hydrothermal alteration along some of the fractures, but it does not penetrate into the wall rock of the fractures. The uppermost rock is weathered and weakened by the overlying soils. Several samples were collected to document the slight variations present. The main pink granite, the darker granite that forms patches on the north and south walls (Figure A.2) and a sample of the hydro-thermally altered material were sampled for testing.

Figure A.2 - South Wall of the Granite Quarry

Soft Limestone Quarry

The soft limestone quarry is operated by Martin Marietta Materials and located at the Beckman plant near San Antonio, TX and is quarried from the Edwards Limestone. The quarried section is at least 150 ft thick. The interval currently being quarried and the interval sampled for this study is the lower 80 ft of the section (Figure A.3). The entire quarry consists of 10 layers of thick limestone separated by thin layers of tan and red shale. Several caves, filled with red sand and mud are evident in the quarry walls. There are also many fractures that show red and tan muds and where the limestone has been dissolved.

Three types of limestone are evident and were sampled (Figure A.4). The basal part of some layers is composed of a limestone, containing numerous mollusk fossils. This layer is formed of interlocked crystals 1/16 in. to ½ in. in diameter. The second rock type makes up the bulk of each layer. This layer is a light beige colored lime mudstone. This is pure limestone, but composed of microscopic crystals that allow the rock to break with smooth curving fractures. This limestone contains numerous large irregular open cavities, called vugs, which are lined with large calcite crystals. The upper part of each layer is a yellowish sandy limestone that contains scattered quartz grains intermixed into the limestone The interval forms more distinct layers and varies internally more than the underlying layers.

Sandstone Quarry

The sandstone quarry is operated by Capitol Aggregate and located in Brownlee, TX. The sandstone quarry, which is developed in the Cambrian Cap Mountain Sandstone, is a 150 ft-thick carbonate-cemented feldspathic sandstone. The sandstone is a dark gray, medium grained sandstone that grades down into a feldspar-rich, sandstone with a greater density of shale interbeds. The sandstone in the quarry is folded into an open anticline, and the resistant cap of the quarried sandstone forms a hard cap that forms the hill slope in most of the quarry area.

The quarried strata can be divided into three layers (Figure A.5). The upper 15 to 45 ft is a more carbonate rich resistant caprock that is better cemented than the underlying sandstone (Figure A.5). The basal section is composed of a tan layer that appears different than the overlying strata. Accessible samples for coring and a thin section from this horizon were not able to be

Figure A.3 - Soft Limestone Quarry

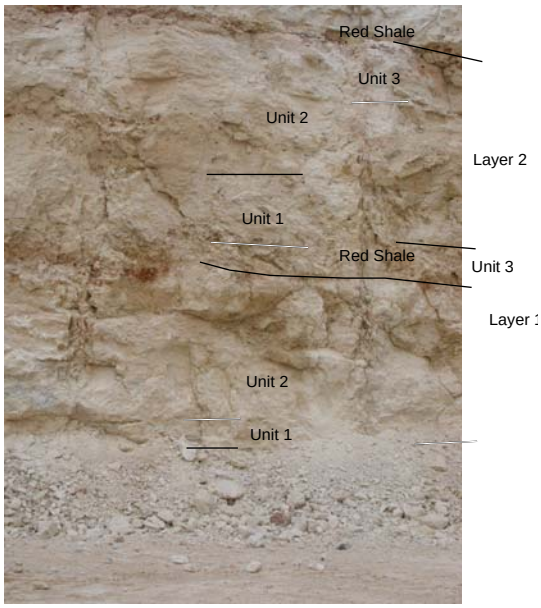

Figure A.4 - Detail Showing Units for Layers in Soft Limestone Quarry

found. The quarry operator indicates this is not depositional differences, but only a weathering feature. The central 30 m of the quarry is formed of alternations of thickly bedded gray cross-stratified sandstone and ripple cross-stratified sandstone with thin shale partings (Figure A.5). The units form upward coarsening sequences, with the shale partings becoming less abundant and finally disappearing and the sandstone becoming coarser upward into the massive cross stratified sandstone.

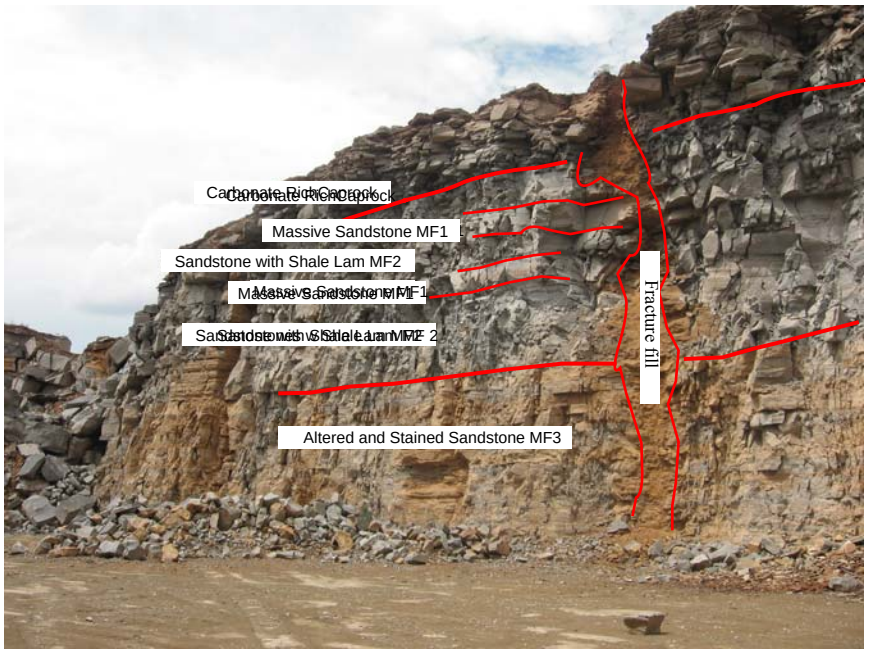

Figure A.5 – Stratigraphy of Sandstone Quarry

Cutting across the entire quarry are vertical, irregularly sided fractures filled with loose tan sand (Figure A.5). The sand is unlithified and the fractures are solution widened. Evidently the sand is a recent fill of fractures formed by dissolution of the carbonate cemented sandstone. The sand is similar to the soil above the quarry and probably was washed in from the surface.

Gravel Quarry

The gravel aggregates are mined by Fordyce Co. and located at Murphy Plant, TX. The hard gravel quarry is located along the Guadalupe River in the Texas Gulf Coastal plain. The gravel is being mined from terraces that flank the river. The quarry mines sands and gravels that were deposited by the river earlier in its history and are derived from distant outcrops. The deposits consist of three to four stacked channel fills that underlie the terrace (Figure A.6). Gravel lenses range from 1 to 3 m thick and contain a wide variety of sizes. According to the operators, coarse sand and gravel form approximately 10% of the deposit. Coarser gravel lenses within the deposit are cemented to rock with calcite cement (Figure A.7). The gravel is crushed for aggregate to provide rough surfaces.

Samples were collected from the 1 ½" to 6" pile; they consist of 80 to 90 percent chert. Four different chert types were identified. The remainder is limestone; two types are prevalent, tan micrite or lime mudstone, and gray coarsely crystalline limestone.

Lightweight Aggregate Plant

The lightweight aggregate is produced by Texas Industries (TXI) and located at the Streetman, TX plant. The shale aggregate quarry is developed in the Midway Shale, a Paleocene, dark gray marine shale. The shale is mined and cooked at over 2,000º F. The shale is then transformed into a gray, hardened low density aggregate. The quarry is developed in three benches. The lowest is not being mined as quartz (silica) content is higher and the aggregate that would be produced from this bench does not meet current TXDOT specifications. The upper two benches are mined for shale.

The benches are relatively homogenous (Figure A.8) except for calcium carbonate nodules that may reach up to 3 m long and 0.75 m across. The nodules are screened out prior to cooking of the shale. The two quarried benches are relatively homogenous and cannot be subdivided on inspection. Due to the the transformation of the shale during processing, no samples were collected, as these would not be representative of the product. Samples were collected from each bench for X-ray spectrographic analysis.

PETROGRAPHIC ANALYSIS

Hard Limestone Quarry

Samples from units 2 and 3 were studied together. These form the bulk of the quarried limestone shown in Figure A.1. Unit 2 is a lighter gray lime packstone-wackestone with small fossils, thicker bedded and more widespread than unit 1 in the quarry. Figure A.9 illustrates an 8 in. polished slab of Unit 2 material showing the void filling texture and the fossils floating in a mud

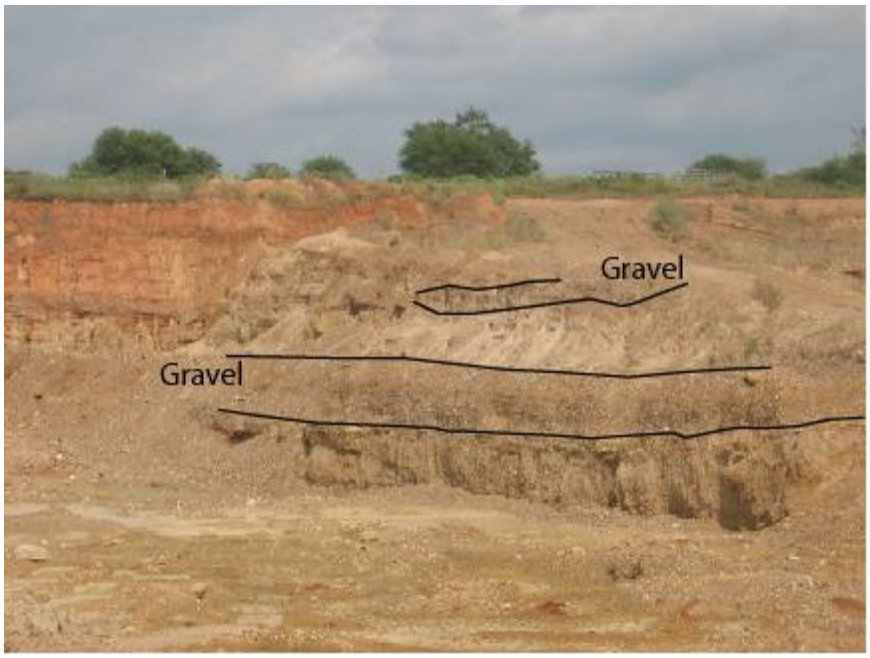

Figure A.6 - Stratigraphy in the Gravel Quarry

Figure A.7 - Characteristics of the Gravels Mined from Quarry.

Figure A.8 - Upper Bench at the Shale Quarry

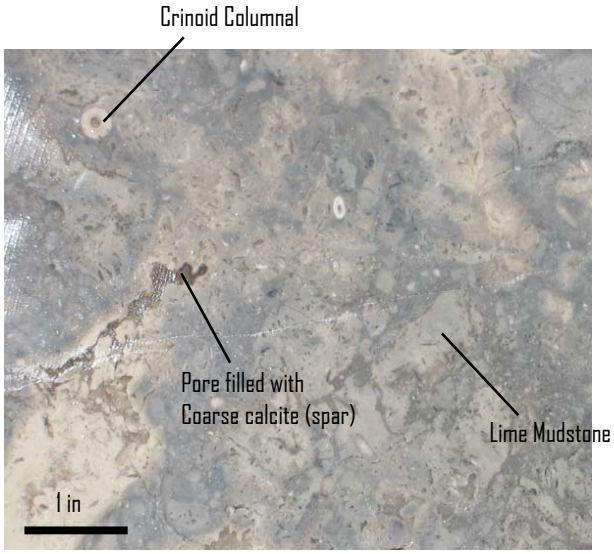

Figure A.9 - Polished Slab of Unit Two from the Hard Limestone Quarry

matrix. In polished slabs and thin sections, the unit is composed of fossils that have been micritized. The open interiors of the fossils were filled with void filling calcite spar. The original rock matrix is dominantly filled with lime mudstone.

There is very little evident porosity, accounting for the hard nature of the limestone. Almost all the porosity is molds where fossil fragments have been dissolved. A photomicrograph of the middle of unit 2 in Figure A.10 shows the typical lack of porosity in this formation. Light colored areas in the figure are filled fossil fragments. Dark matrix in the figure is lime mud (micrite). The arrow points to a blue ring in the center which is a pore that formed through dissolution of a brachiopod spine. Letters "M" indicate some of the molds filled with coarsely crystalline calcite. The field of view is 1.2 mm. The only visible pore is a mold around a brachiopod spine in the center of the photo. The fossil fragments have been replaced with calcite

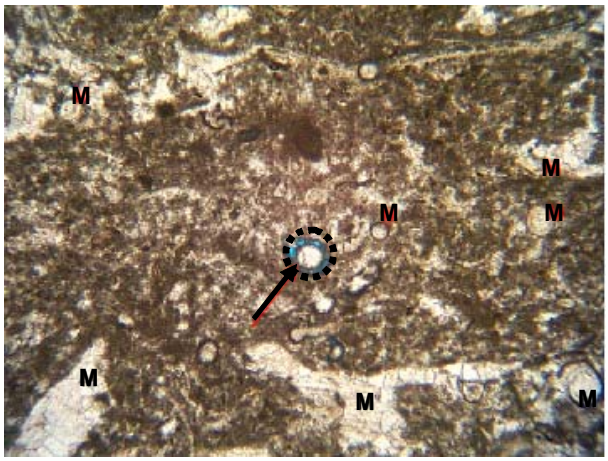

Figure A.10 - Photomicrograph of the Interior of Unit 2

spar and the matrix between them is composed of micrite, (calcite mud). The field of view from Figure A.10 is 0.8 mm. The sample is composed of 45% micrite and 30% spar that fill the molds. Another 13% is micritized shells and 10% spar filling irregular vuggy pores. The remaining 2% is filled with fossil molds.

Unit 3 is a grainstone/packstone; a limestone composed of large crystals that essentially acted as sand grains when the limestone was deposited. Fossils are common in this unit, the most common being crinoid stems brachiopods and fusulinids. This unit is darker grey than the underlying lime mud and is continuous throughout the quarry. It forms the base of the quarried interval in the northeastern part of the quarry. The layers in the unit are 0.5 ft to 1 ft thick and pinch and swell in the quarry wall.
The petrography supports the macroscopic interpretation. Diverse fossils are cemented with lime mud and spar creating a dense limestone without microscopically visible pores as shown in Figure A.11. The vuggy pore filled with blue epoxy is large, but because these are rare, they make up only 1% of the sample. The laminar of coarser and finer grained material in this unit will probably make it less brittle than the underlying micrite. About 37% of the sample is micrite while 22% is micritized fossil fragments. However, in contrast to unit 2, only 11% of the sample is sparry mold fill, whereas 28% is interstitial spar that fills the spaces between the fossils. Another 1.1% is unaltered bioclasts. The photomicrograph of unit 3 (Figure A.11) shows micritized fossils cemented together by calcite spar. The field of view from Figure A.11 is 1.2 mm.

Granite Quarry

All the granite samples showed fracturing and filling of fractures with what is probably hematite and clay, followed by quartz (Figures A.12 and A.13). The sample shown in Figure A.12 is 10 inches across. The dark lines shown in the figure are fractures. The granite selected as being darker and more fractured exhibited denser and more frequent fracturing. The granite was dominantly composed of large crystals (up to 0.8 in. in cross section) of microcline potassium feldspar. Microcline composed 59 to 63 percent of the two thin sections. Quartz crystals formed 9 to 17 percent of the samples, being lower in the more highly fractured sample. Plagioclase

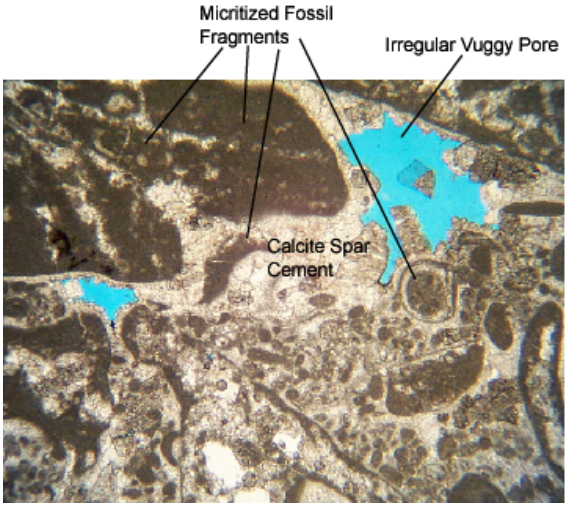

Figure A.11 - Photomicrograph of Unit 3

formed less than 2 percent of each sample and hornblende formed 1 percent of the slides. Alteration products formed 15 to 20 percent of each slide. In the less highly disturbed sample, fractures filled with iron-oxide and shattered grains formed 17 percent of the sample. In the more highly fractured sample, almost all the grains were fractured with hairline, iron-oxide filled cracks (Figure A.13). However, these only formed 6 percent of the sample. Quartz filled fractures formed another 6 percent of the sample and clay filled fractures formed 3 percent of the sample. Thus, 15 percent of the sample was fracture fill. An additional 6 percent of the sample was composed of iron oxide alteration in irregular vugs and 2 percent was open porosity. The field of view is 1.2 mm

Soft Limestone Quarry

The soft limestone quarry exposed repeated layers of limestone, each containing two units. The basal part of some layers is composed of lime sandstone, containing numerous mollusk fossils. The layer is formed of interlocked crystals 1/16 in. to ½ in. in diameter. Unit 1 forms the lowest 1-2 ft of the sampled unit (see Figure A.4).

Figure A.12 - Polished Slab of Granite

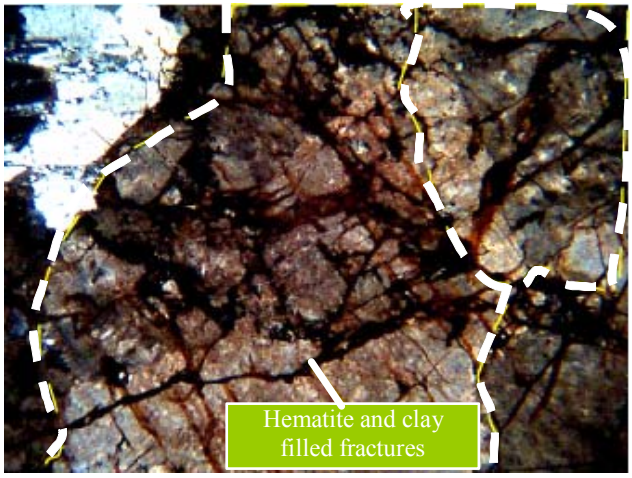

Figure A.13 - Photomicrograph of a Large Fractured Microcline

Petrographically, unit 1 is a pure limestone (Grainstone in Dunham classification scheme), with abundant mollusk and algae fossils as well as peloidal grains (Figure A.14). The fossils had been micritized and the matrix is coarse grained calcite spar. The only porosity present was large irregular late stage dissolution pores shown as darker spots. Micritized fossils form 55% of the sample whereas un-micritized fossil clasts form 15 % of the sample. Coarse Spar cement forms 19 percent of the samples while Peliods forms 6.6 percent of the sample. Porosity forms only 2.6 percent of the thin section in contrast to the overlying unit 2.

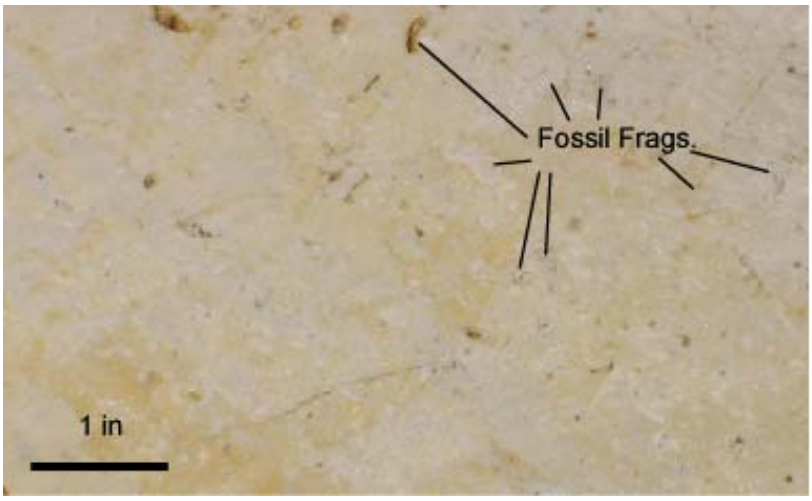

Figure A.14 - Polished Slab of Unit 1 in the Soft Limestone

Figure A.15 shows the photomicrograph of unit 1 showing the abundant fossils separated by sparry cement. The photo is 0.8 mm across and the isolated pores are stained blue. The field of view is 1.2 mm. Letters show features described in texts. Letters “f” show some of the visible fossil fragments; letters “c” show coarse calcite spar cement, and letters “p” show porosity filled with blue stained epoxy.

The second rock type makes up the bulk of each layer. This layer is a light beige colored lime mudstone with a few scatted fossils (Mudstone in the Dunham classification scheme). This is

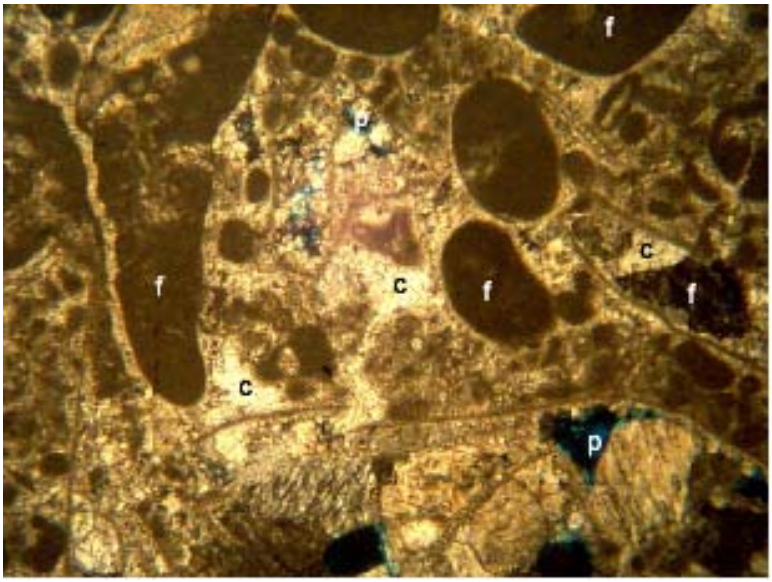

Figure A.15 - Photomicrograph of Unit 1 with Abundant Fossils

pure limestone, but composed of microscopic crystals that allow the rock to break with smooth curving fractures (Figures A.16 and A.17).

Petrographically, the limestone shows abundant micro-porosity where small calcite crystals had been dissolved. Large irregular vugs are also present. However, the most important porosity is the lenticular fracture pores that crosscut the sample (Figures A.16 and A.17). In Figure A.16, the Fractures appear as lighter colored lines. This rock is probably the weakest of the entire sample because of the porosity at all scales. The slab illustrated in Figure A.16 is 10 inches across while the field of view in Figure A.17 is .03 inches. In Figure A.17, porosity appears as blue stained epoxy. Micro-porosity appears as tiny blue spots. Fractures are blue lines that cross

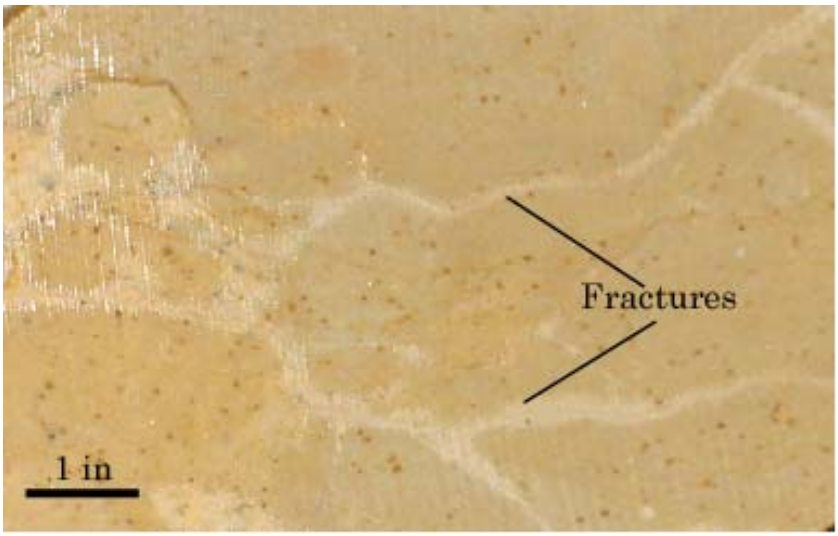

Figure A.16 - Polished Slab of Unit 2 Showing Fractures and Vuggy Porosity Widened by Solution

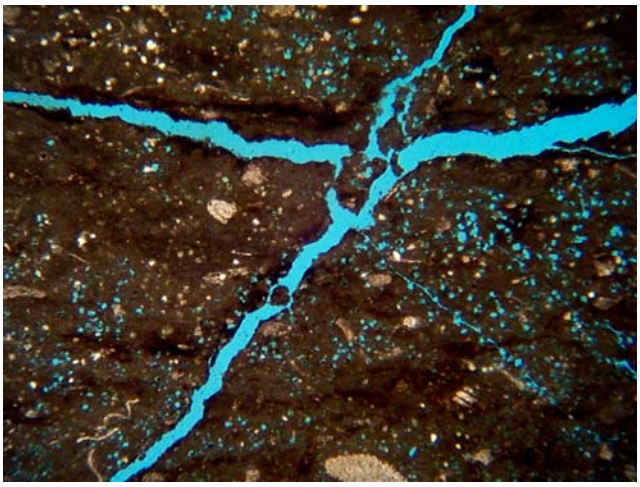

Figure A.17 - Photomicrograph Showing Solution Widened Fractures and Micro Porosity due to Dissolution of Grains in the Dark Micrite

the slide. The field of view is 1.2 mm. Porosity forms a total of 19 percent of the sample, with 11% of this being micro porosity and 8 percent of the slide being large solution widened fractures and vugs. Micrite forms 67 percent of the sample and small patches of pores form 12 percent of the samples. Biotic clasts make up 0.5 percent of the slide and small oxide spots, probably altered pyrite grains, make up 2.5% of each sample.

Sandstone Quarry

The bulk of the hard sandstone was composed of carbonate cemented sandstone interbedded on a micoscopic scale with sandy dolomite and sandy limestone. Patches of highly compacted sandstone make up approximately half of the thin section (Figure A.18). The rest of the thin section is composed of a sandy carbonate, approximately 60% calcite and dolomite crystals enclosing small patches of sand grains. The detrital grains are well sorted and average 0.157 mm in diameter (2.7 phi, from 100 measurements). The sandstone is quartz rich and only 4% of the grains are potassium feldspar.

For the entire thin section, Quartz composes 44% of the thin section, with feldspar grains forming another 4%. Dolomite cement is the next most common at 25%. The dolomite cement is a diagenetic replacement of grains and earlier cements, and formed in several distinct generations. Very large crystals >0.5 mm are intergrown with very small (0.1 to 0.01 mm) crystals. Detrital clay 13% occurs as thin lenses within the sandstone. Calcite 12% occurs in irregular patches intergrown with the dolomite. Detrital grains of glauconite, a green iron-rich clay make up the remaining 2% of the thin section.

Interbedded with the sandstones are sandstones with shale interbeds (MF-2 in Figure A.5). These are properly siltstones as the grains are 0.01-0.03 mm diameter. There is much less diagenetic alteration. Detrital clay forms 52% of the thin section and coarse-silt sized quartz forms 42% of the sample (Figure A.19). A thin bed of diagenetic calcite forms 6% of the sample.

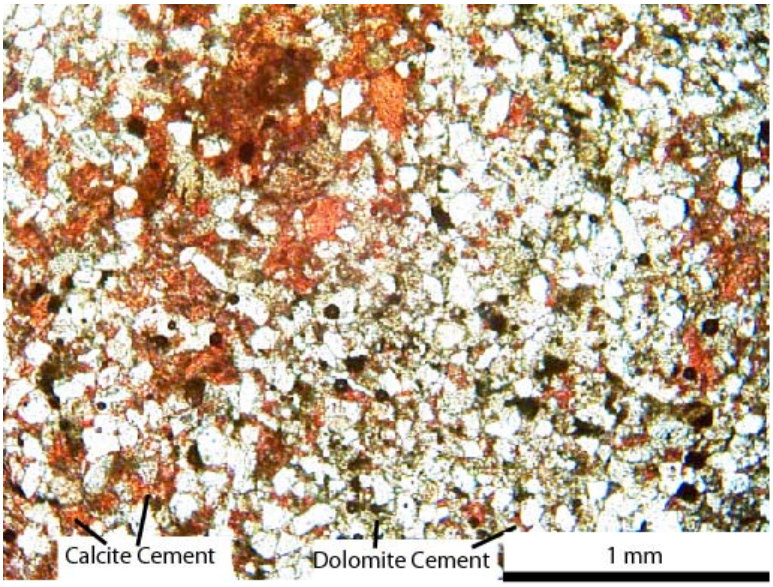

Figure A.18 - Sample 1: Calcite and Dolomite Cemented Sandstone.

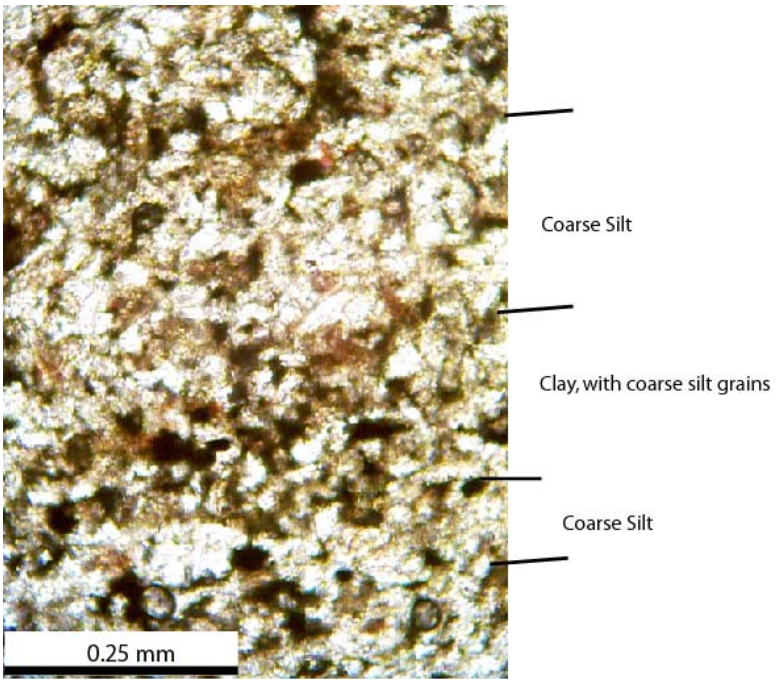

Figure A.19 - Laminated Clay and Coarse Silt that Make Zones Labeled MF-2 in Figure A.5.

The altered zone at the base of the quarry consists of thin laminations of sandstone in a dolomite (Figure A.20). The sediment contains very coarse sand grains and was deposited as a depositional lag. It is much more porous and carbonate-rich than the overlying sandstone, and Detrital Quartz forms only 15% of the sample. Large, irregular secondary pores make up 8% of the sample and the remainder is carbonate cement. Some 1-mm thick layers in the thin section contain highly altered microfossils composed of microcrystalline calcite (Figure A.19).

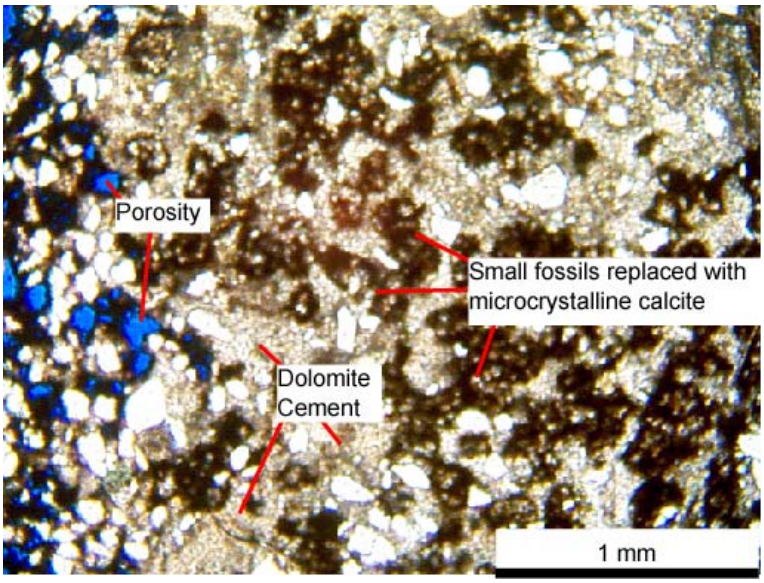

Figure A.20 - Photomicrograph of Altered Zone at Base of Hard Sandstone Quarry

Lightweight Aggregate Plant

The shale samples consisted of sub-microscopic grains. The grains were disaggregated with a mortar and pestle, deflocculated for 48 hours using a 5% solution of sodium hexametaphosphate. The powdered samples were then injected into a Malvern 2000 laser particle size analyzer and analyzed for grain size distribution (Figure A.21). The Malvern 2000 measures particle sizes between 0.02 microns and 2000 microns. Mean grain size was 5.5 microns, with almost the entire sample lying between 0.5 and 10 microns (Figure A.21).

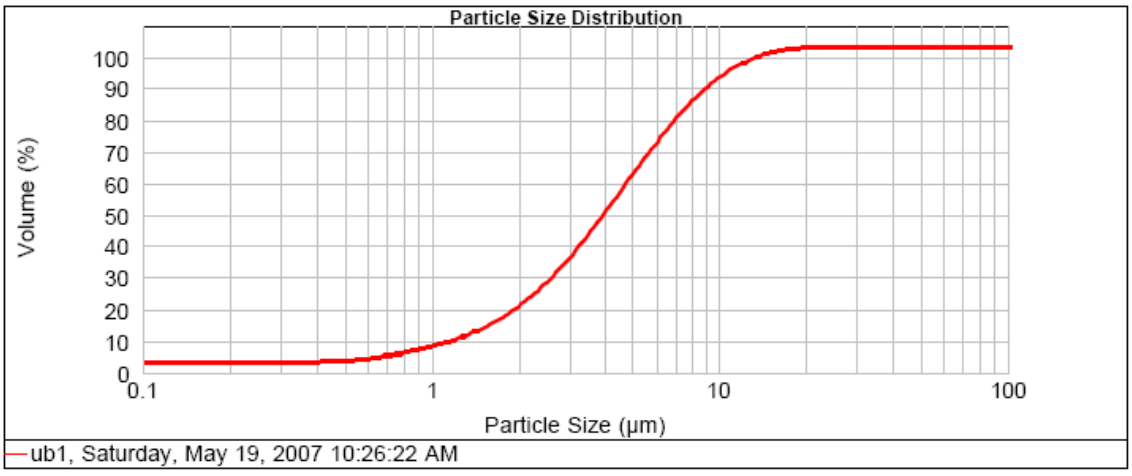

Figure A.21 - Grain size distribution of the clay from the clay quarry.

APPENDIX B - STRENGTH OF INDIVIDUAL AGGREGATE PARTICLES

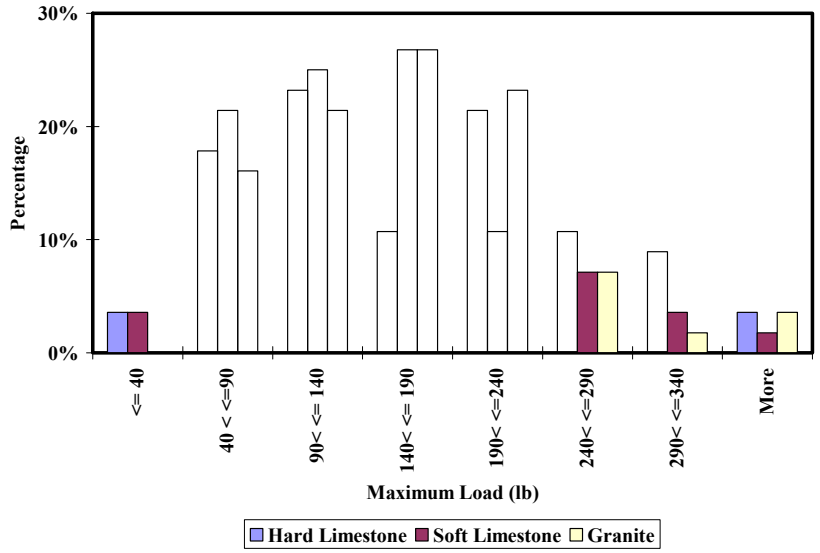

Figure B.1 - Single Aggregate Crushing Results Distribution (Vertical)

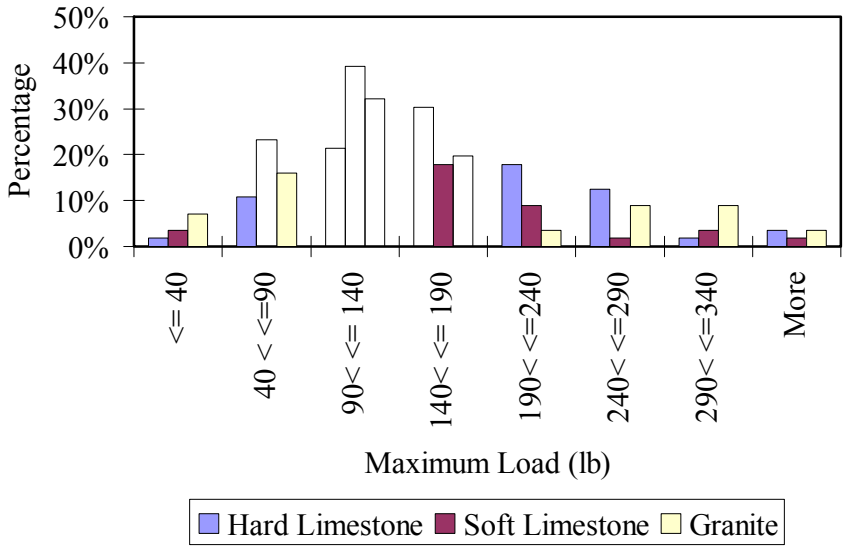

Figure B.2 - Single Aggregate Crushing Results Distribution (Horizontal)

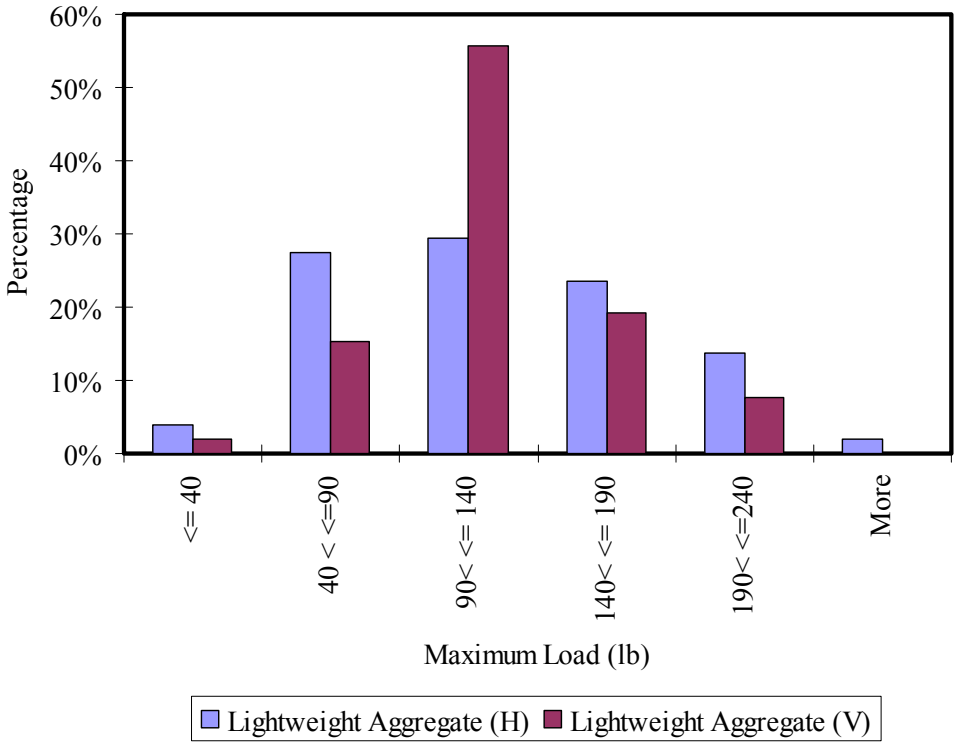

Figure B.3 - Single Aggregate Crushing Results Distribution (Lightweight Aggregate)

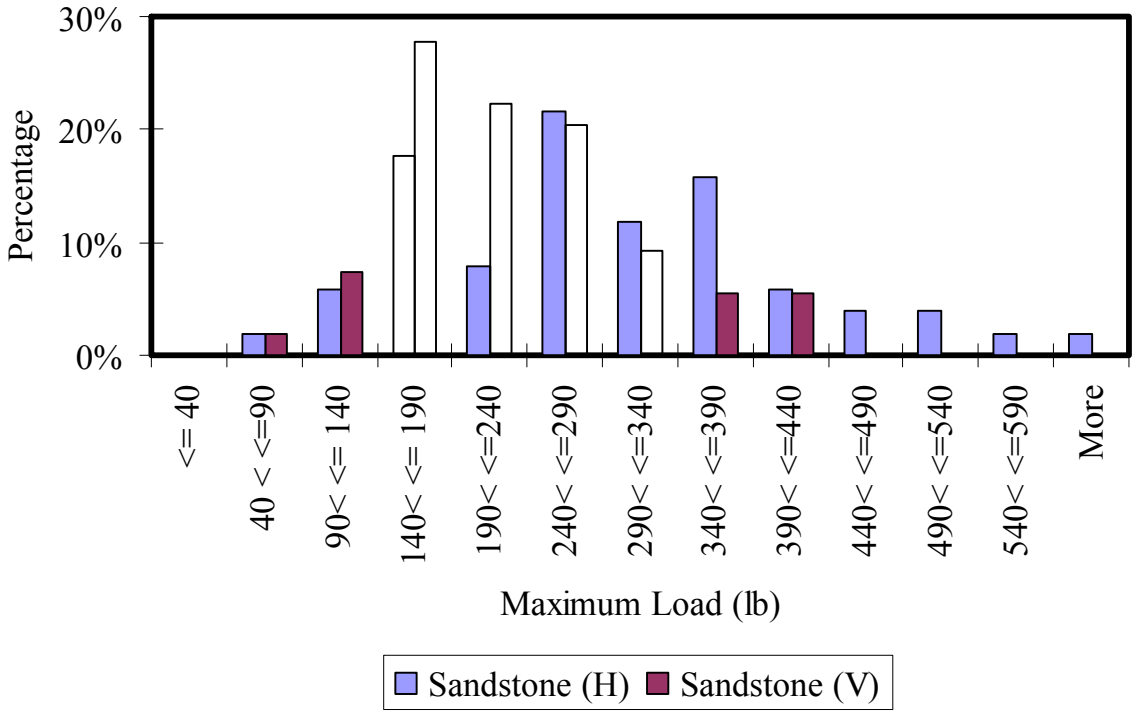

Figure B.4 - Single Aggregate Crushing Results Distribution (Sandstone)

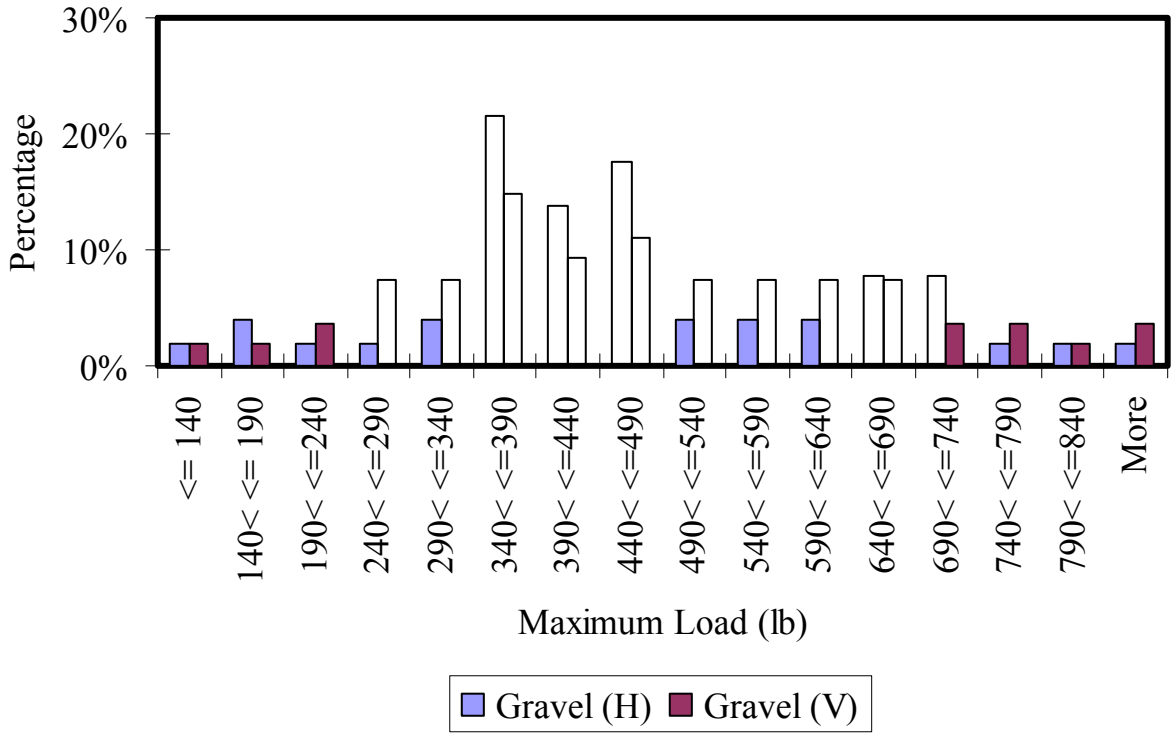

Figure B.5 - Single Aggregate Crushing Results Distribution (Gravel)

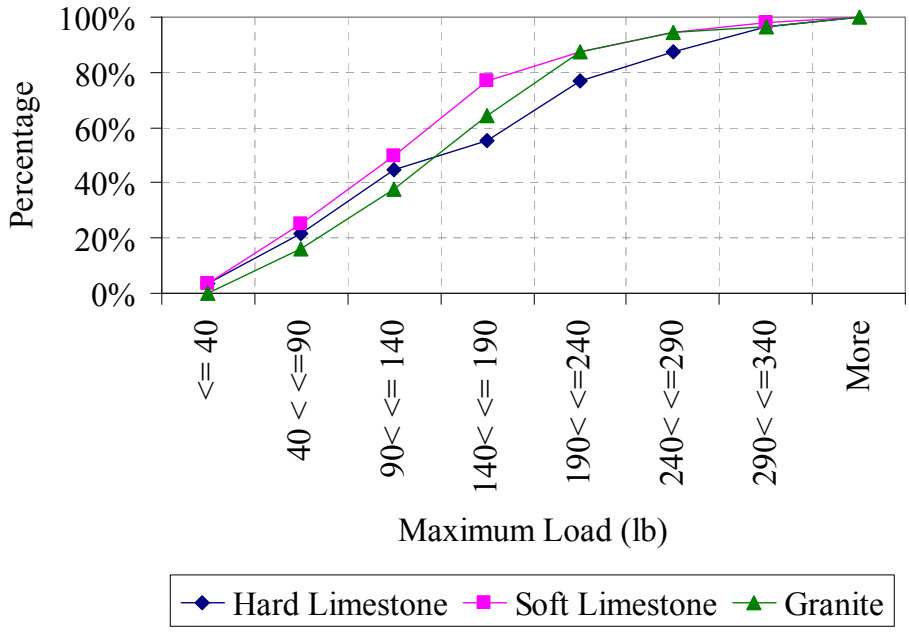

Figure B.6 - Single Aggregate Crushing Cumulative Distribution (Vertical)

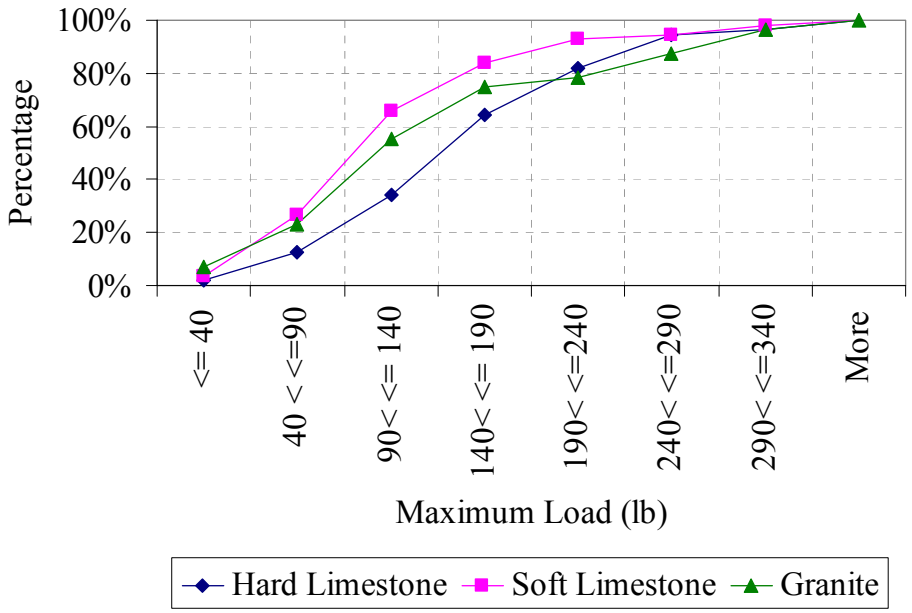

Figure B.7- Single Aggregate Crushing Cumulative Distribution (Horizontal)

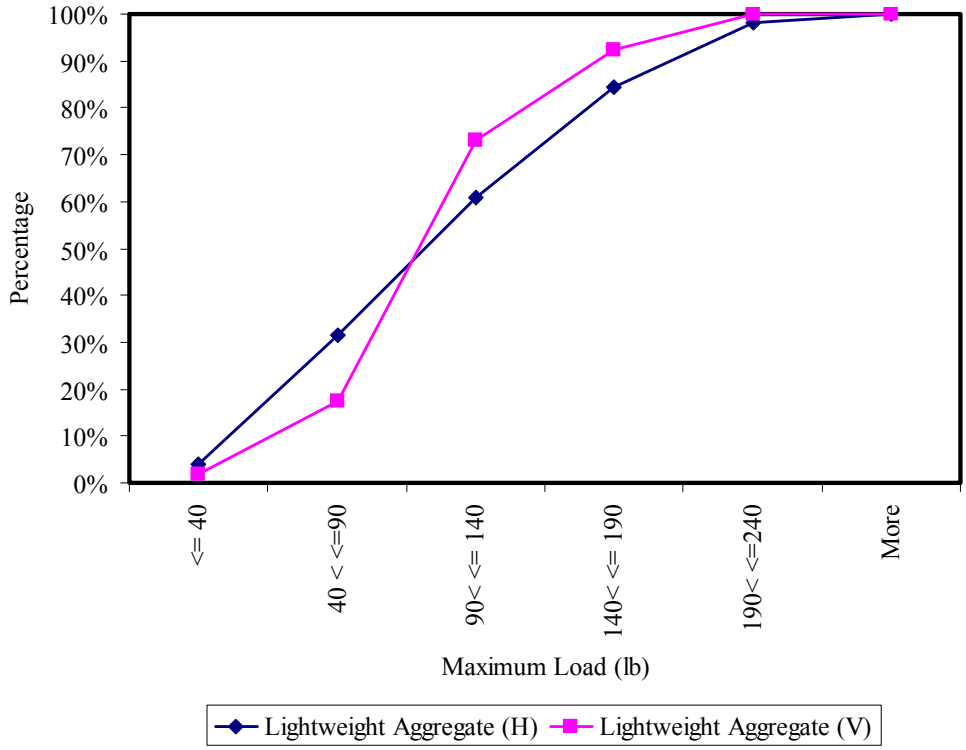

Figure B.8 - Single Aggregate Crushing Cumulative Distribution (Lightweight Aggregate)

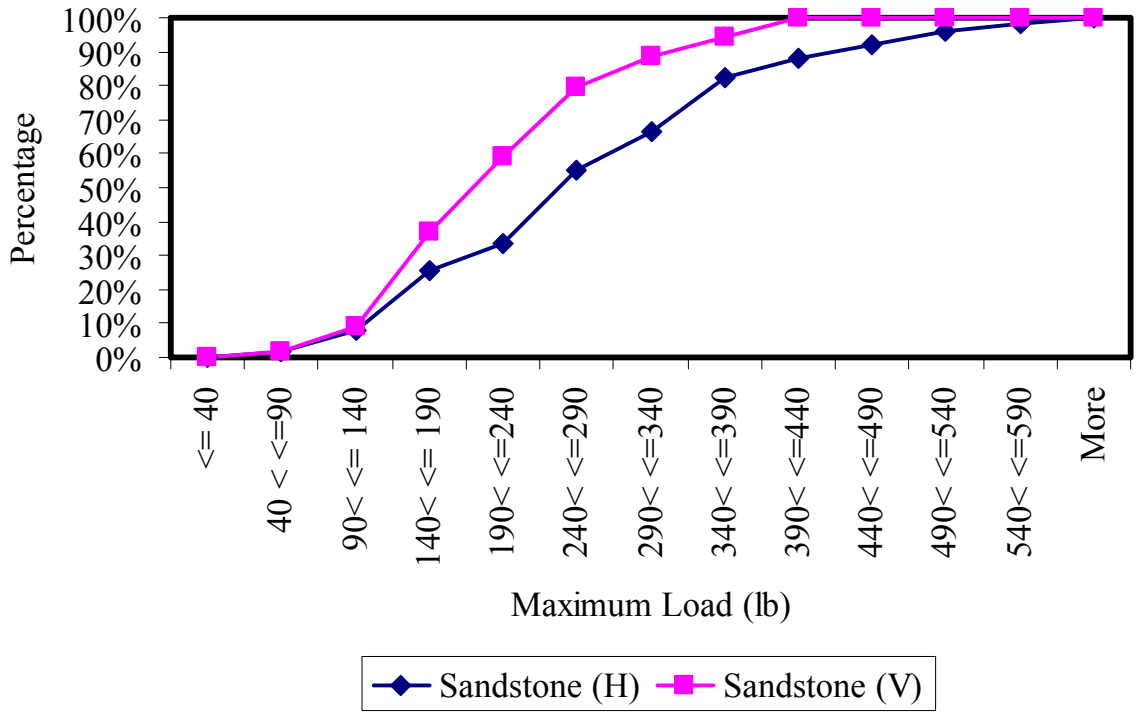

Figure B.9 - Single Aggregate Crushing Cumulative Distribution (Sandstone)

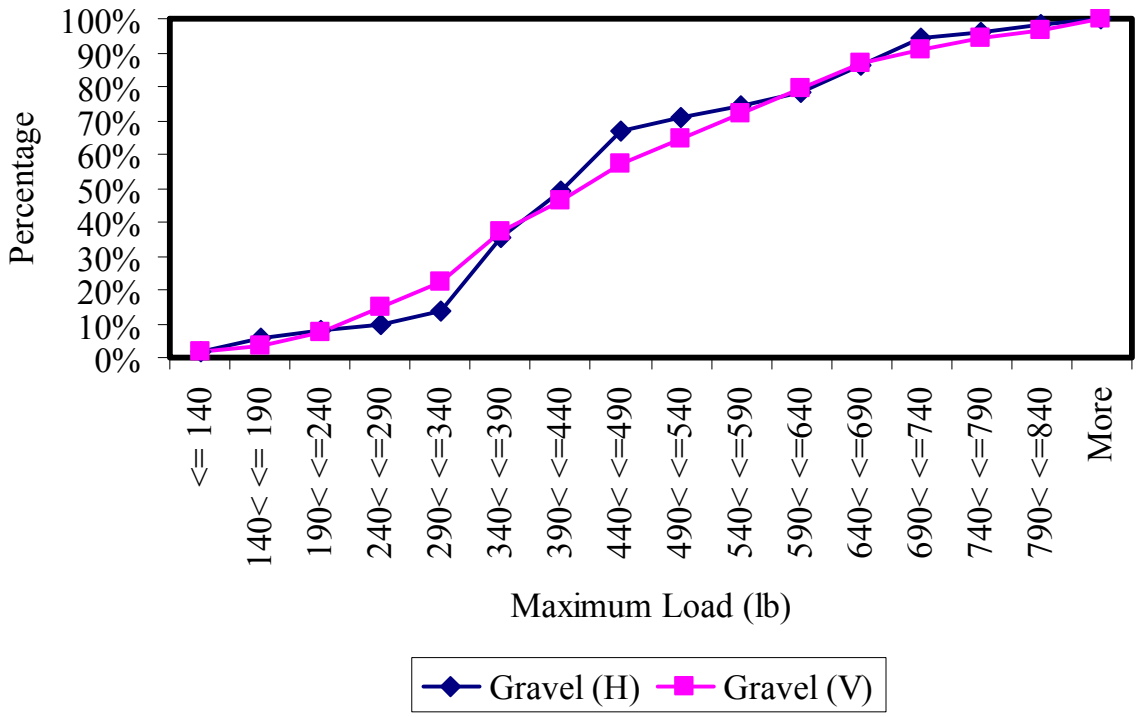

Figure B.10 - Single Aggregate Crushing Cumulative Distribution (Gravel)

APPENDIX C - MICROMECHANICAL MODELING

Figures C.1 through C.27 present the stress distributions within the different mixes for the hard limestone, soft limestone, granite, gravel, and sandstone. The figures compare the results based on the aggregate type and based on the mix. Each figure contains two plots. For each comparison group, there are three pairs. The first pair represents the compression forces, followed by shear forces, and finally tension forces. The first plot of each pair is a histogram plot followed by cumulative distribution curves in the second plot. Please note that only positive shear forces are considered here as the negative shear forces are identical to the positive ones (typically). The only difference is the sign. The numerical results were as expected as the negative and positive shear forces were almost identical and their distributions were the same.

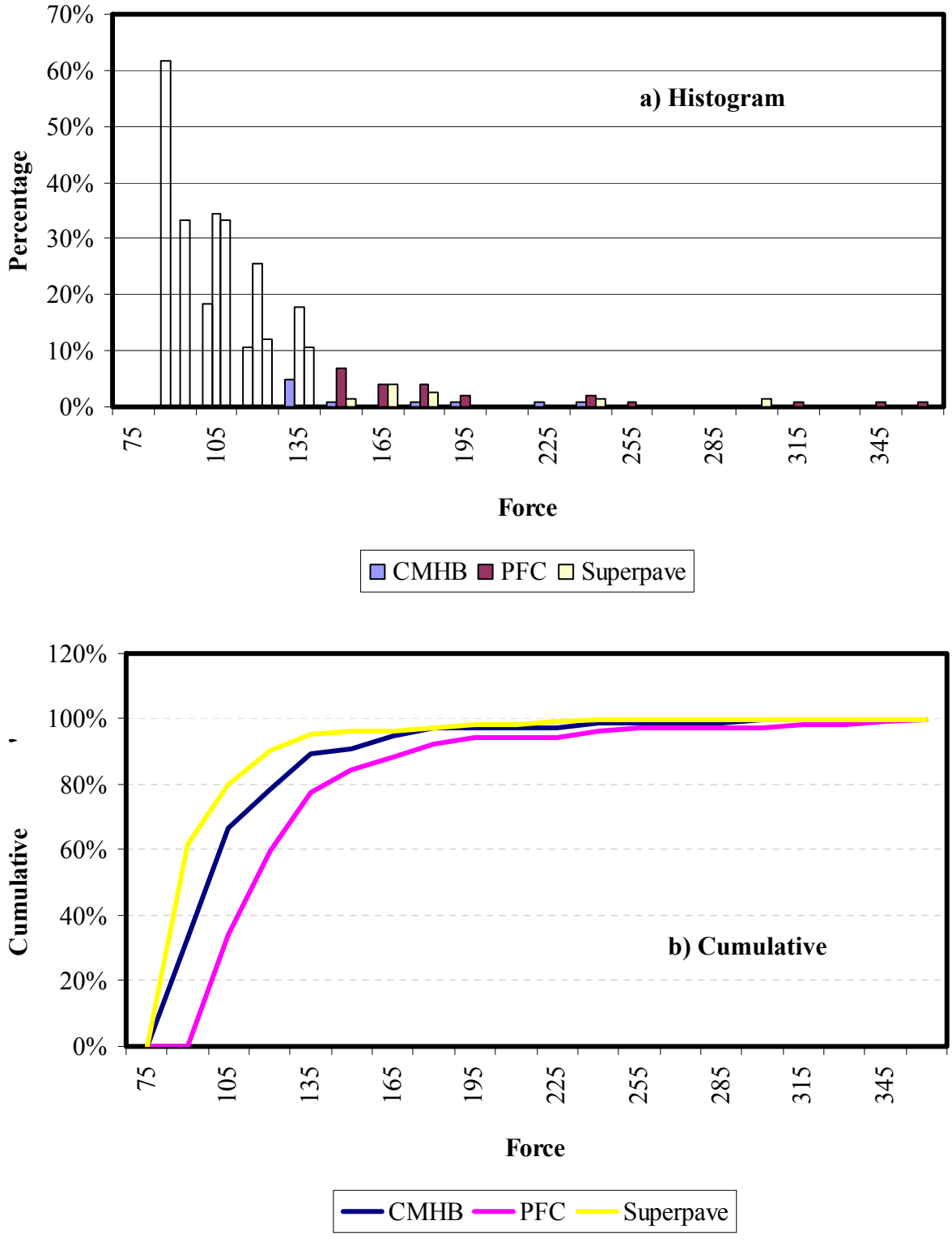

Figure C.1 – Internal Compression Forces Distribution Results for Hard Limestone

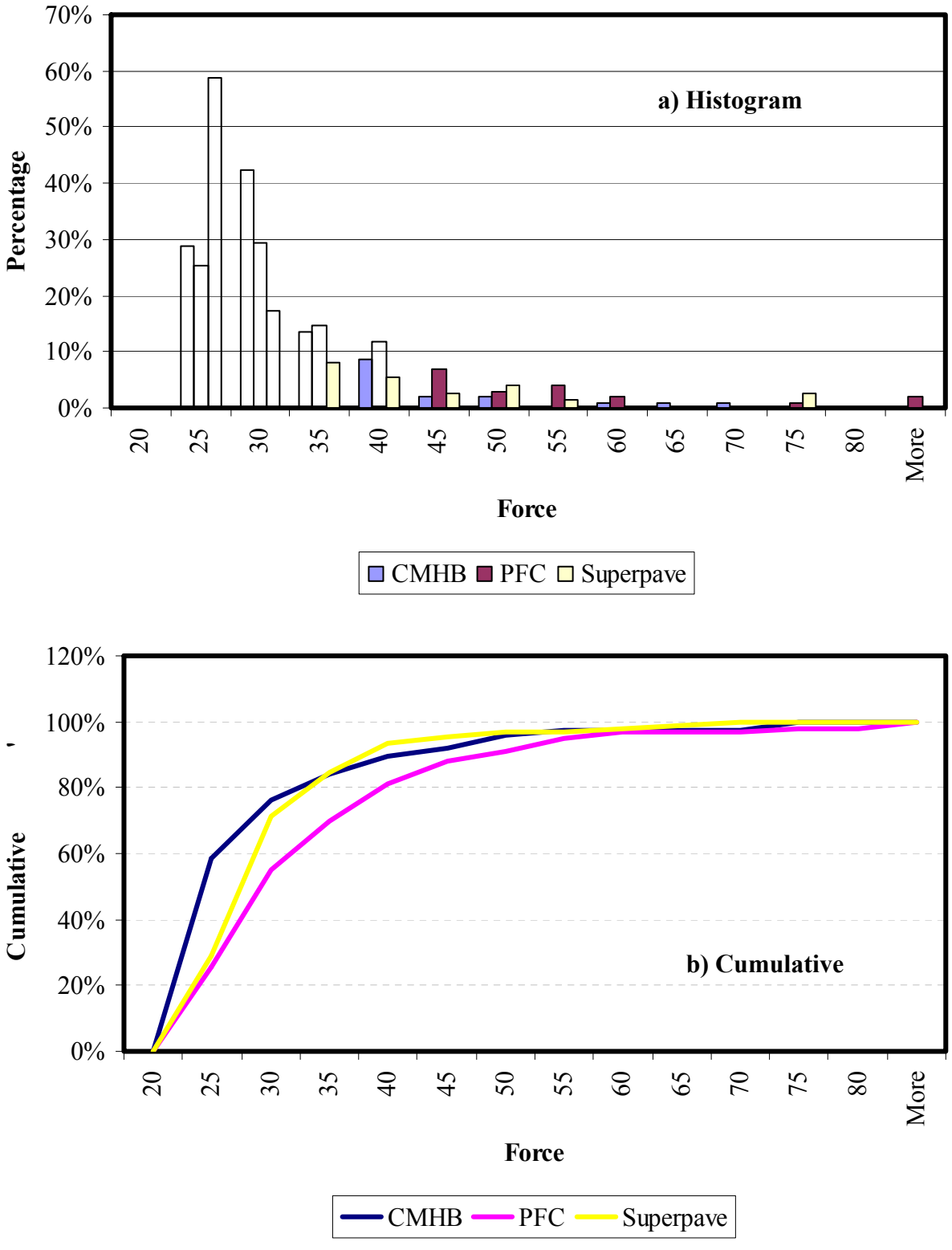

Figure C.2 – Internal Shear Forces Distribution Results for Hard Limestone

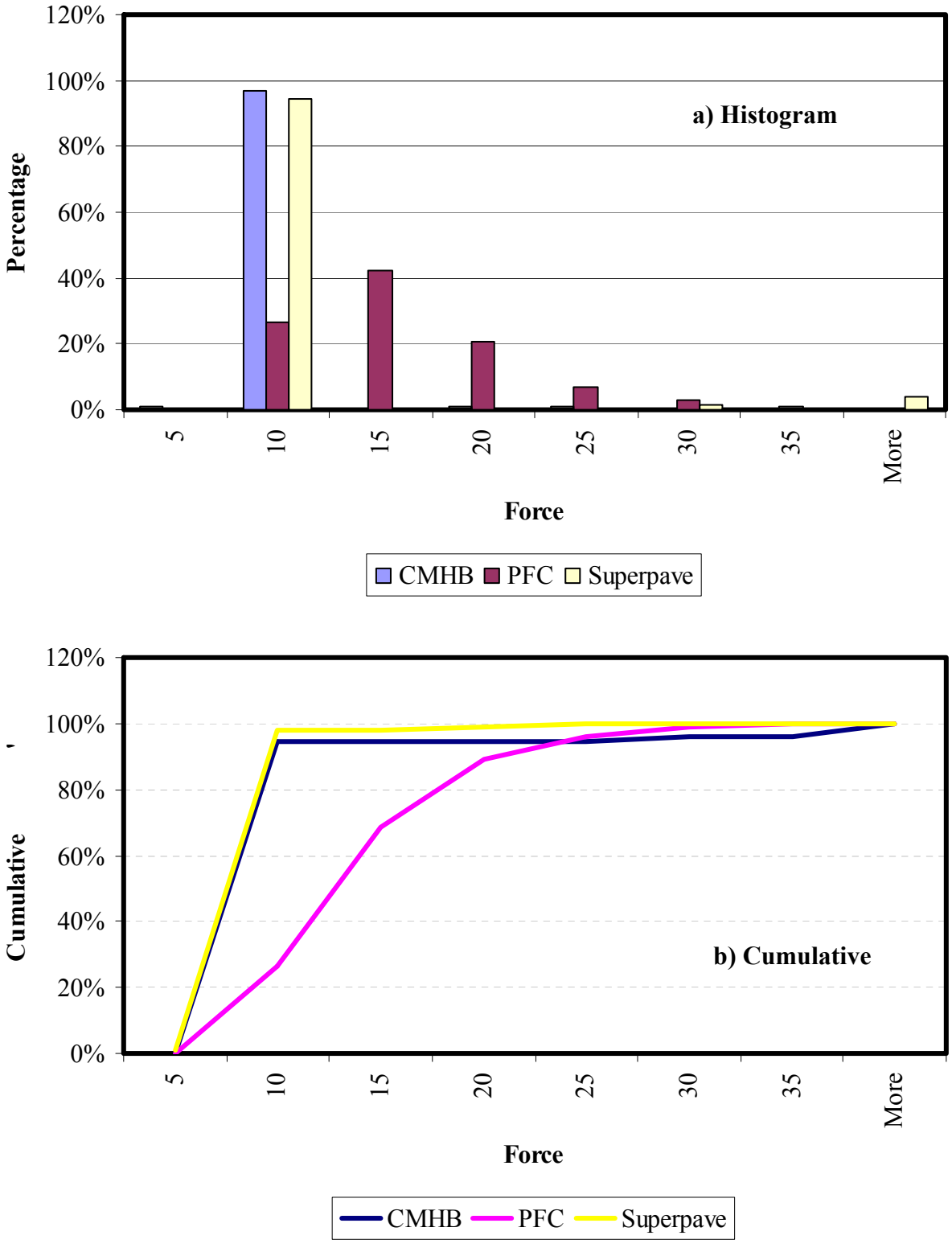

Figure C.3 – Internal Tension Forces Distribution Results for Hard Limestone

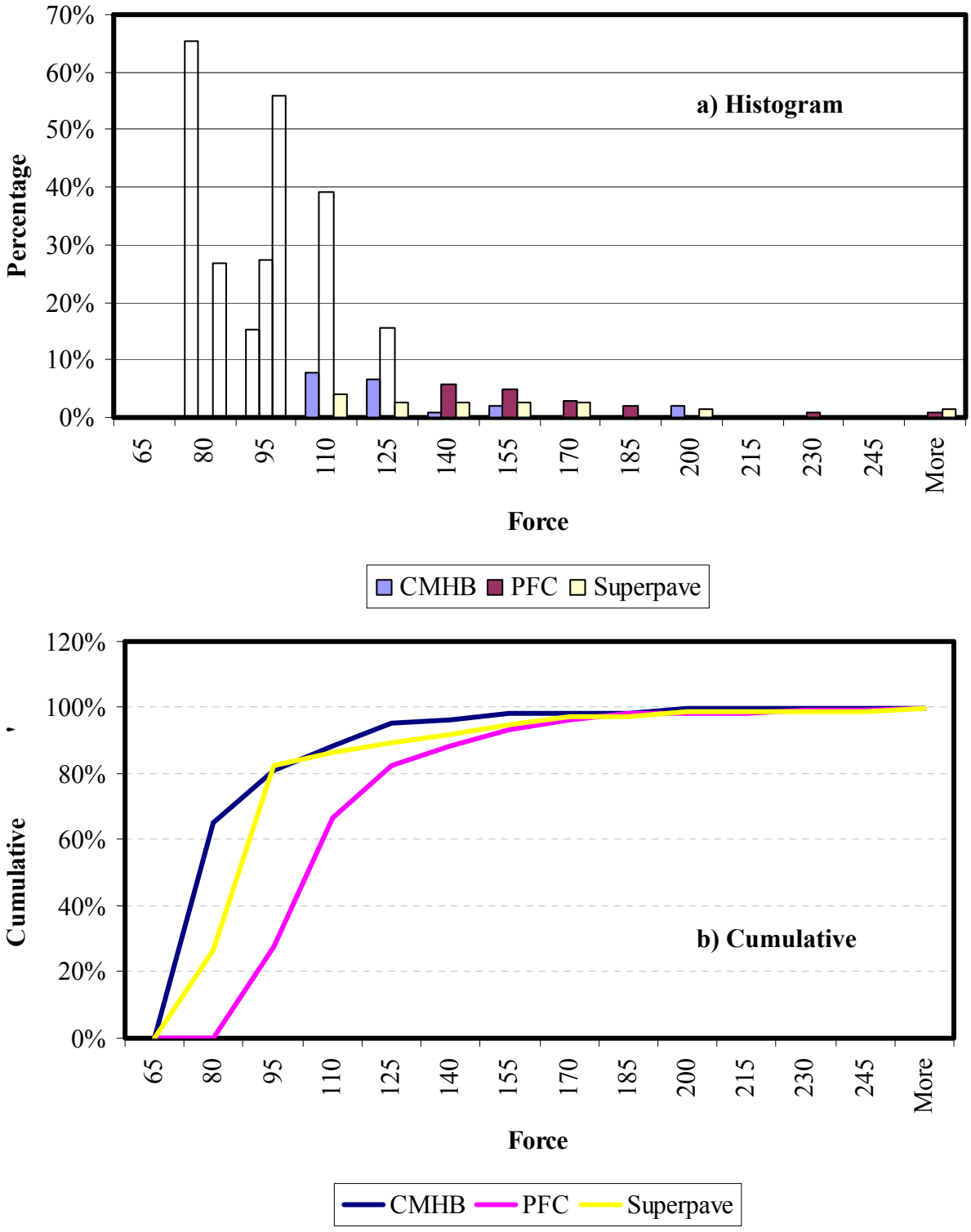

Figure C.4 – Internal Compression Forces Distribution Results for Soft Limestone

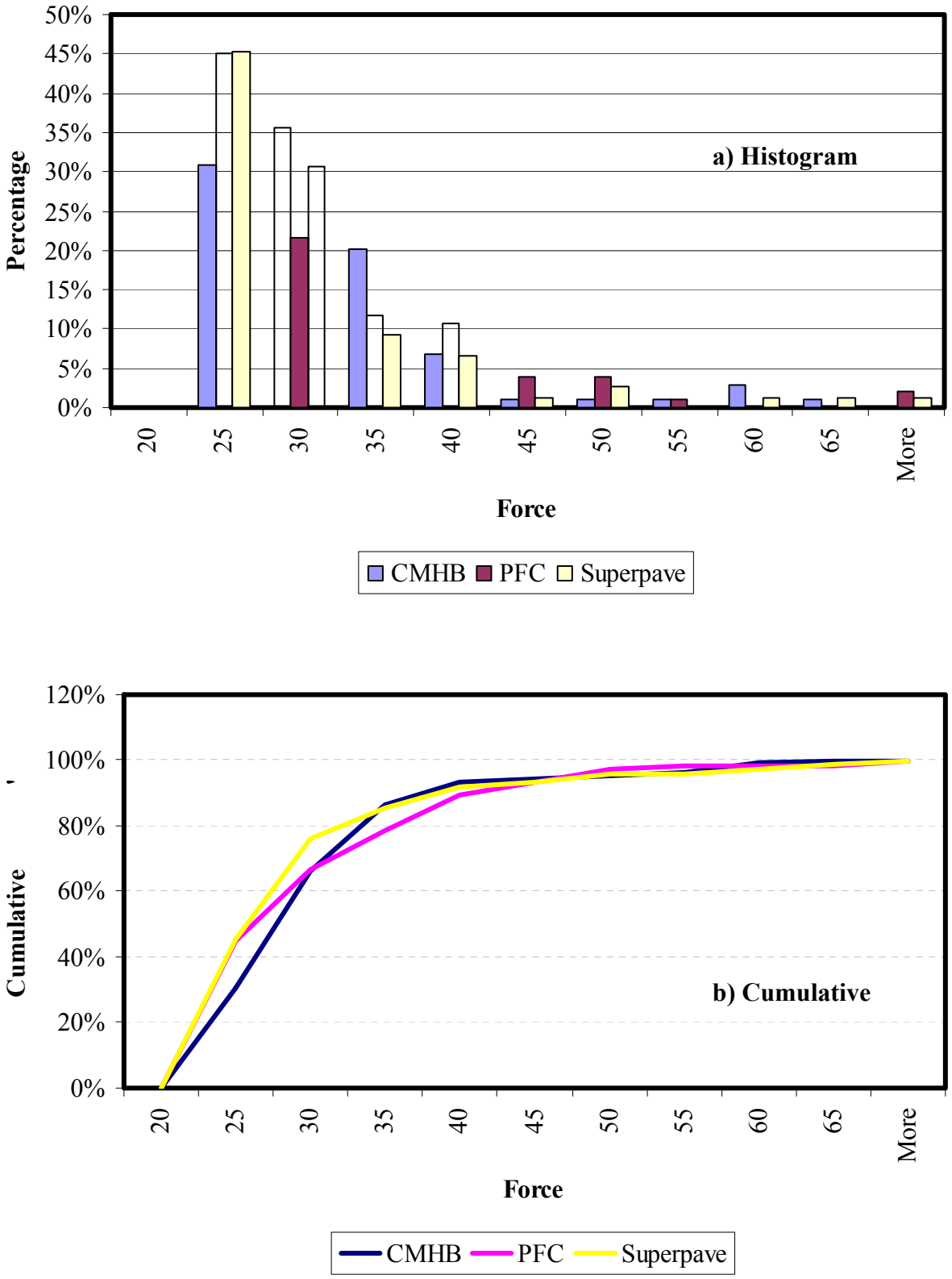

Figure C.5 – Internal Shear Forces Distribution Results for Soft Limestone

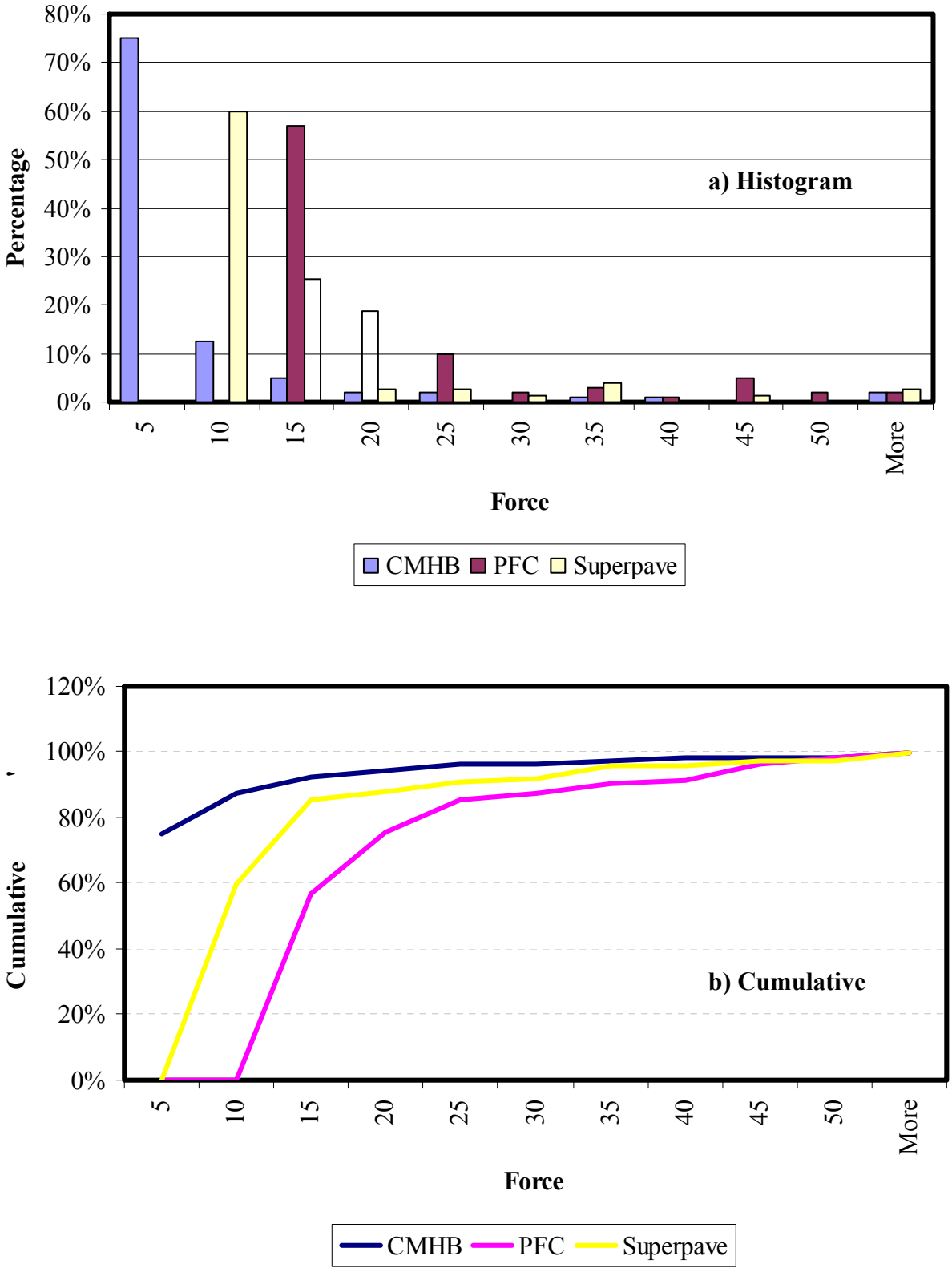

Figure C.6 – Internal Tension Forces Distribution Results for Soft Limestone

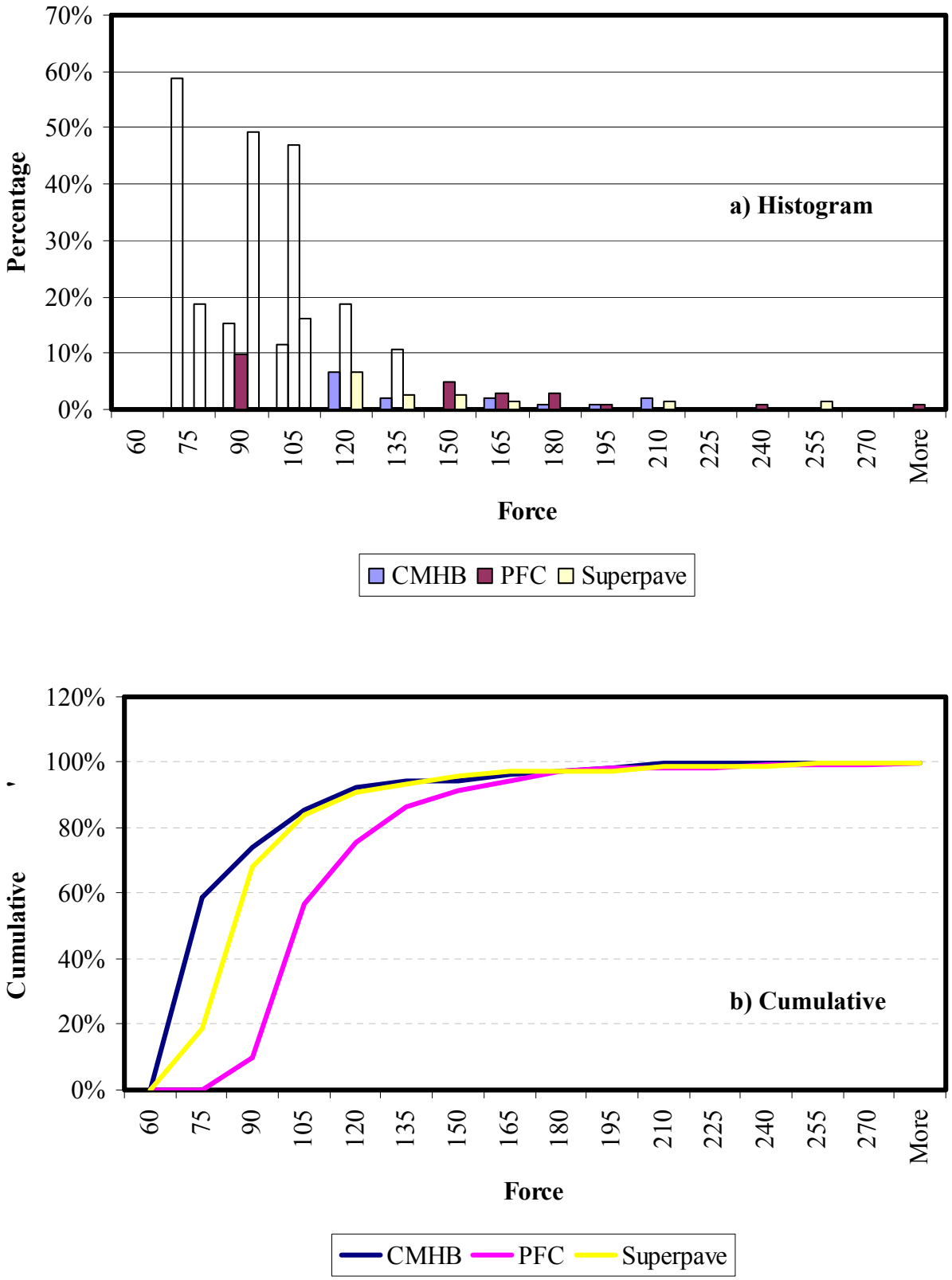

Figure C.7 – Internal Compression Forces Distribution Results for Granite

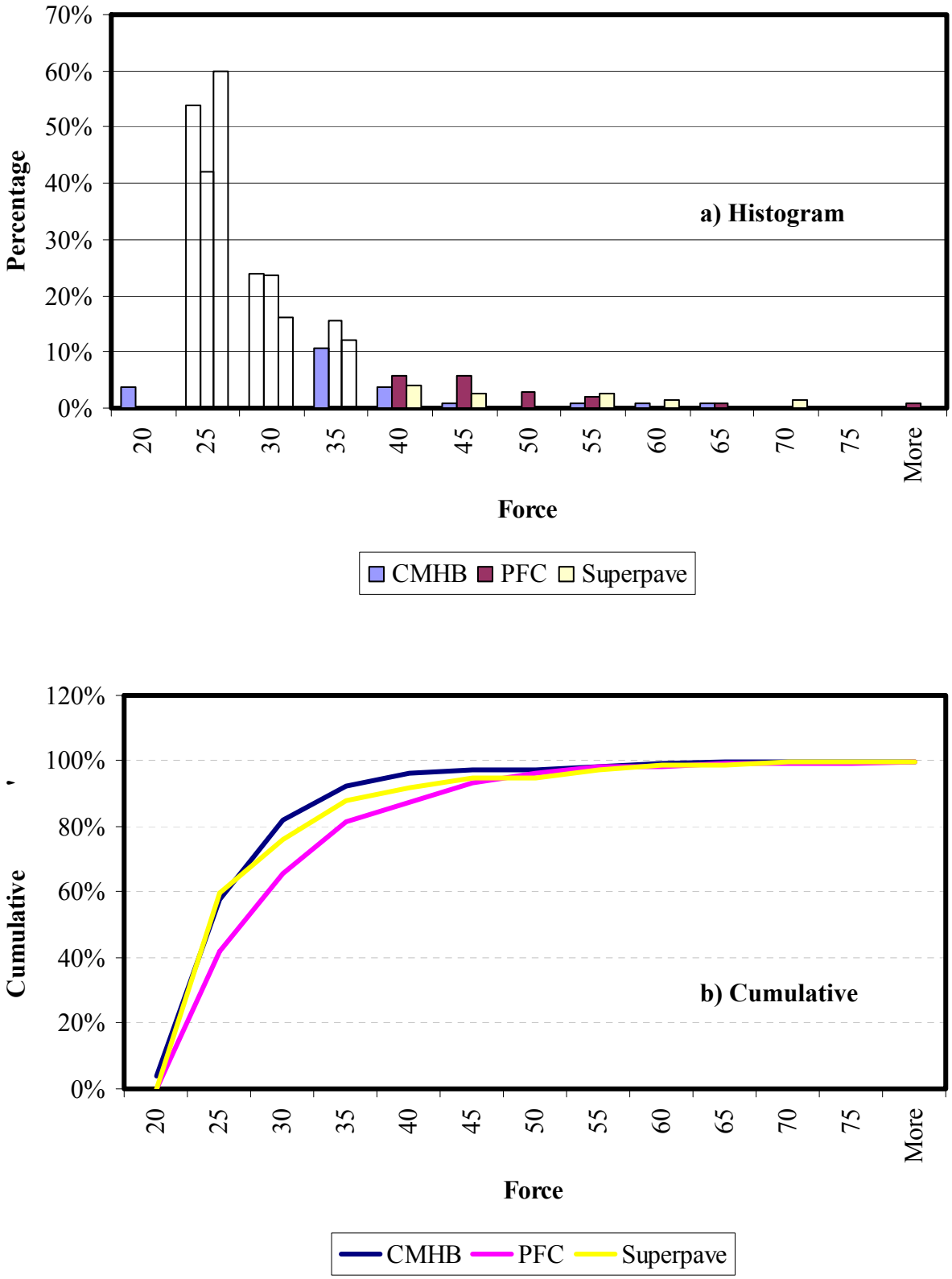

Figure C.8 – Internal Shear Forces Distribution Results for Granite

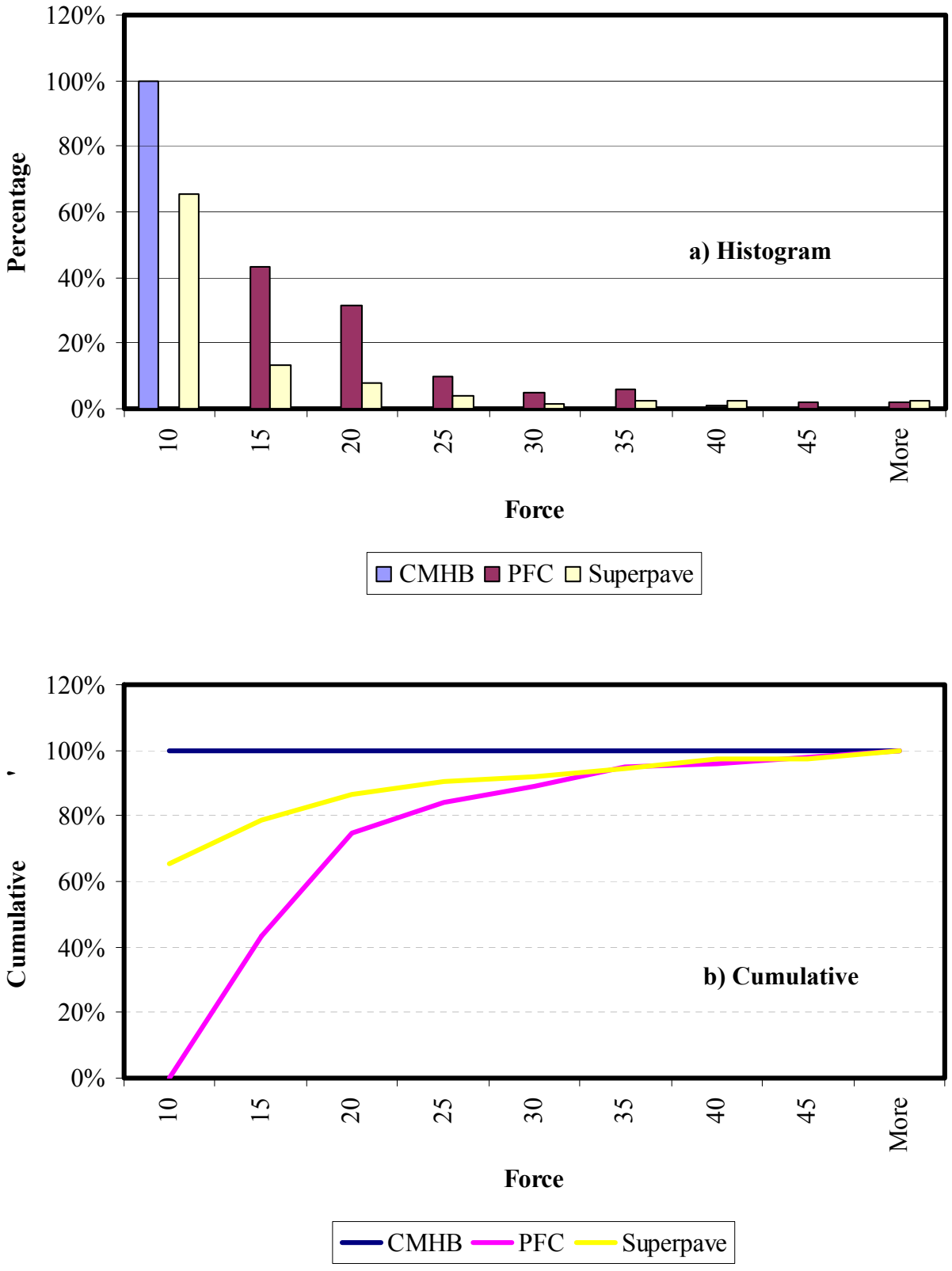

Figure C.9 – Internal Tension Forces Distribution Results for Granite

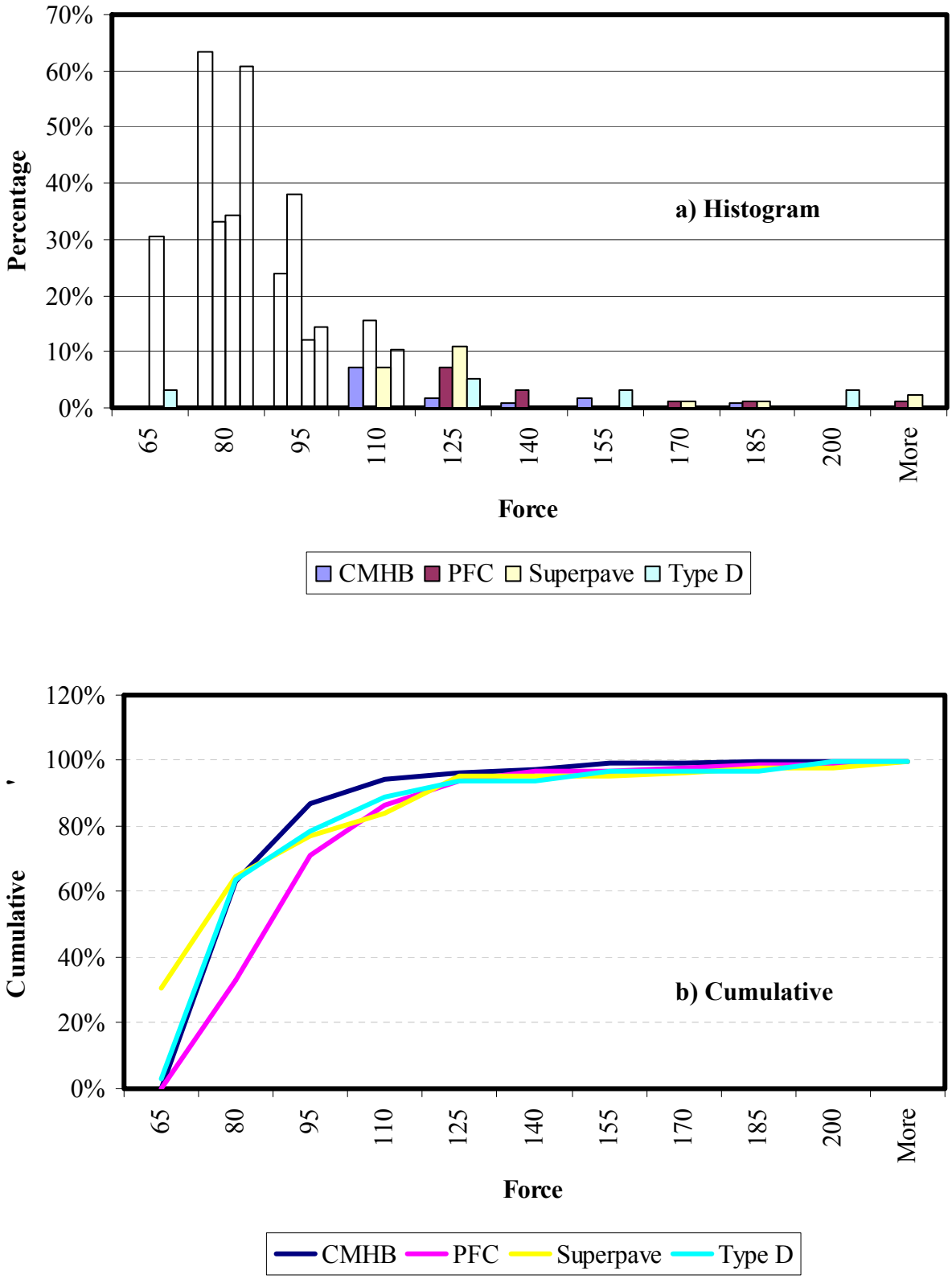

Figure C.10 – Internal Compression Forces Distribution Results for Gravel

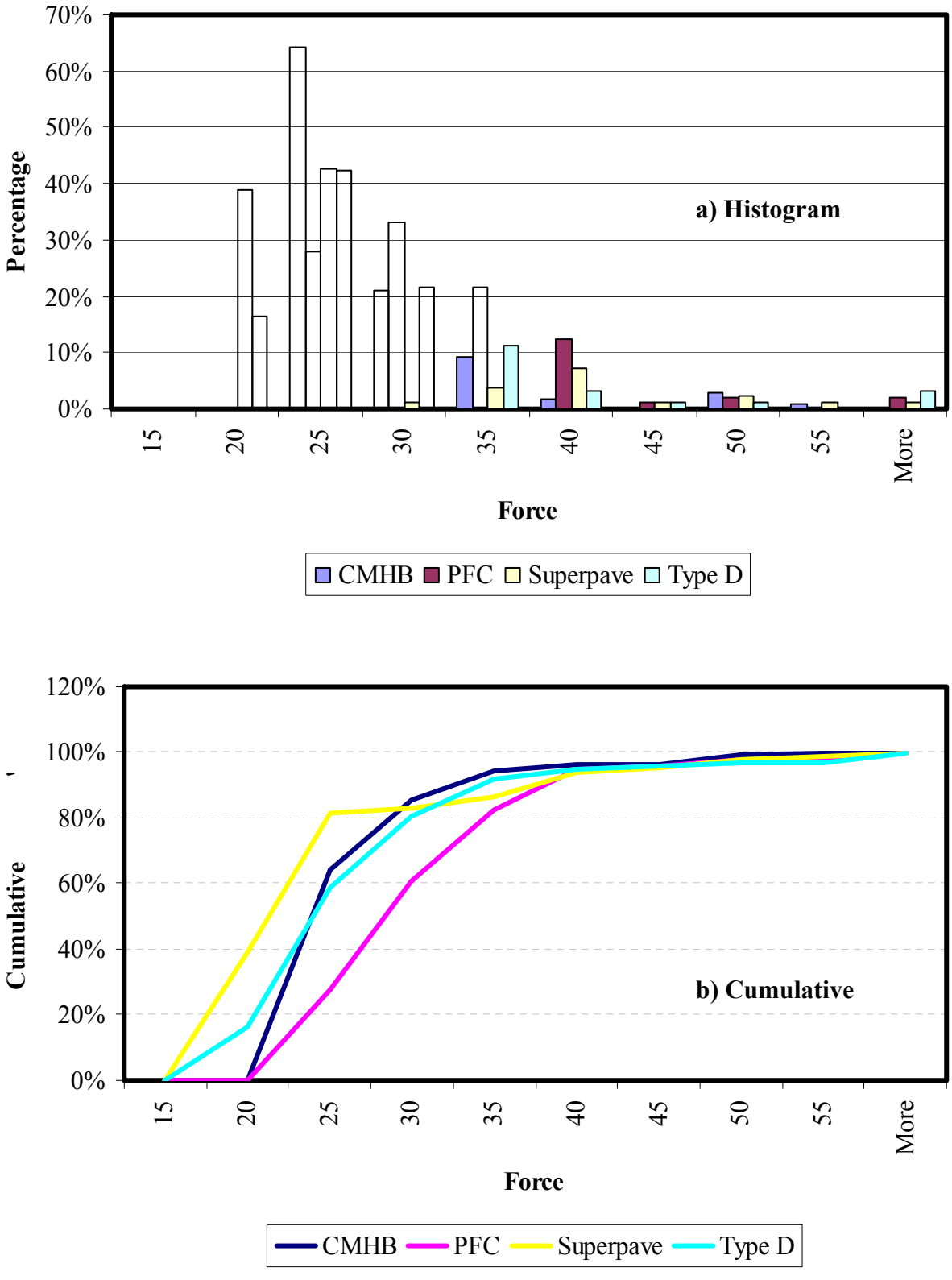

Figure C.11 – Internal Shear Forces Distribution Results for Gravel

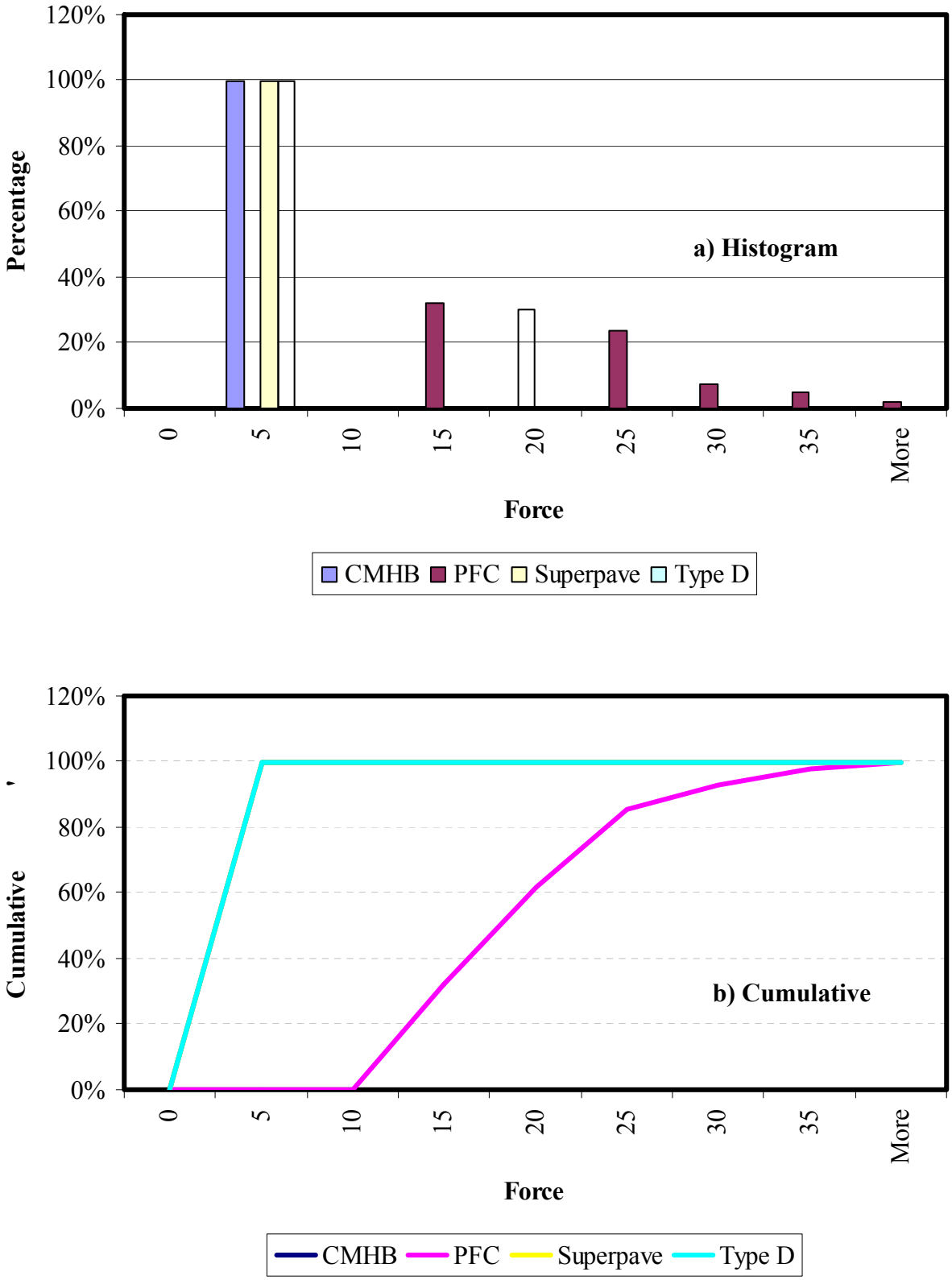

Figure C.12 – Internal Tension Forces Distribution Results for Gravel

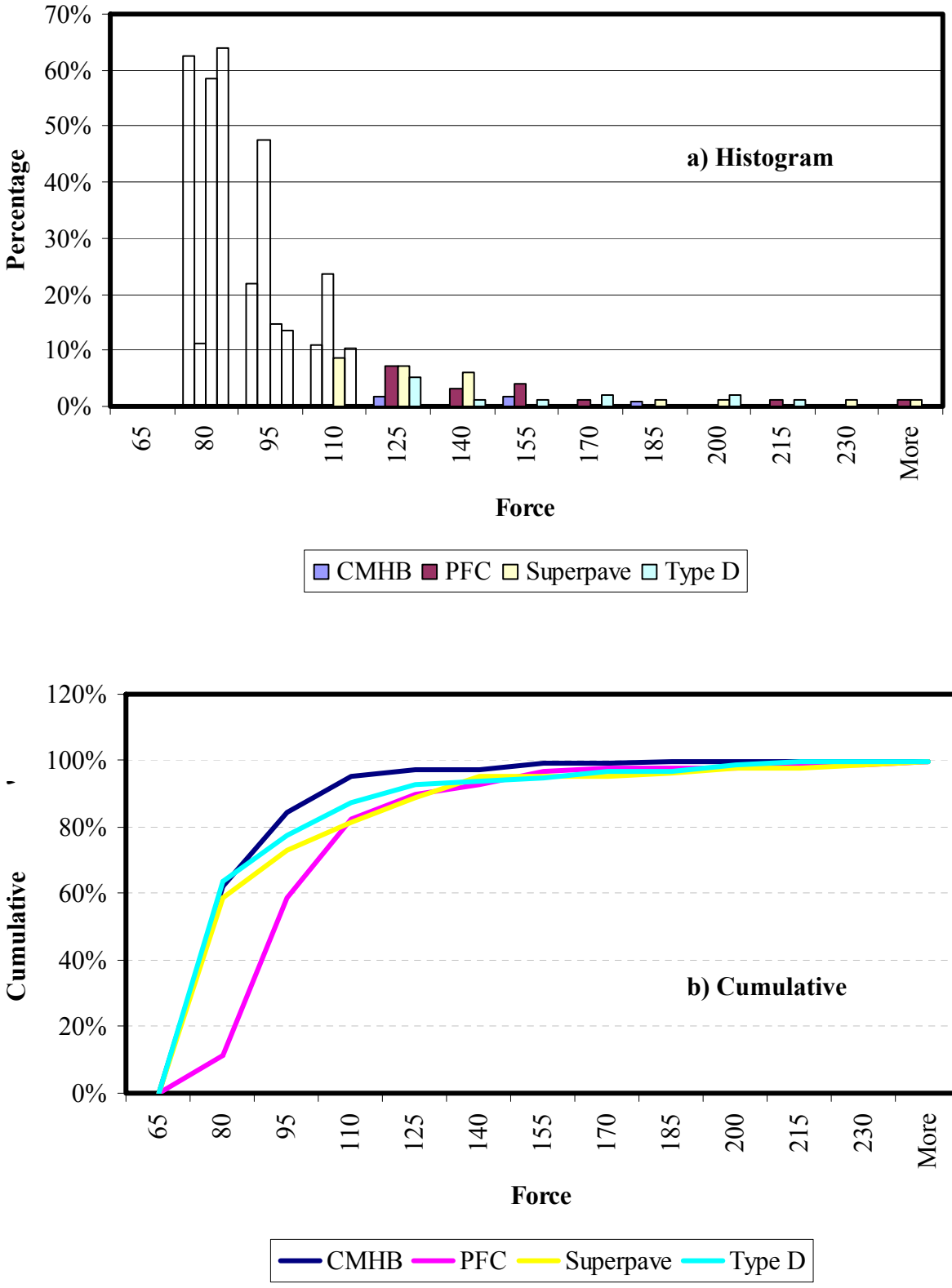

Figure C.13 – Internal Compression Forces Distribution Results for Sandstone

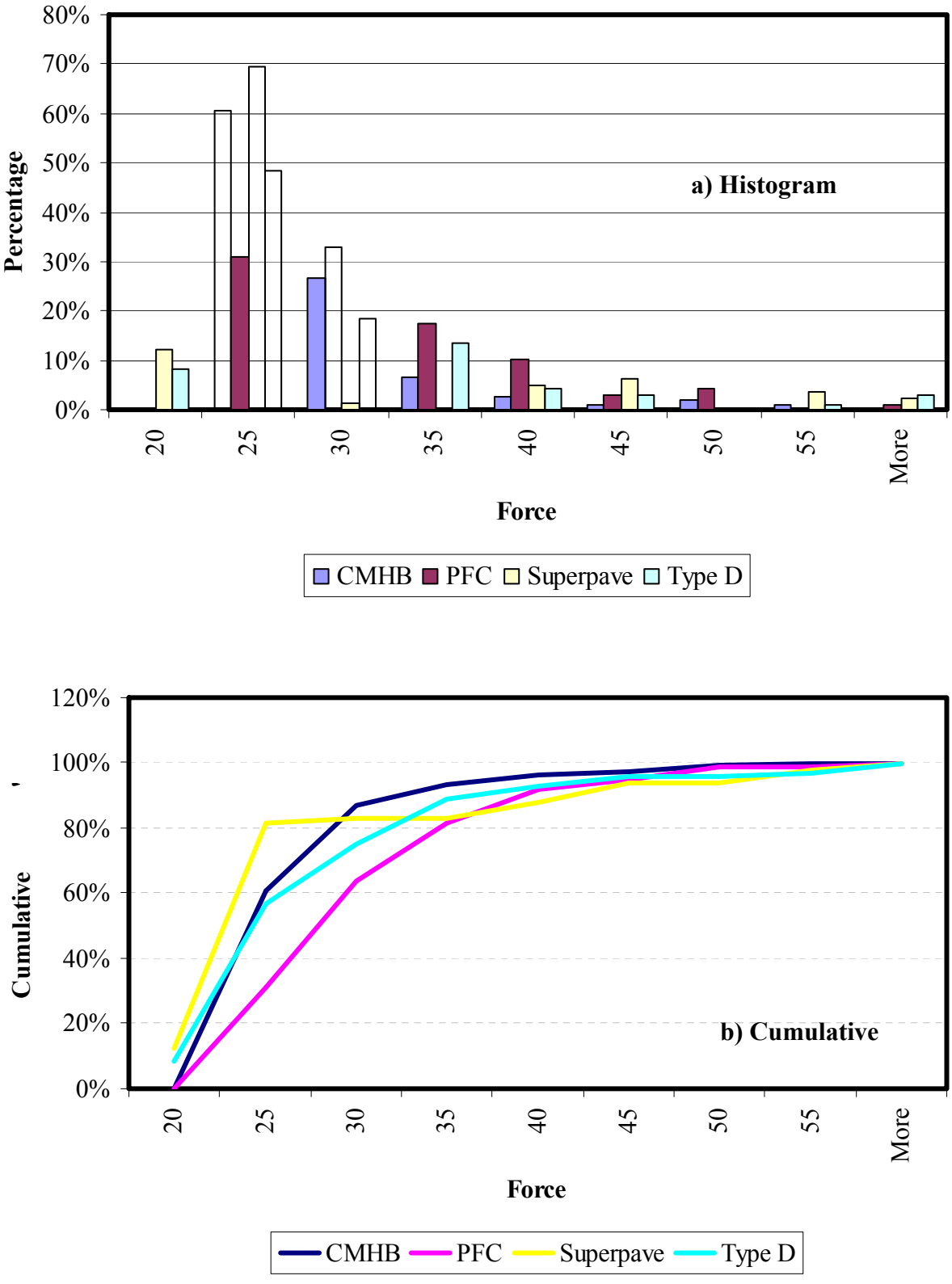

Figure C.14 – Internal Shear Forces Distribution Results for Sandstone

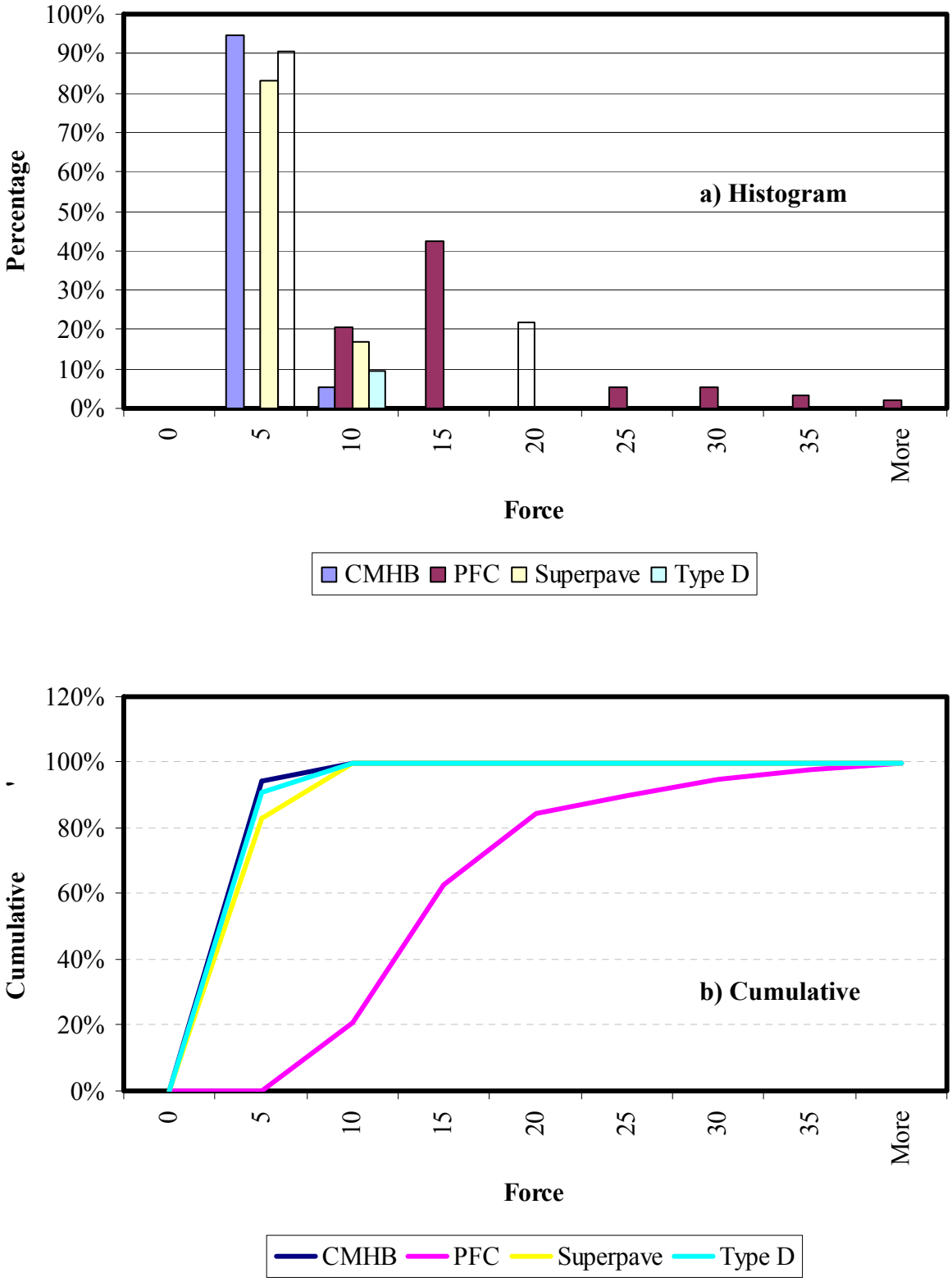

Figure C.15 – Internal Tension Forces Distribution Results for Sandstone

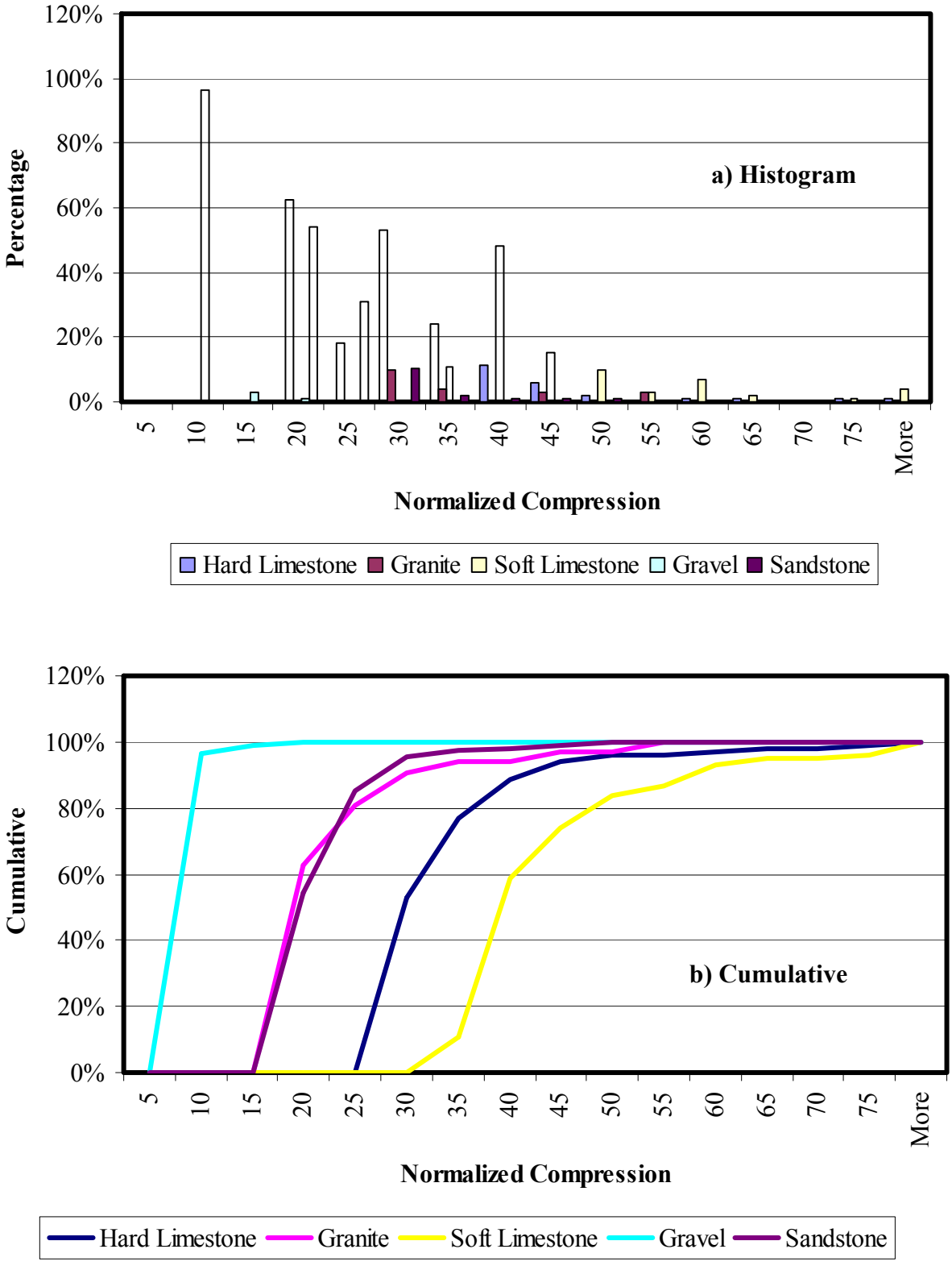

Figure C.16 – Internal Compression Forces Distribution Results for CMHB-C

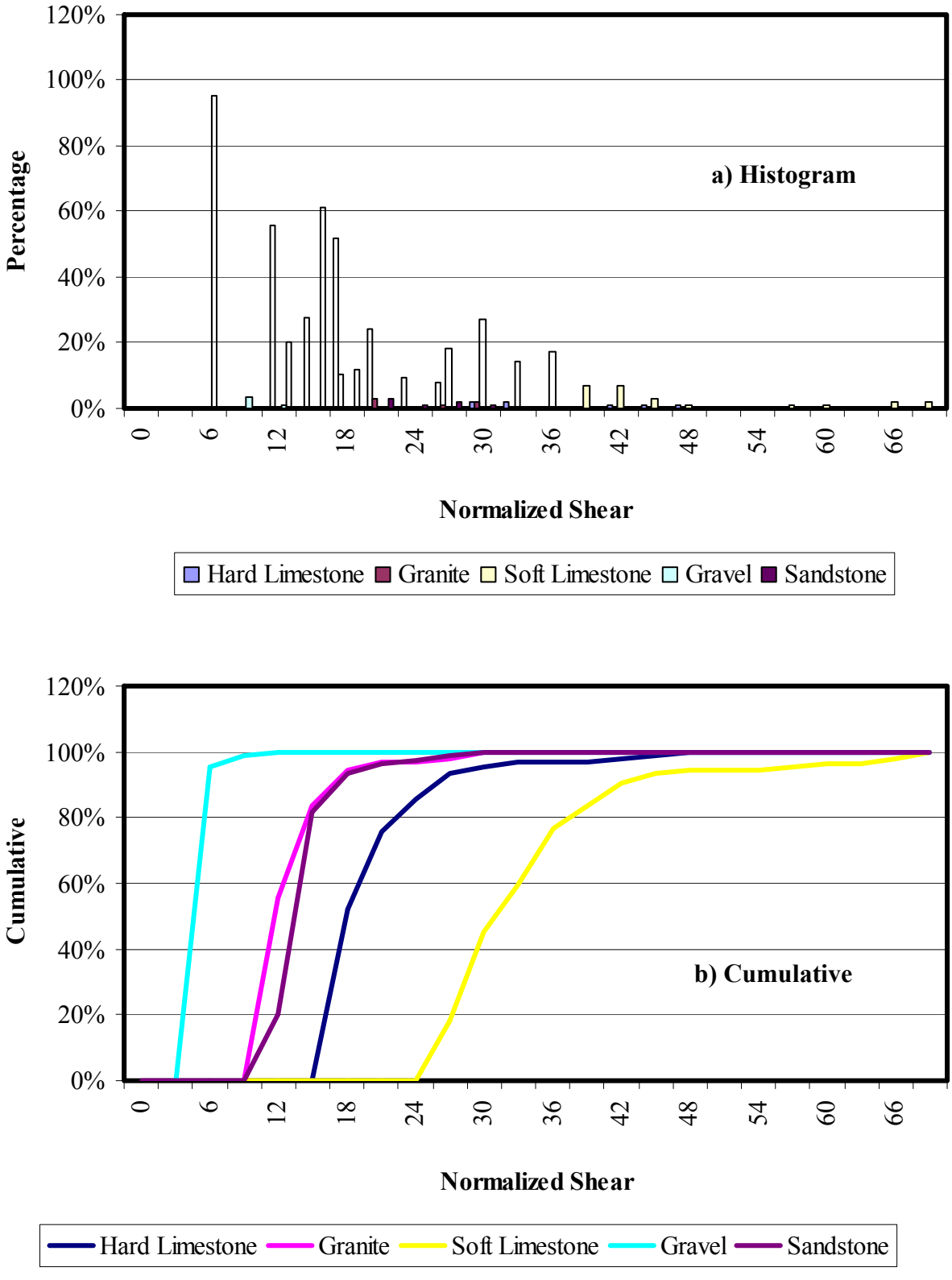

Figure C.17 – Internal Shear Forces Distribution Results for CMHB-C

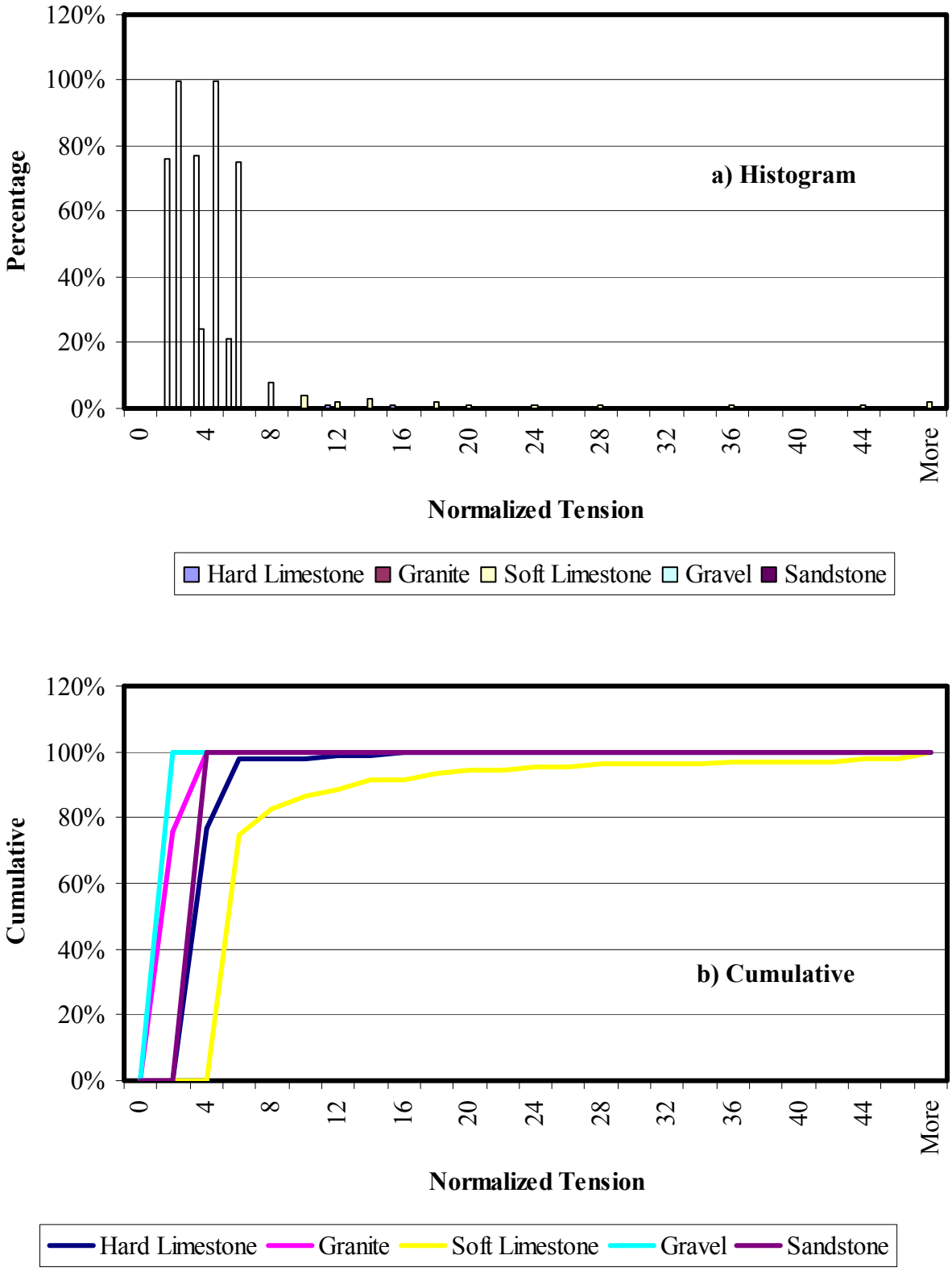

Figure C.18 – Internal Tension Forces Distribution Results for CMHB-C

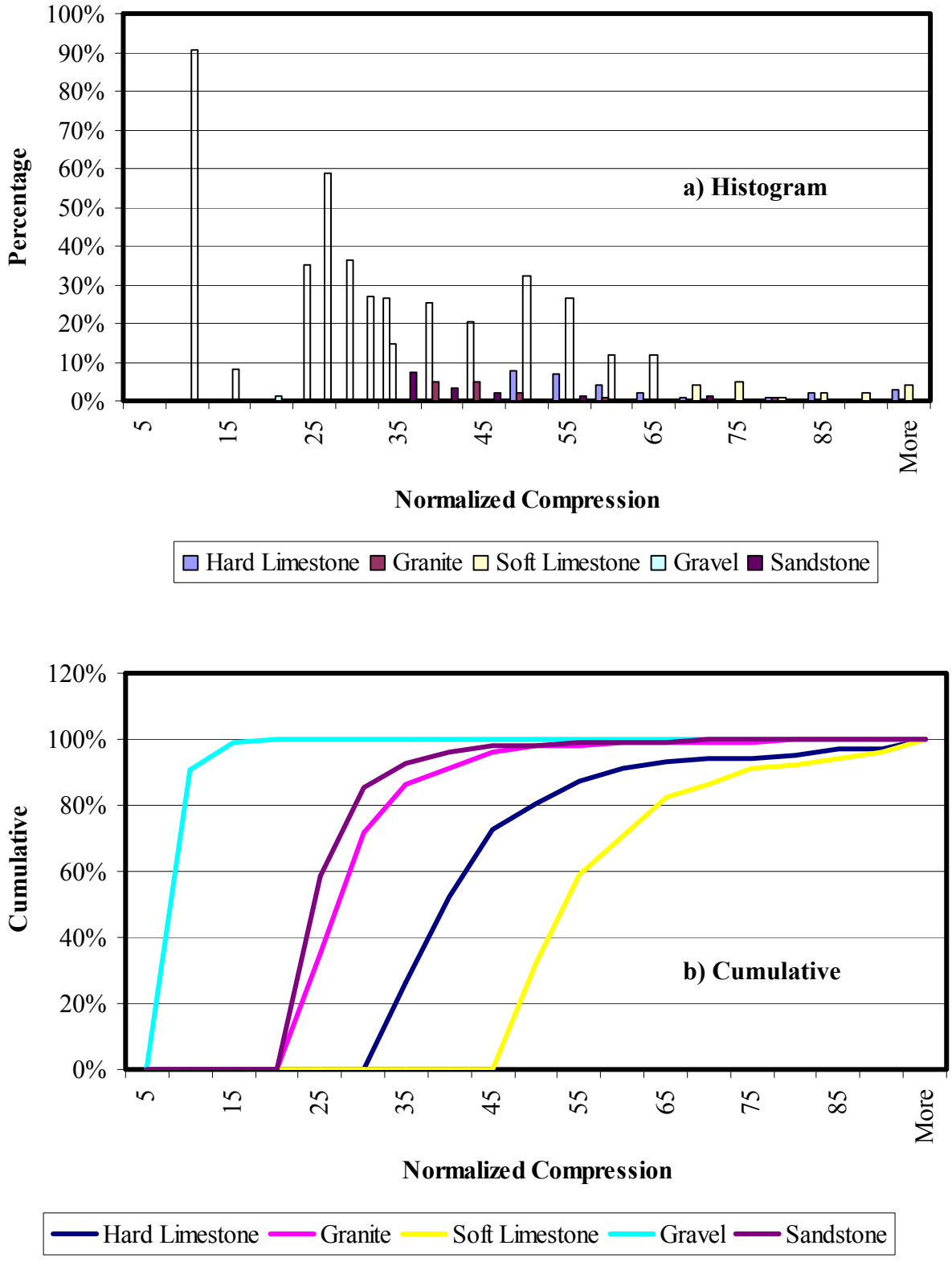

Figure C.19 – Internal Compression Forces Distribution Results for PFC

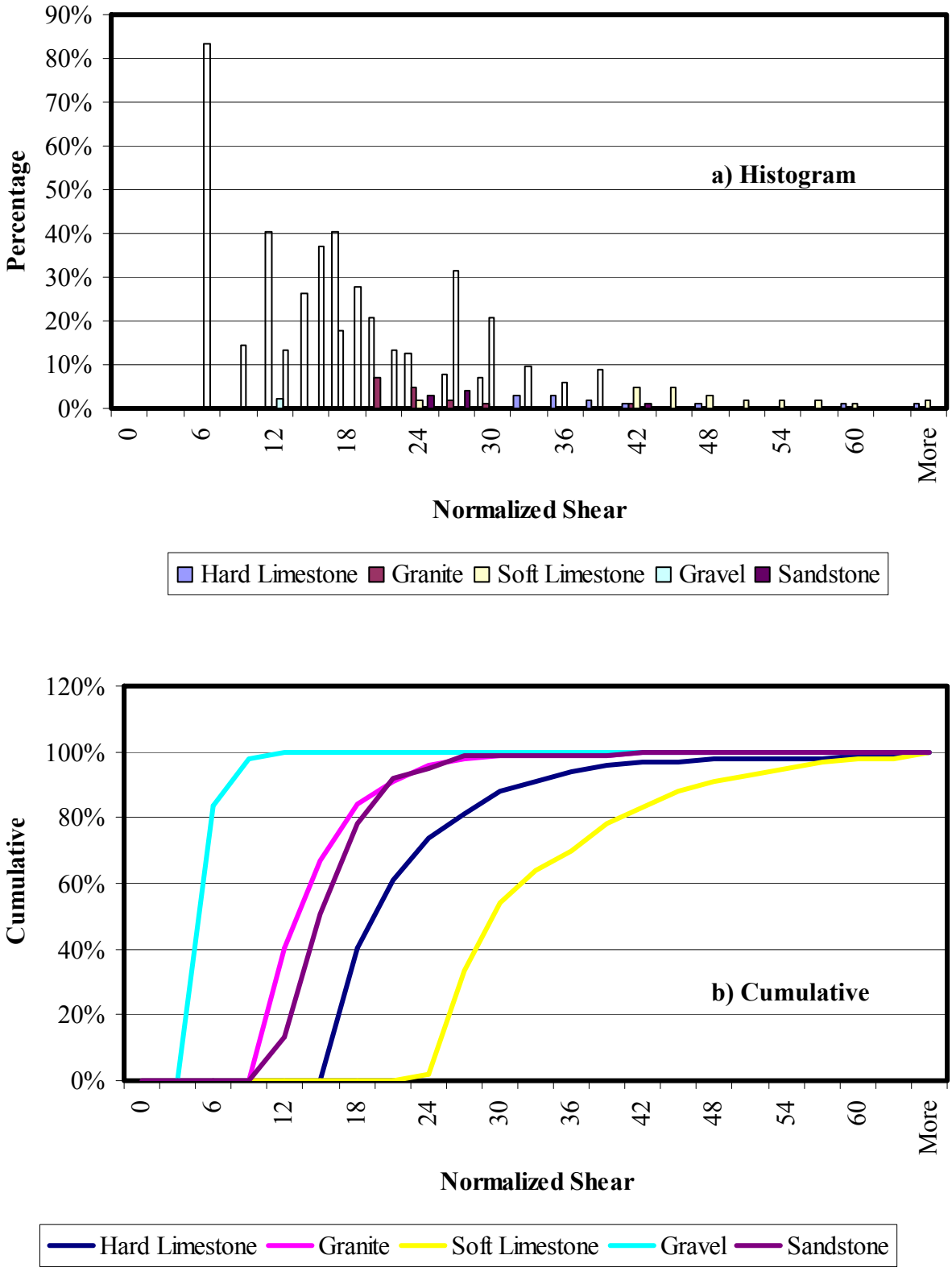

Figure C.20 – Internal Shear Forces Distribution Results for PFC

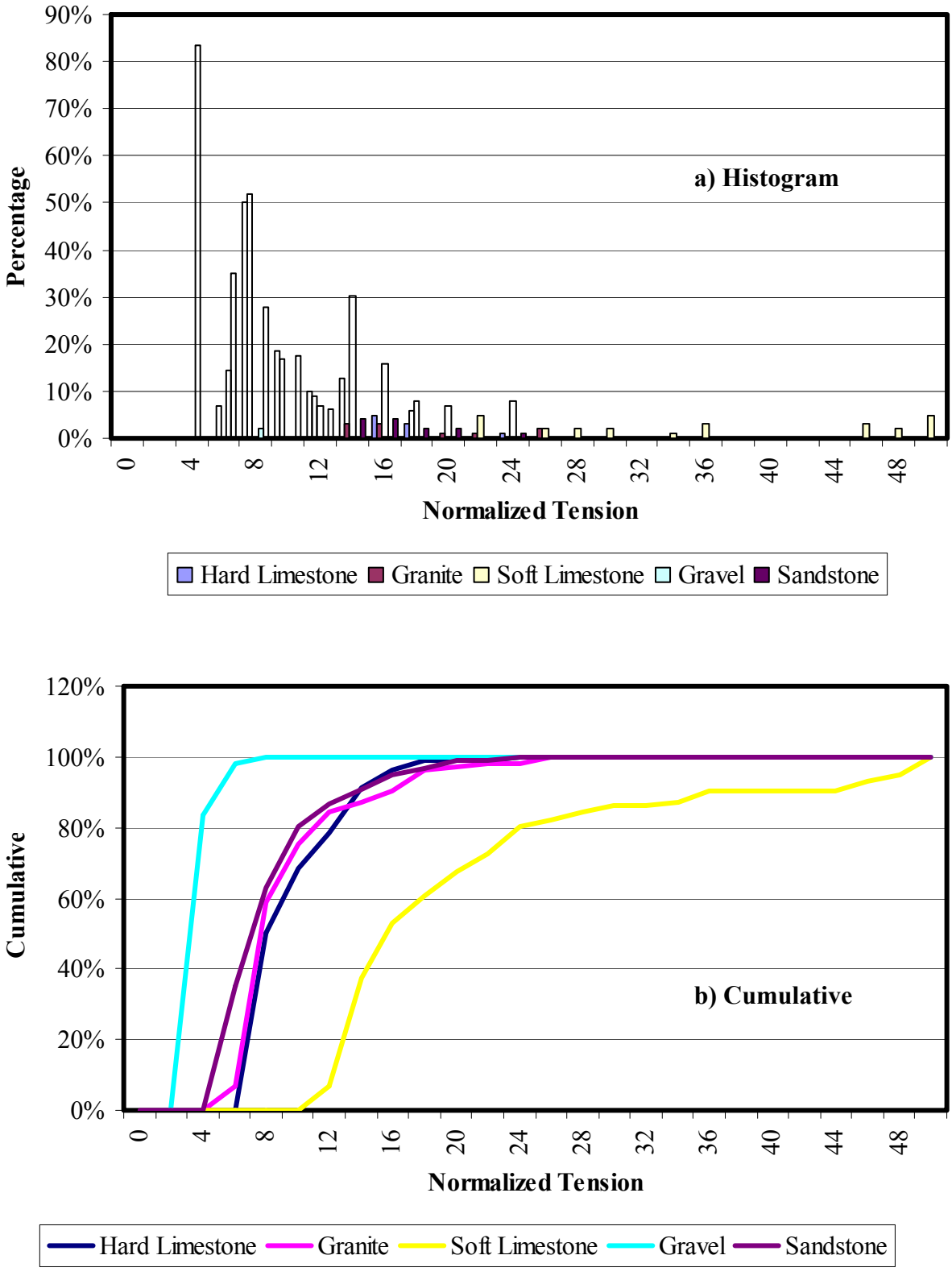

Figure C.21 – Internal Tension Forces Distribution Results for PFC

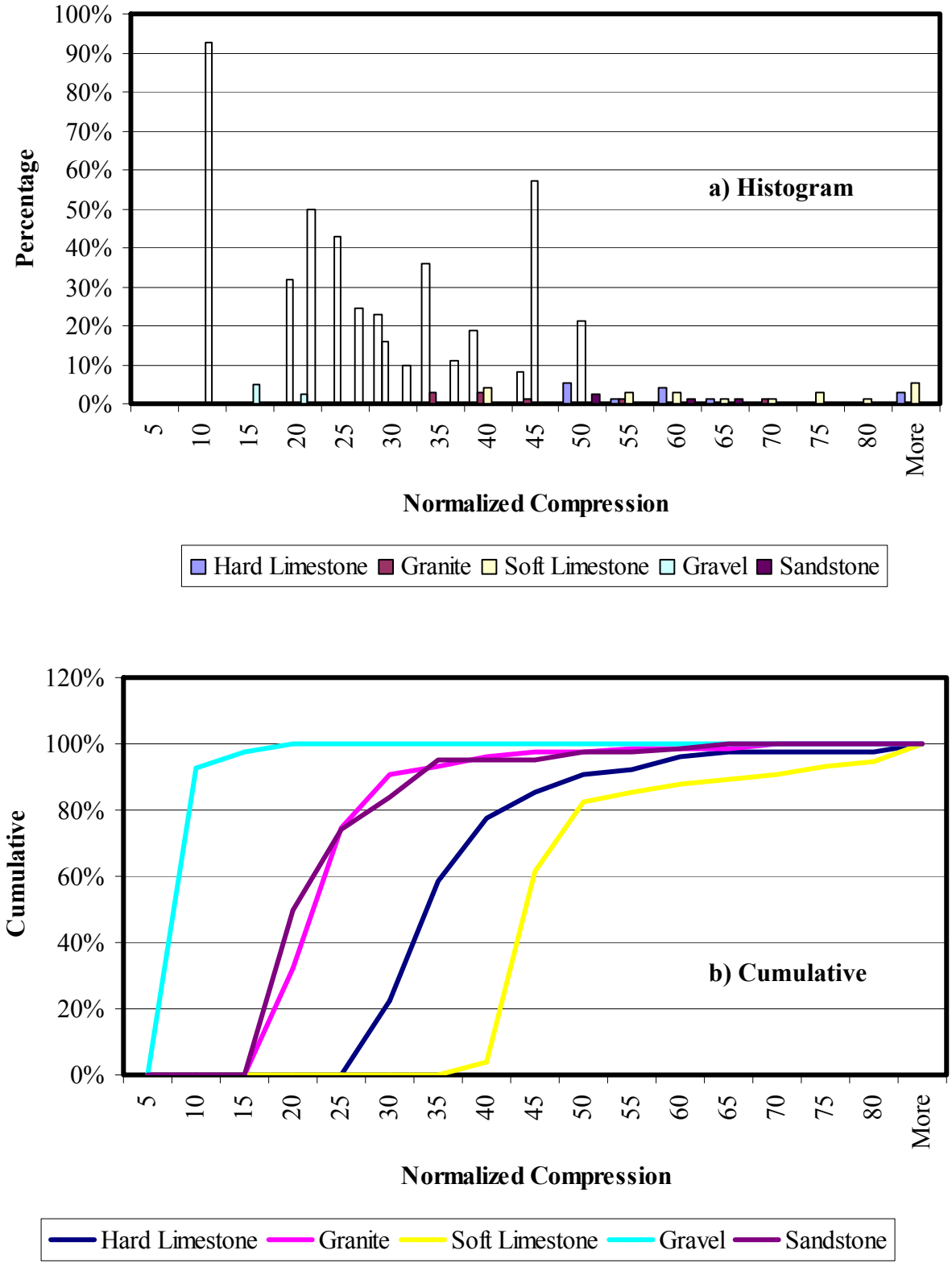

Figure C.22 – Internal Compression Forces Distribution Results for Superpave

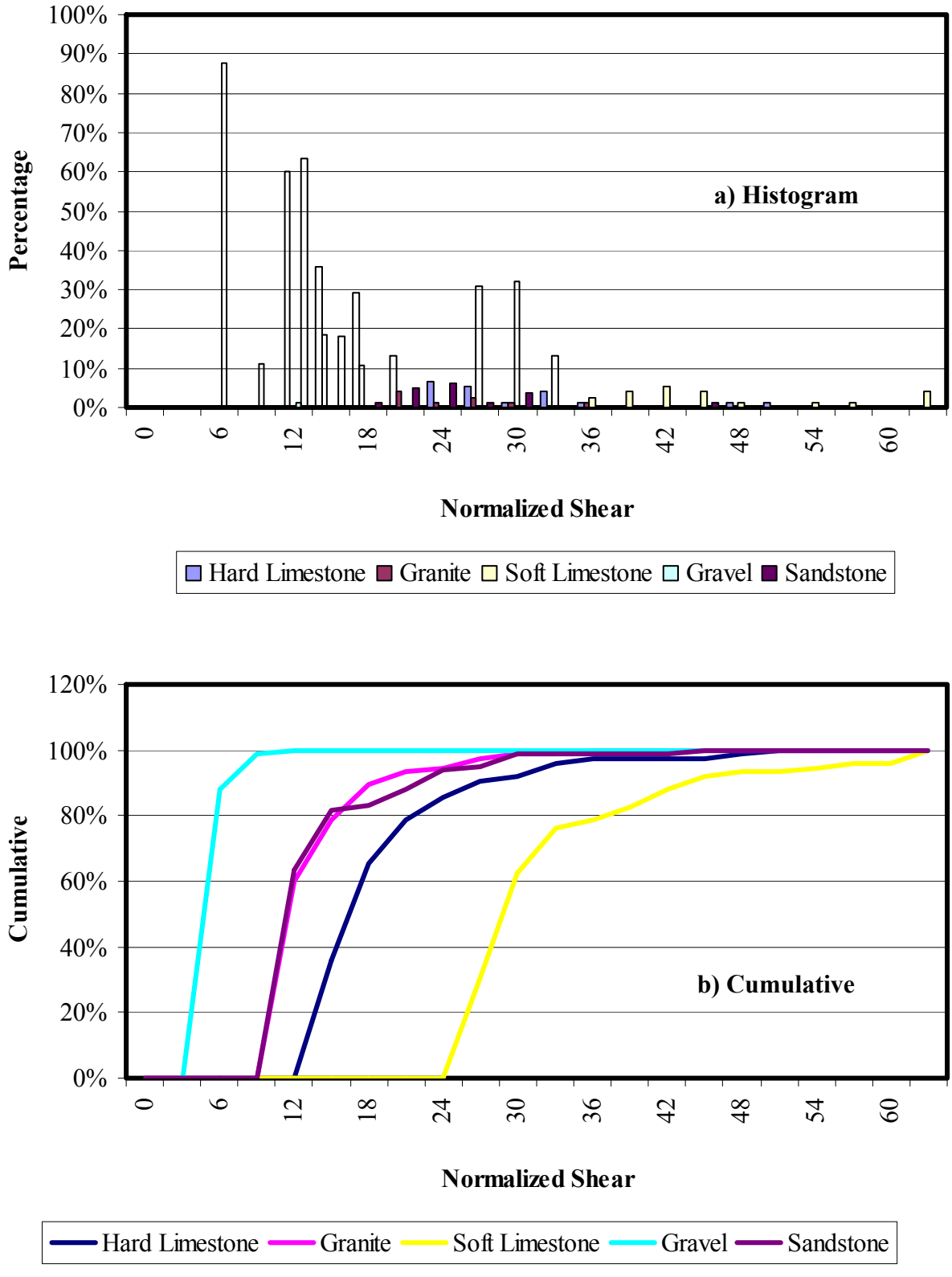

Figure C.23 – Internal Shear Forces Distribution Results for Superpave

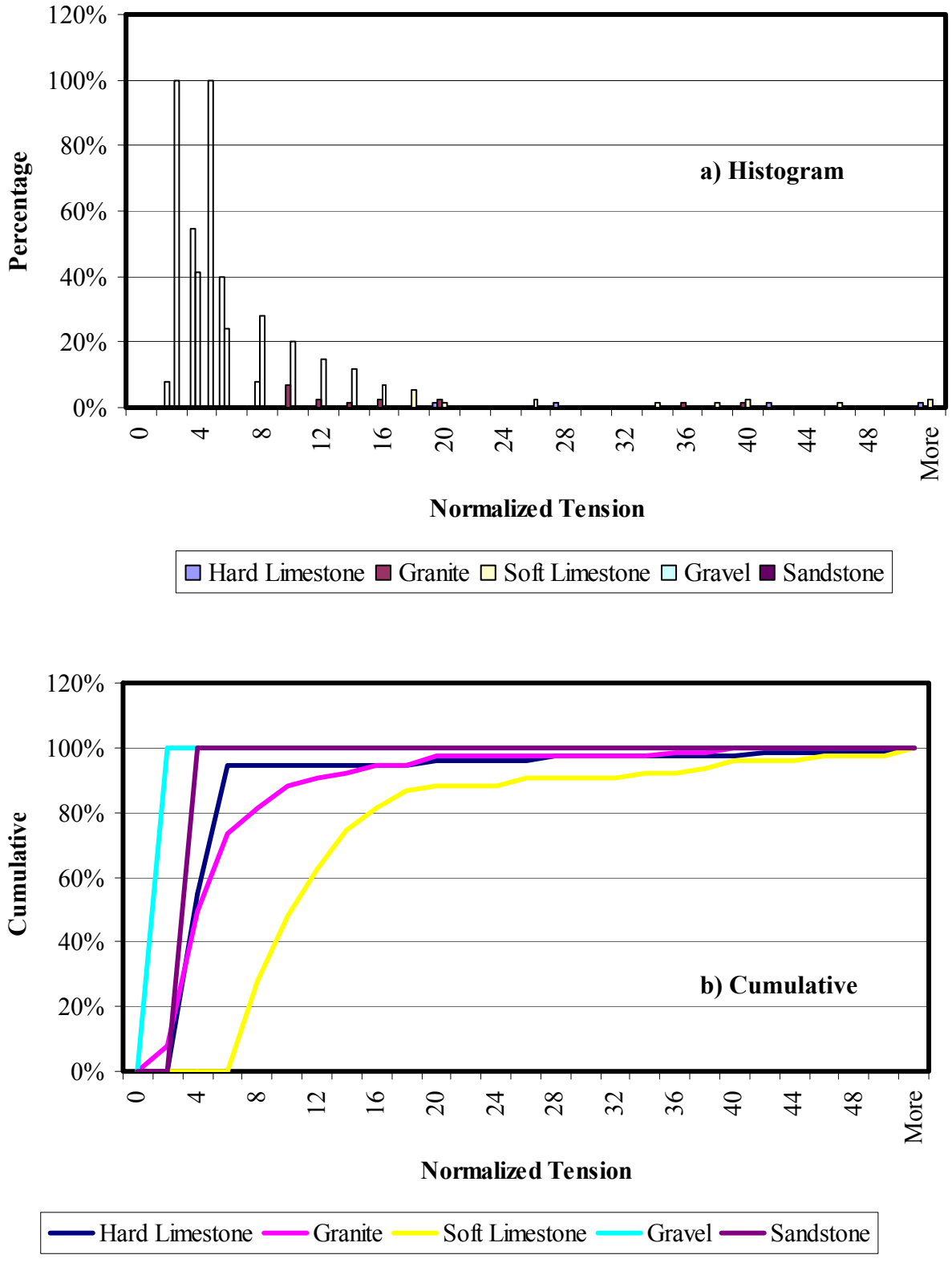

Figure C.24 – Internal Tension Forces Distribution Results for Superpave

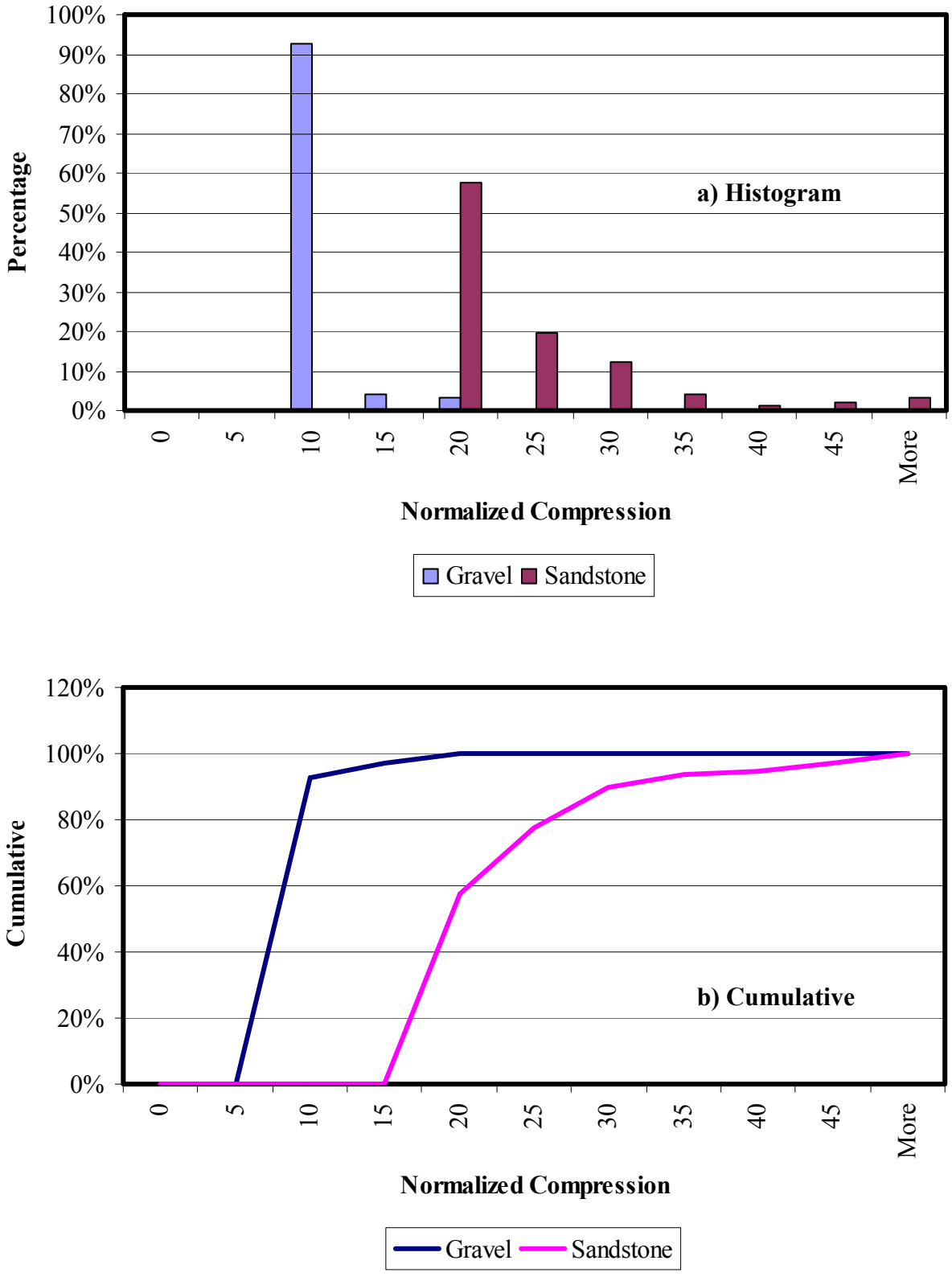

Figure C.25 – Internal Compression Forces Distribution Results for Type-D

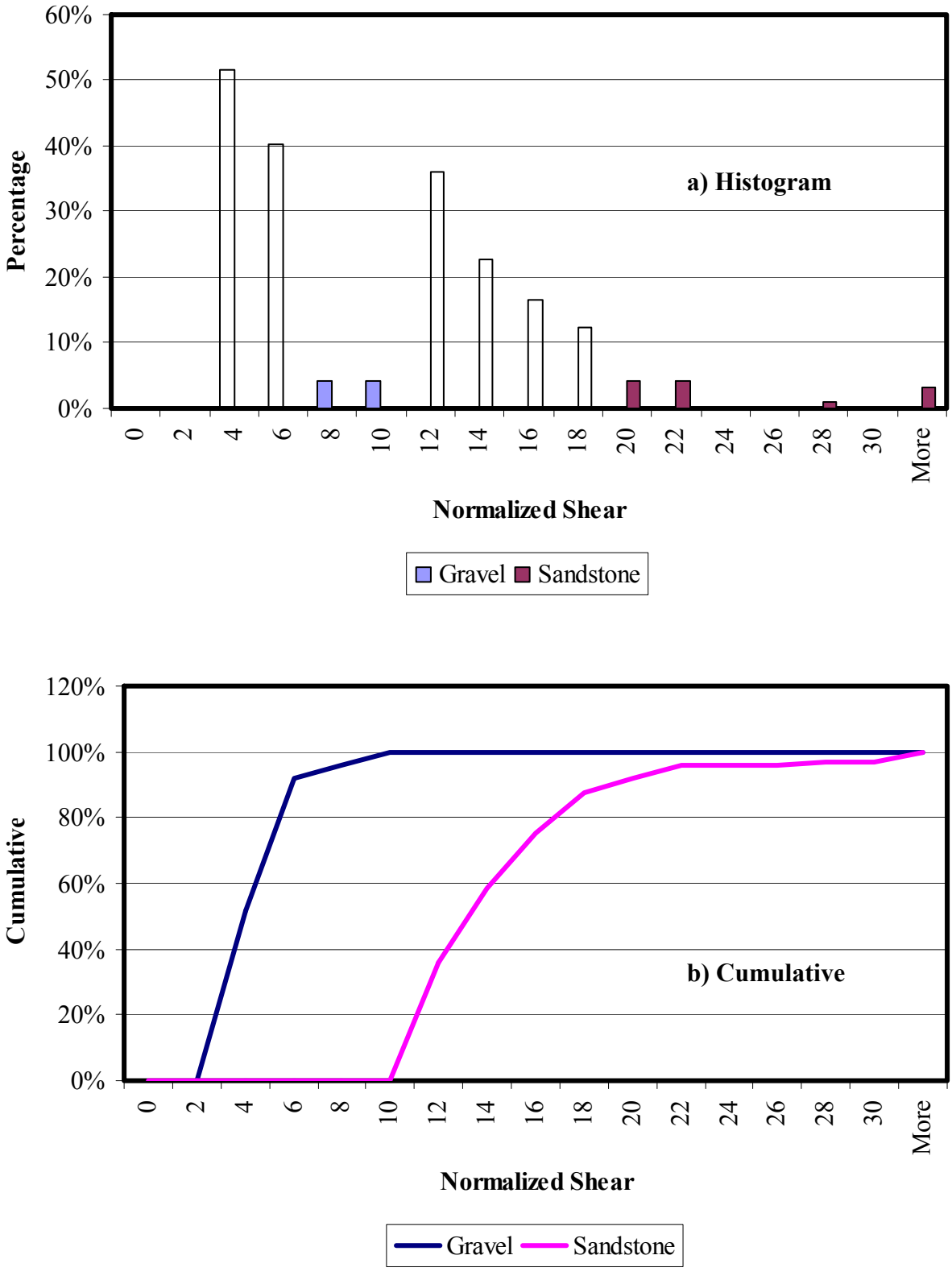

Figure C.26 – Internal Shear Forces Distribution Results for Type-D

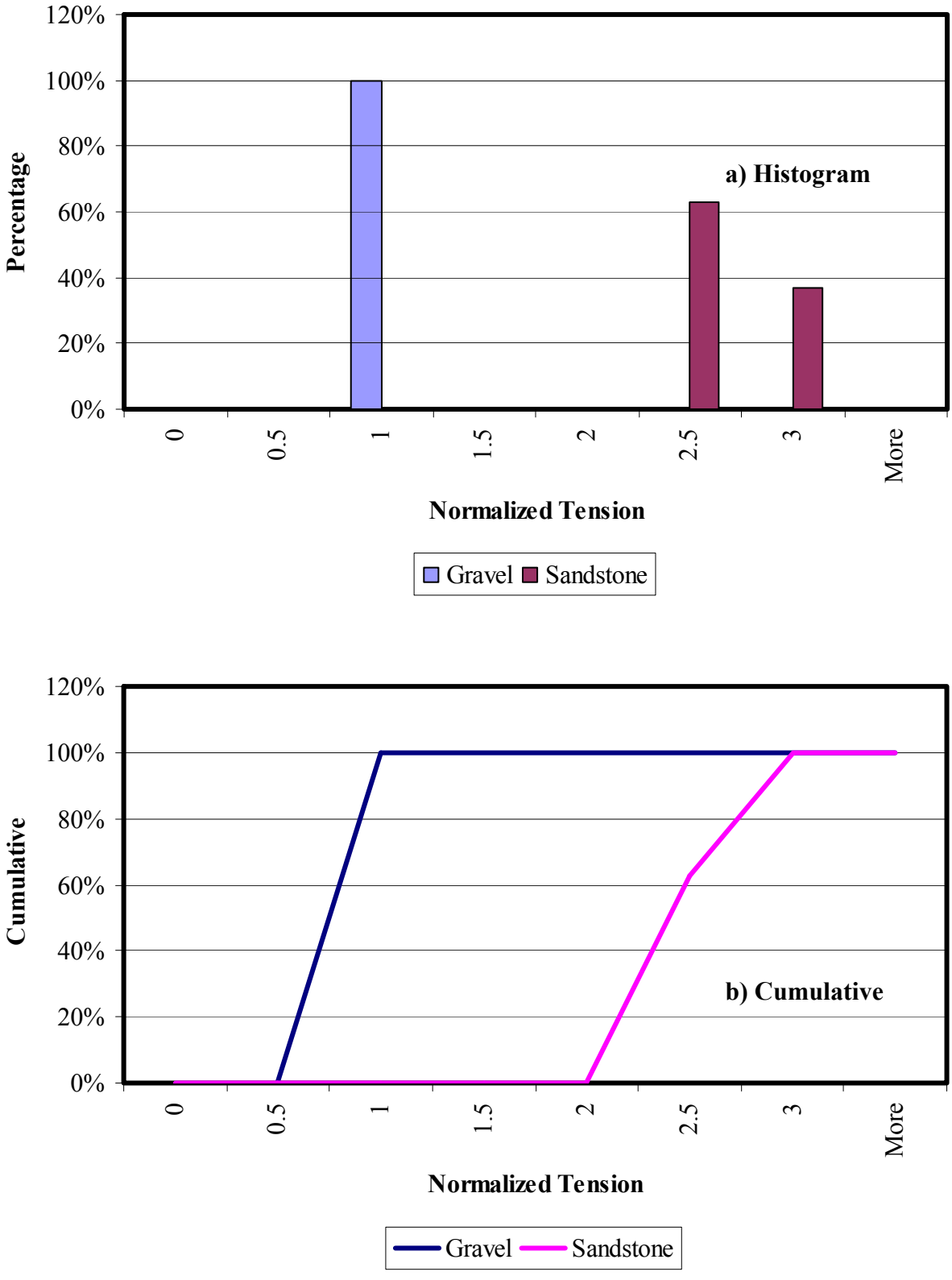

Figure C.27 – Internal Tension Forces Distribution Results for Type-D

APPENDIX D - AGGREGATE IMPACT VALUE (AIV)

Section D.1

Overview

This specification describes methods for the determination of the Aggregate Impact Value (AIV) which gives a relative measure of the resistance of an aggregate to sudden shock or impact.

Two procedures are described; one in which the aggregate is tested in a dry condition, and the other in a soaked condition.

The methods are applicable to aggregates passing at 1/2 in. (12.7 mm) sieve and retained on a 3/8 in. (9.5 mm) sieve.

A specimen is compacted, in a standardized manner, into an open steel cup. The specimen is then subjected to a number of standard impacts from a drop weight. This action breaks the aggregate to a degree which is dependent on the impact resistance of the material. This degree is assessed by a sieving test on the impacted specimen and is taken as the Aggregate Impact Value (AIV).

Units of Measurement

> The values given in parentheses (if provided) are not standard and may not be exact mathematical conversions. Use each system of units separately. Combining values from the two systems may result in nonconformance with the standard.

Section D.2

Apparatus

The following apparatus is required:

- The machine shall be of the general form shown, have a total mass of between 88 lb (45 kg) and 132 lb (60 kg) and shall comprise the parts described in **Figure D.1**.
- A circular metal base, with a mass of 50 lb (22.7 kg), with a plane lower surface of not less than 8 in. (200 mm) diameter and shall be supported on a level and plane concrete or stone block floor at least 18 in. (450 mm) thick. The machine shall be prevented from rocking either by fixing it to the block or floor or by supporting it on a level and plane metal plate cast into the surface of the block or floor.
- A cylindrical steel cup, having an internal diameter of 4 ± 0.02 in. (102 ± 0.5mm) and an internal depth of 2 ± 0.01 in. (50.8 ± 0.25 mm) The walls shall be not less than 0.25 in. (6.35 mm) thick and the inner surfaces shall be case hardened. The cup shall be rigidly fastened at the center of the base and be easily removed for emptying.
- A metal hammer, with a mass of 30 lb (13.6 kg), the lower end of which shall be cylindrical in shape, 3.94 ± 0.02 in. (100 ± 0.5 mm) diameter and 2 ± 0.01 in. (50 ± 0.25 mm) long, with a 0.5 in. (1.5 mm) chamfer at the lower edge, and case hardened. The hammer shall slide freely between vertical guides so arranged that the lower (cylindrical) part of the hammer is above and concentric with the cup.
- Means for raising the hammer, and allowing it to fall freely between the vertical guides from a height of 15 ± 0.2 in. (380 ± 5 mm) on to the sample in the cup, and means for adjusting the height of fall within 0.2 in. (5 mm).
- Means for supporting the hammer, while fastening or removing the cup.
  NOTE: Some means for automatically recording the number of blows is desirable.
- Square-hole perforated-plate sieves, of sizes 1/2 in. (12.7 mm) test sieve, a 3/8 in. (9.5 mm), a #4 (4.76 mm), a #8 (2.36 mm), a #40 (0.42 mm), and a #200 (0.074 mm) test sieve.
- A tamping rod, made out of straight iron or steel bar of circular cross section, 0.63 ± 0.04 in. (16 ± 1 mm) diameter and 23.5 ± 0.2 in. (600 ± 5 mm) long, with both ends hemispherical.
- A balance, of capacity not less than 1 lb (500 g) readable to 0.01 lb (0.1 g).
- A well-ventilated oven, thermostatically controlled at a temperature of 220 ± 10 °F (105 ± 5 °C).
- A rubber mallet.
- A metal tray, of known mass large enough to contain 2 lb (1 kg) of aggregate.
- A brush, with stiff bristles.
- Additional items for testing aggregates in a soaked condition
    - Drying cloths or absorbent paper, for the surface-drying of the aggregate after it has been soaked in water, e.g. two hand-towels of a size not less than 30. in. × 18 in. (750 mm × 450 mm) or rolls of absorbent paper of suitable size and absorbency.

- One or more wire-mesh baskets, having apertures not larger than 0.25 in. (6.5 mm) or a perforated container of convenient size with hangers for lifting purposes.
- A stout watertight container, in which the basket(s) may be immersed.
- A supply of clean water, of drinking quality.

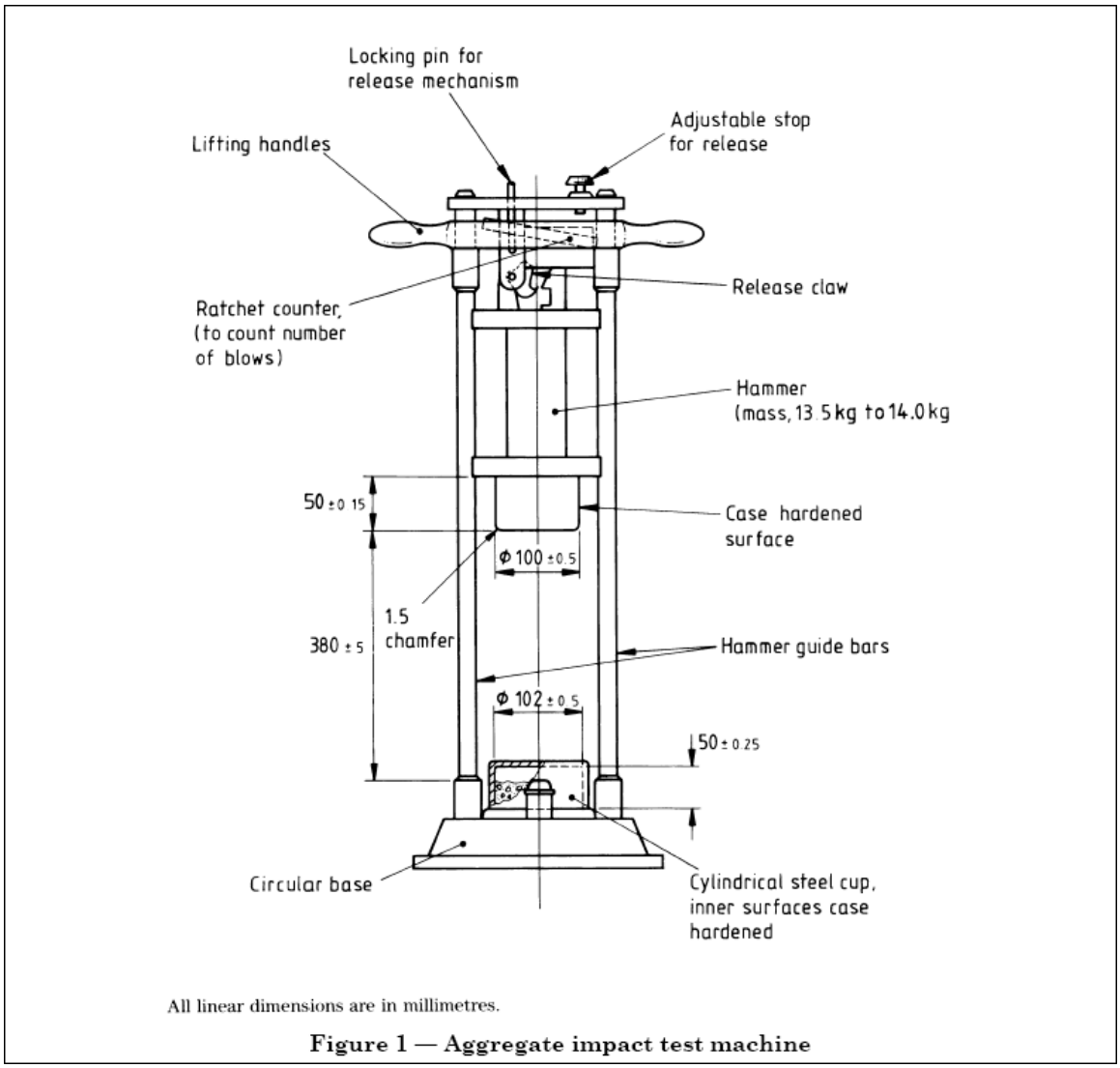

Figure 1 — Aggregate impact test machine

Figure D.1 – Aggregate Impact Test Machine

Section D.3

Preparation of Specimen

For test specimens in a dry condition

- Produce a sample of sufficient mass to acquire three specimens of 1/2 in. (12.7 mm) and 3/8 in. (9.5 mm) size fraction.

- Thoroughly sieve the entire sample on the 1/2 in. (12.7 mm) and3/8 in. (9.5 mm) sieves to remove the oversize and undersize fraction. Divide the resulting 1/2 in. (12.7 mm) and 3/8 in. (9.5 mm) size fractions to produce three specimens each of sufficient mass to fill the container.

- Dry the specimens by heating at a temperature of 220 ± 10 °F (105 ± 5 °C) for a period of not more than 4 hrs. Cool to room temperature before testing.

- Fill the cup to overflowing with the aggregate comprising the specimen by means of a scoop. Tamp the aggregate with 25 blows of the rounded end of the tamping rod, each blow being given by allowing the tamping rod to fall freely from a height of about 2 in. (50 mm) above the surface of the aggregate and the blows being evenly distributed over the surface. Remove the surplus aggregate by rolling the tamping rod across, and in contact with, the top of the container. Remove by hand any aggregate which impedes its progress and fill any obvious depressions with added aggregate. Record the net mass of aggregate in the cup and use the same mass for the subsequent specimens.

For test specimens in a soaked condition

- Prepare the sample using the procedure described for dry condition except that the sample is tested in the as-received condition and not oven-dried. Place each specimen in the wire basket and immerse it in the water in the container with a cover of at least 2 in. (50 mm) of water above the top of the basket. Immediately after immersion remove the entrapped air from the specimen by lifting the basket 1 in. (25 mm) above the base of the container and allowing it to drop 25 times at a rate of about once a second. Keep the basket and aggregate completely immersed during the operation and for a subsequent period of 24 ± 2 h and maintain the water temperature at 70 ± 4 °F (20 ± 5 °C).

- After soaking, remove the specimen from the basket and blot the free water from the surface with the absorbent cloths. Carry out the completion of preparation and testing immediately after this operation.

Section D.4

Procedure

This part explains the steps followed to perform the Aggregate Impact Value test.

Dry Condition	
Step	Action
1	Rest the impact machine, without wedging or packing, upon the level plate, block or floor, so that it is rigid and the hammer guide columns are vertical. Before fixing the cup to the impact machine, place the specimen in the cup and then compact by 25 strokes of the tamping rod as discussed above. With the minimum of disturbance to the specimen, fix the cup firmly in position on the base of the machine. Adjust the height of the hammer so that its lower face is 15 ± 0.2 in (380 ± 5 mm) above the upper surface of the aggregate in the cup and then allow it to fall freely on to the aggregate. Subject the specimen to a total of 25 such blows. NOTE: No adjustment for hammer height is required after the first blow.
2	Remove the crushed aggregate by holding the cup over a clean tray and hammering on the outside with the rubber mallet until the particles are sufficiently disturbed to enable the mass of the specimen to fall freely on to the tray. NOTE 1: If this fails to remove the compacted aggregate other methods should be used but take care not to cause further crushing of the particles. Transfer fine particles adhering to the inside of the cup and the underside of the hammer to the tray by means of the stiff bristle brush. Weigh the tray and the aggregate and record the mass of aggregate used (M_1) to the nearest 0.01 lb (0.1 g).
3	Sieve the entire specimen on the tray with the #8 (2.36 mm), #4 (4.76 mm), #40 (0.42 mm) , and #200 (0.074 mm) sieves until no further significant amount passes during a further period of 1 min. Weigh and record the masses of the fractions passing and retained on the sieve to the nearest 0.01 lb (0.1 g), and if the total mass differs from the initial mass by more than 0.02 lb (2 g), discard the result and test a further specimen.
4	Repeat the procedure as described in **Steps 1** to **3** inclusive using a second specimen of the same mass as the first specimen.

Soaked Condition	
Step	Action
1	Follow the test procedure described in the dry condition.
2	Remove the crushed specimen from the cup and dry it in the oven at a temperature of 220 ± 10 °F (105 ± 5 °C) either to constant mass or for a minimum period of 12 hrs. Allow the dried material to cool and weigh to the nearest gram and record the mass of the specimen (M_1). Complete the procedure as described in **Step 2 for the dry condition**, starting at the point where the specimen is sieved on the #8 (2.36 mm), #4 (4.76 mm), #40 (0.42 mm), and #200 (0.074 mm) sieves.

Section D.5

Calculations

- Calculate the Aggregate Impact Value (AIV) expressed as a percentage to the first decimal place for each test specimen from the equation:

$$AIV = \frac{M_2}{M_1} \times 100\% \quad \text{(D.1)}$$

where

M_1 is the mass of the test specimen (in lbs);
M_2 is the mass of the material passing the #8 (2.36 mm) test sieve (in lbs).

- Calculate the aggregate passing the #4 (4.76 mm) test sieve expressed as a percentage to the first decimal place, of the mass of fines formed to the total mass of the test specimen from the following equation:

$$AIV4 = \frac{M_3}{M_1} \times 100\% \quad \text{(D.2)}$$

where

M_1 is the mass of the test specimen (in lbs);
M_3 is the mass of the material passing the #4 (4.76 mm) test sieve (in lbs).

- Calculate the aggregate passing the #40 (0.42mm) test sieve expressed as a percentage to the first decimal place, of the mass of fines formed to the total mass of the test specimen from the following equation:

$$AIV40 = \frac{M_4}{M_1} \times 100\% \quad \text{(D.3)}$$

where

M_1 is the mass of the test specimen (in lbs);
M_4 is the mass of the material passing #40 (0.42 mm) test sieve (in lbs).

- Calculate the aggregate passing the #200 (0.074 mm) test sieve expressed as a percentage to the first decimal place, of the mass of fines formed to the total mass of the test specimen from the following equation:

$$AIV200 = \frac{M_5}{M_1} \times 100\% \quad \text{(D.4)}$$

where

M_1 is the mass of the test specimen (in lbs);
M_5 is the mass of the material passing the #200 (0.074 mm) test sieve (in lbs).

- Calculate the mean of the two values from the above equations to the nearest whole number. Report the mean as the Aggregate Impact Value, unless the individual results differ by more than 0.15 times the mean value. In this case repeat the test on two further specimens, calculate the median of the four results to the nearest whole number, and report the median as the Aggregate Impact Value.

NOTE: The median of four results is calculated by excluding the highest and the lowest result and calculating the mean of the two middle results.

Section D.6

Report

The report shall contain the following information:

- Material description of sample;
- Conditions under which sample was tested, i.e. dry or soaked condition;
- Number of blows;
- The Aggregate Impact Value (AIV) of the dry aggregate;
- The Aggregate Impact Value (AIV) of the aggregate under soaked conditions;
- Parameters AIV4, AIV40 and AIV200

APPENDIX E - AGGREGATE CRUSHING VALUE (ACV)

Section E.1

Overview

The Aggregate Crushing Value (ACV) is a method that gives a relative measure of the resistance of an aggregate to crushing under a gradually applied compressive load. In this test an aggregate specimen is compacted in a standardized manner into a steel cylinder fitted with a freely moving plunger. The specimen is then subjected to a standard loading applied through the plunger. This action crushes the aggregate to a degree which is dependent on the crushing resistance of the material. This degree is assessed by a sieving test on the crushed aggregate and is taken as a measure of the Aggregate Crushing Value (ACV).

The methods are applicable to aggregates passing at 1/2 in. (12.7 mm) sieve and retained on a 3/8 in. (9.5 mm) sieve.

A specimen is compacted in a standardized manner into a steel cylinder fitted.

Units of Measurement

The values given in parentheses (if provided) are not standard and may not be exact mathematical conversions. Use each system of units separately. Combining values from the two systems may result in nonconformance with the standard.

Section E.2

Apparatus

The following apparatus is required:

- A steel cylinder, open-ended, of nominal 6 in. (150 mm) internal diameter with plunger and base plate of the general form and dimensions shown in Figure E.1 and given in Table E.1.
- A tamping rod, made out of straight iron or steel bar of circular cross section, 0.63 ± 0.04 in. (16 ± 1 mm) diameter and 23.5 ± 0.2 in. (600 ± 5 mm) long, with both ends hemispherical.
- A balance, of at least 7 lb (3 kg) capacity, readable and accurate to0.01 lb (1 g).
- Square-hole perforated-plate sieves, of sizes 1/2 in. (12.7 mm) sieve, a 3/8 in. (9.5 mm), a #8 (2.36 mm), a #4 (4.76 mm), a #40 (0.42 mm), and a #200 (0.074 mm) sieve.
- A well-ventilated oven thermostatically controlled at a temperature of 220 ± 10 °F (105 ± 5 °C).
- A compression testing machine, capable of applying any force up to 112 kips (500 kN) and which can be operated to give a uniform rate of loading so that this force is reached in 10 min. (a machine that can record the load and deformation is preferred).
- A cylindrical metal measure, for measuring the samples, of sufficient rigidity to retain its form under rough usage and having an internal diameter of 4.5 ± 0.04 in. (115 ± 1 mm) and an internal depth of 7 ± .05 in. (180 ± 1 mm).
- A rubber mallet.
- A metal tray, of known mass large enough to contain 6.6 lb (3 kg) of aggregate.
- A brush, with stiff bristles.

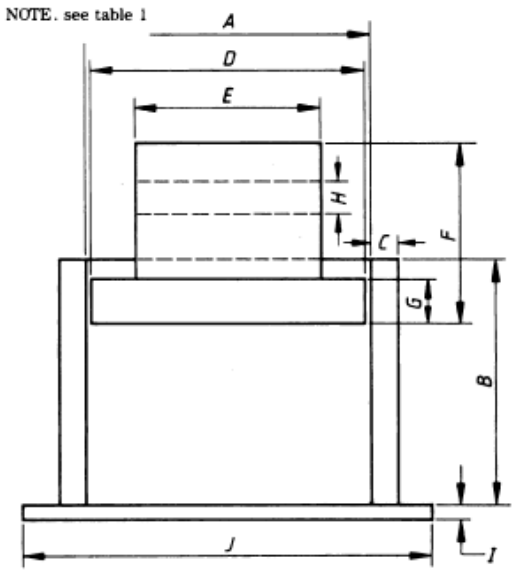

Figure 1 — Outline form of cylinder and plunger apparatus for the aggregate crushing value

Figure E.1 – Outline form of Cylinder and Plunger Apparatus for the Aggregate Crushing Value

Table E.1 — Principal Dimensions of Cylinder and Plunger Apparatus

Component	Dimensions (see Figure 1)	Nominal 150 mm internal diameter of cylinder	
		in	mm
Cylinder	Internal diameter, *A*	6.1 ± 0.02	154 ± 0.5
	Internal depth, *B*	5.0 to 5.5	125 to 140
	Minimum wall thickness, *C*	6.3	16.0
Plunger	Diameter of piston, *D*	5.9 ± 0.02	152 ± 0.5
	Diameter of stem, *E*	< 3.7 to ≤ *D*	< 95 to ≤ *D*
	Overall length of piston plus stem, *F*	4.0 to 4.5	100 to 115
	Minimum depth of piston, *G*	not less than 1.0	not less than 25.0
	Diameter of hole, *H*	0.75 ± 0.004	20.0 ± 0.1
Base Plate	Minimum thickness, *I*	0.4	10.0
	Length of each side of square, *J*	8.0 to 9.0	200 to 230

Section E.4

Preparation of Specimen

- Produce a sample of sufficient mass to acquire three specimens of 1/2 in. (12.7 mm) and 3/8 in. (9.5 mm) size fraction.
  NOTE: A single specimen is that quantity of material required to fill the cylinder
- Thoroughly sieve the entire sample on the 1/2 in. (12.7 mm) and 3/8 in. (9.5 mm) sieves to remove the oversize and undersize fractions. Divide the resulting 1/2 in. (12.7 mm) and 3/8 in. (9.5 mm) size fractions to produce three specimens each of mass such that the depth of the material in the cylinder is approximately 4 in. (100 mm) after tamping (see note 1).
  NOTE 1: The appropriate quantity of aggregate may be found conveniently by filling the cylindrical measure in three layers of approximately equal depth. Tamp each layer 25 times, from a height of approximately 2 in. (50 mm) above the surface of the aggregate, with the rounded end of the tamping rod. Level off using the tamping rod as a straightedge.
  NOTE 2: Mechanical sieving should only be used for aggregates which do not degrade under this action.
- Dry the specimens by heating at a temperature of 220 ± 10 °F (105 ± 5 °C) for a period of not more than 4 hours. Cool to room temperature and record the mass of material comprising the specimens before testing.

Section E.5

Procedure

This part explains the steps followed to perform the Aggregate Crushing Value test.

Step	Action
1	Place the cylinder of the test apparatus in position on the base plate and add the specimen in three layers of approximately equal depth, each layer being subjected to 25 strokes from the tamping rod distributed evenly over the surface of the layer and dropping from a height approximately 2 in. (50 mm) above the surface of the aggregate. Carefully level the surface of the aggregate and insert the plunger so that it rests horizontally on this surface. Take care to ensure that the plunger does not jam in the cylinder.
2	Place the apparatus, with the specimen prepared as described in **Section 3** and plunger in position, between the platens of the testing machine and load it at as uniform a rate as possible (see note) so that the required force of 90 kips (400 kN) is reached in 10 min ± 30 s. NOTE: When, during the early stages of the test, there is a significant deformation, it may not be possible to maintain the required loading rate and variations in the loading rate may occur especially at the beginning of the test. These variations should be kept to a minimum with the principal object of completing the test in the overall time of 10 min ± 30 s.
3	Record and save time, loading, and deformation of progress of the test.
4	Release the load and remove the crushed material by holding the cylinder over a clean tray of known mass and hammering on the outside of the cylinder with the rubber mallet until the particles are sufficiently disturbed to enable the mass of the specimen to fall freely onto the tray. NOTE: If this fails to remove the compacted aggregate other methods may be used but take care not to cause further crushing of the particles. Transfer any particles adhering to the inside of the cylinder, to the base plate and the underside of the plunger, to the tray by means of a stiff bristle brush. Weigh the tray and the aggregate and determine the mass of aggregate used ($M1$) to the nearest gram.
5	Sieve the specimen on the tray with the #8 (2.36 mm), #4 (4.76 mm), #40 (0.42 mm), and #200 (0.074 mm) sieves until no further significant amount passes during a further period of 1 min. Weigh and record the masses of the fractions passing and retained on the sieve to the nearest gram. If the total mass of the individual fractions differs from the initial mass by more than 0.05 lb (25 g), discard the result and repeat the complete procedure using a new specimen. NOTE 1: In all of the procedures described in Steps 3 and 5 take care to avoid loss of fines and overloading the sieves. NOTE 2: Mechanical sieving should only be used for aggregates which do not degrade under its action.
5	Repeat the whole procedure described in Steps 1 to 5 with a second and third test specimen.

Section E.6

Calculations

- Calculate the Aggregate Crushing Value (ACV) expressed as a percentage to the first decimal place, of the mass of fines formed to the total mass of the test specimen from the following equation:

$$ACV = \frac{M_2}{M_1} \times 100\% \quad \text{(E.1)}$$

where

M_1 is the mass of the test specimen (in lbs);
M_2 is the mass of the material passing the #8 (2.36 mm) test sieve (in lbs).

- Calculate the aggregate passing the #4 (4.76 mm) test sieve expressed as a percentage to the first decimal place, of the mass of fines formed to the total mass of the test specimen from the following equation:

$$ACV4 = \frac{M_3}{M_1} \times 100\% \quad \text{(E.2)}$$

where

M_1 is the mass of the test specimen (in lbs);
M_3 is the mass of the material passing the #4 (4.76 mm) test sieve (in lbs).

- Calculate the aggregate passing the #40 (0.42 mm) test sieves expressed as a percentage to the first decimal place, of the mass of fines formed to the total mass of the test specimen from the following equation:

$$ACV40 = \frac{M_4}{M_1} \times 100\% \quad \text{(E.3)}$$

where

M_1 is the mass of the test specimen (in g);
M_4 is the mass of the material passing the #40 (0.42 mm) test sieves (in g).

- Calculate the aggregate passing the #200 (0.074mm) test sieve expressed as a percentage to the first decimal place, of the mass of fines formed to the total mass of the test specimen from the following equation:

$$ACV200 = \frac{M_5}{M_1} \times 100\% \quad \text{(E.4)}$$

where

M_1 is the mass of the test specimen (in g);
M_5 is the mass of the material passing the #200 (0.074mm) test sieve (in g).

- Calculate the mean of the three results to the nearest whole number for ACV, ACV4, ACV40 and ACV200. Report the mean as the Aggregate Crushing Value, unless the individual results differ by more than 0.1 times the mean value. In this case repeat the test on a fourth specimen, calculate the median of the four results to the nearest whole number, and report the median as the Aggregate Crushing Value.
  NOTE: The median of four results is calculated by excluding the highest and the lowest result and calculating the mean of the two middle results.

- Quantify the behavior under loading by using the data recorded during the test (if available)
  - Plot the stress-strain curve as shown in Figure E.2.
  - Fit two straight lines to the stress-strain curve as shown in Figure E.2.
  - Calculate the compacting modulus by using two points on the straight line covering the initial part of the stress strain curve, using the following equation:

$$Compacting\ Modulus = \frac{\sigma_2 - \sigma_1}{\varepsilon_2 - \varepsilon_1} \quad \text{(E.5)}$$

where

σ_1 is the stress for the first point chosen (in psi)
σ_2 is the stress for the second point chosen (in psi)
ε_1 is the strain for the first point chosen (in in./in.)
ε_2 is the strain for the second point chosen (in in./in.)

  - Calculate the crushing modulus by using two points on the straight line covering the final part of the stress strain curve, using the following equation:

$$Crushing\ Modulus = \frac{\sigma_2 - \sigma_1}{\varepsilon_2 - \varepsilon_1} \quad \text{(E.6)}$$

where

σ_1 is the stress for the first point chosen (in psi)
σ_2 is the stress for the second point chosen (in psi)
ε_1 is the strain for the first point chosen (in in./in.)
ε_2 is the strain for the second point chosen (in in./in.)

  - Find the maximum compacting stress and strain from the stress-strain curve at the intersection of the two straight lines as shown in Figure E.2.

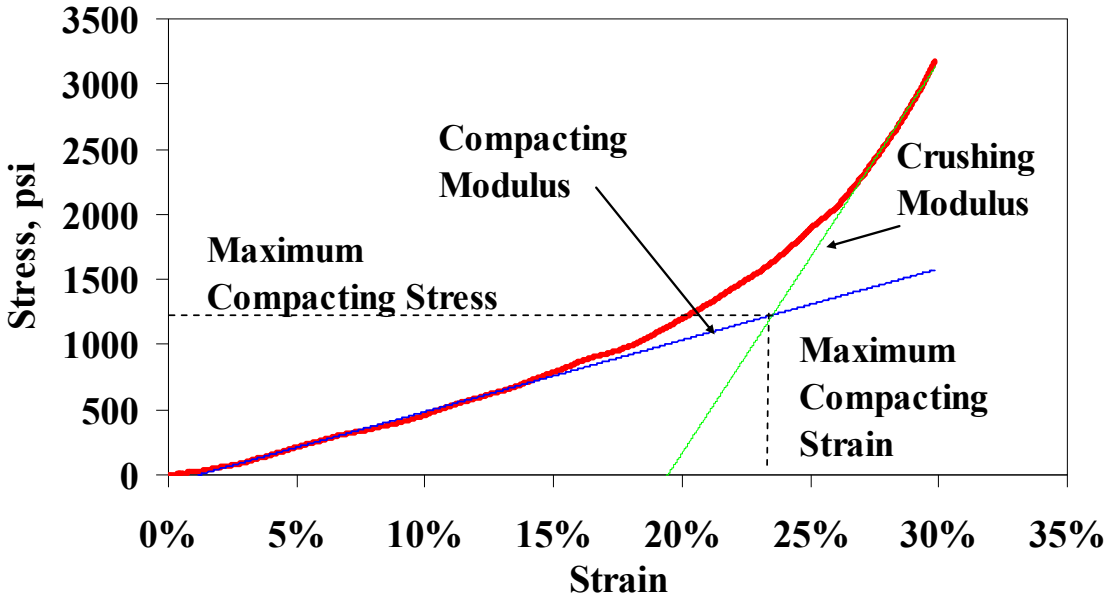

Figure E.2 - Typical Results for the ACV Test

Section E.7

Report

The report shall contain the following information:

- Material description of sample;
- The Aggregate Crushing Value (ACV) of the aggregate;
- Parameters ACV4, ACV40 and ACV200;
- Stress-strain curve and two lines fitted to it;
- Maximum compacting stress value;
- Maximum compacting strain value;
- Compacting modulus value;
- Crushing modulus value;